TREATMENT OF ALGAL TOXINS IN DRINKING WATER WITH UV-BASED ADVANCED OXIDATION PROCESSES

by

Fateme Barancheshme

A dissertation submitted to the faculty of
The University of North Carolina at Charlotte
in partial fulfillment of the requirements
for the degree of Doctor of Philosophy in
Civil Engineering

Charlotte

2020

Approved by:

_____
Dr. Olya Keen

_____
Dr. Gina Kimble

_____
Dr. John Diemer

_____
Dr. Jacelyn Rice-Boayue

_____
Dr. James Amburgey

©2020
Fateme Barancheshme
ALL RIGHTS RESERVED

ABSTRACT

FATEME BARANCHESHME. Treatment of Algal Toxins in Drinking Water with UV-Based Advanced Oxidation Processes. (Under the direction of DR. OLYA KEEN)

The occurrence of algal blooms and the possibility of production of algal toxins and contamination of drinking water resources have become a significant concern worldwide. Advanced oxidation processes (AOPs) are currently known as one of the most effective methods to remove algal toxins. However, little is known about the formation of toxic oxidation products and how the presence of algal organic matter may affect disinfection byproducts (DBPs) formation. Microcystin (MC) is one of the most common toxins associated with freshwater harmful algal blooms. In this study, AOPs, specifically UV/H_2O_2 and UV/Cl_2, were investigated as a means of mitigating microcystins (LR, RR and YR variants). The goal of this study is to compare mentioned advanced oxidation processes in terms of effectiveness to detoxify algal hepatotoxin microcystin and their potential to produce the regulated and unregulated disinfection byproducts, namely trihalomethanes (THMs), haloacetic acids (HAAs), and *N*-nitrosodimethylamine (NDMA). Protein phosphatase inhibition assay (PP2A) and Ames II were conducted to assess the toxicity of the transformation products of each toxin. Analysis of byproducts was done using GC-ECD and LC-MS/MS based on the EPA methods (551.1, 552.3, and 521) modified using recent publications. Both UV/H_2O_2 and UV/Cl_2 processes were effective in oxidizing MC-LR, -RR, and -YR, although the relative effectiveness varied based on additional direct reaction of some of the toxins with chlorine. The background matrix had different inhibitory effects for each toxin because of their relative reactivity with radicals. Higher oxidant dose and higher UV dose helped to minimize the impact of the matrix. The effect of dissolved organic matter (DOM) as a radical scavenger was higher than the impact of nitrate, creating additional radicals. Some of the products in the UV/Cl_2 process are chlorinated,

but may not be toxic, as ADDA group responsible for toxicity was cleaved in most of the detectable transformation products. The formation of DBPs was affected by the background matrix. Different treatment methods did not affect the formation of the THMs. Chloroform appeared to be suppressed by nitrate and enhanced by DOM. The background matrix also impacted HAAs formation. However, there was no correlation between the type of treatment process or level of treatment and HAAs formation. Both nitrate and algal DOM increased the formation of NDMA. NDMA was below the threshold of 10 ng/L followed by some states in all samples even though the nitrate and algal DOM concentration in this study was at a high end of the environmentally relevant range.

Keyword:

Advanced oxidation processes, Disinfection byproducts, Drinking water treatment, Algal toxins, Microcystins, UV irradiation, Chlorination

Table of Contents

List of Tables

List of Figures

List of Abbreviations

AOPs	Advanced Oxidation Processes
AOM	Algal Organic Matter
BSA	Bovine Serum Albumin
CECs	Contaminants of Emerging Concern
CCL 4	Contaminant Candidate List 4
DBPs	Disinfection Byproducts
DOM	Dissolved Organic Matter
DWTP	Drinking Water Treatment Plant
ESI	Electrospray Ionization
EPA	Environmental Protection Agency
ELISA	Enzyme-Linked Immunosorbent Assay
EOM	Extracellular Organic Matter
HAAs	Haloacetic Acids
HABs	Harmful Algal Blooms
IOM	Intracellular Organic Matter
KHP	Potassium Hydrogen Phthalate
LC	Liquid Chromatography
LLE	Liquid-Liquid Extraction
LP	Low Pressure
MCL	Maximum Contaminant Level
MS	Mass Spectrometry
MP	Medium Pressure
MCs	Microcystins
MW	Molecular Weight
MRM	Multiple-Reaction Monitoring
NDMA	*N* –Nitrosodimethylamine
NOM	Natural Organic Matter
OD	Optical Density
PP2A	Protein Phosphatase Inhibition Analysis
SPE	Solid-Phase Extraction
T&O	Taste and Odor
TKN	Total Kjeldahl Nitrogen
TN	Total Nitrogen
TOC	Total Organic Carbon
THMs	Trihalomethanes
UFC	Uniform Formation Condition
WTP	Water Treatment Plant

CHAPTER 1. INTRODUCTION

1.1. Harmful Algal Blooms and Algal Toxins in Drinking Water

Harmful algal blooms (HABs) refer to all marine and inland, brackish and freshwater blooms that result in adverse effects (Anderson, Boerlage, and Dixon 2017; Carmichael and Boyer 2016).

Occurrence, duration, and intensity of HABs are intensifying worldwide due to anthropogenic nutrient addition to aquatic ecosystems and increasing water temperature (Danner et al. 2018; Deng et al. 2017)

Harmful effects are toxic seafood, death of fish, birds and other animals, indirect and direct human illnesses (Carmichael and Boyer 2016), production of neurotoxins, bad taste and odor, and skin-irritating compounds (Anderson et al. 2017; Deng et al. 2017). HABs in freshwater and close to a water treatment plant (WTP) can negatively affect the water treatment processes by increasing the influent turbidity and leading to the higher formation of algal toxins, taste and odor (T&O)-causing compounds, algal organic matter (AOM), and disinfection byproducts (DBPs) (Deng et al. 2017). Hence, HABs result in adverse economic impacts and long-term ecosystem changes.

HABs are mainly formed by cyanobacteria, also called blue-green algae, that are photosynthetic and microscopic organisms in aquatic environments (Chae et al. 2019). Some cyanobacteria can produce toxic compounds as cyanotoxins or algal toxins. Algal toxicity is a significant public health concern in water resources worldwide and drinking water utilities have experienced water intake shutdowns caused by algal toxins (Graham, Loftin, and Kamman 2009; Rodríguez et al. 2007; Rositano et al. 2001).

Microcystins (MCs), cylindrospermopsin, saxitoxin, and anatoxin-a are algal toxins that have been found in drinking water resources (Chae et al. 2019) and are on the EPA Contaminant Candidate List 4 (CCL 4) as unregulated contaminants of emerging concern (CECs) (US EPA 2016).

The majority of unregulated contaminants of emerging concern do not have documented human health effects. However, algal toxins can cause acute and chronic effects in humans (Carmichael and Boyer 2016), and utilities monitor them and try to control their concentrations (Szlag et al. 2015). Based on the NSF report on an international water quality survey, 82% of consumers are concerned about trace levels of contaminants of emerging concern in drinking water (Flechtner 2017; Sanders 2018; Sun et al. 2016).

Microcystins are the most common cyanobacterial toxins found in water (Chae et al. 2019). Microcystins are liver toxins that increase the serum of liver enzymes, a sign of liver cell death and increase liver weight. Based on studies with mice and rats, injection of microcystin-LR caused death within a few hours (Butler et al. 2009). Microcystins inhibit the protein phosphatases, which cause hyperphosphorylation of the cellular proteins (Badar et al. 2017; Carmichael and Boyer 2016; Liu and Sun 2015). This mechanism can result in tumor promotion activity or programmed cell suicide (apoptosis) (Butler et al. 2009; Liu and Sun 2015).

Microcystins LR, RR, and YR have been detected in freshwater samples (Jurczak et al. 2005; Kaloudis et al. 2013; Shang et al. 2018). Microcystins LR, RR, and YR inhibit the same phosphatases and induce changes in the liver; therefore, the same toxicity criteria are used for all of them (Butler et al. 2009). These microcystins are targets of the research

reported in this dissertation as they are frequently detected in water resources and MC-LR is the most prevalent variant found during HABs.

CHAPTER 2. LITERATURE REVIEW

2.1. Regulation of Microcystins

Cyanobacterial toxins were not included in the first three editions of the World Health Organization's (WHO) International Standards for Drinking water published in 1958, 1963 and 1971. Also, cyanobacterial toxins were not regulated in the first two editions of the WHO guidelines for drinking-water quality that was published in 1984 and 1993. The addendum to the second edition of the guidelines was published in 1998, and a health-based guideline value of 1 µg/L was derived for total MC-LR (free plus cell-bound), concluding that there were not enough data to allow a guideline value to be acquired for any other algal toxins. The guideline value was designated as provisional and covered only MC-LR. This guideline value was brought to the third and fourth editions of the guidelines in 2004 and 2011, respectively. The safe drinking water concentration for MC-LR advised by the USEPA is 0.3 µg/L for infants and pre-school children and 1.6 µg/L for school-age children and adults (US EPA 2016).

2.2. Drinking Water Treatment Methods to Remove Microcystins

Studies have explored the fate of microcystins and other algal toxins in water and wastewater in full-scale (Shang et al. 2018), pilot-scale (Cook and Newcombe 2008), and bench-scale (Song et al. 2006). These studies have been using physical, chemical, and biological methods (Jiang et al. 2017). An overview of treatment methods that have been utilized for algal toxins removal in drinking water is elaborated in this section. Different methods have varying levels of success in the treatment of algal toxins. Table 1 shows some of the critical studies on microcystins removal in drinking water treatment plants.

Table 1. Removal of Microcystin by Chemical Drinking Water Treatment Processes

Target Variant	Treatment Method	Removal	Application	Reference
LR	Powdered Activated carbon	50 to 80%	Bench-Scale	(Bajracharya, Liu, and Lenhart 2019)
LR	Hybrid photocatalytic composites	> 95%	Bench-Scale	(Chae et al. 2019)
LR	Adsorption onto Clay Minerals	Up to 65%	Bench-Scale	(Liu, Walker, and Lenhart 2019)
LR	Solar/chlorine	96.7%	Bench-Scale	(Sun et al. 2019)
LR	vacuum UV	40 – 60%	Bench-Scale	(Visentin et al. 2019)
LR	UV/chlorine	92.5%	Bench-Scale	(X. Zhang et al. 2019)
LR	Ozonation, biofiltration membrane	100%, 70%	Bench-Scale	(Eke, Wagh, and Escobar 2018)
LR, RR, YR	Chlorination	47.9 to 90.9%	Full-Scale	(Shang et al. 2018)
LA, LF, LR, LY, RR, YR	Chlorination	> 98%	Bench-Scale	(Mash and Wittkorn 2016)
LR, LA	Powdered Activated carbon	40%, 15%	Bench and Pilot -Scale	(Cook and Newcombe 2008)
LR, RR	Ultrasonically Induced H_2O_2	95%, 80%	Bench-Scale	(Song et al. 2006)

2.2.1. Conventional Drinking Water Treatment

Traditional drinking water treatment methods like coagulation and flocculation can successfully remove algal cells but cannot effectively remove cyanotoxins that are already released and dissolved in water (Afzal et al. 2010; He et al. 2016; Senogles et al.

2001). For example, lime and alum coagulation effectively remove *Microcystis* cells but have no impact on its associated toxins (Ma et al. 2012).

Coagulation and sedimentation units are often followed by filtration. Filter materials, such as sand, gravel, or both have no considerable impact on algal toxins removal and disrupt cells and release toxins into water (He et al. 2016).

2.2.2. Disinfection

Disinfection treatment methods include chlorine, chlorine dioxide, chloramines, ozone, and ultraviolet light. The effect of disinfection processes on algal toxins depends on certain cyanotoxins, types of oxidants, and operational conditions (He et al. 2016).

Chlorine: In an extensive study on six microcystins, including MCs-LA, -LF, -LR, -LY, -RR, and -YR, the toxins were exposed to chlorine oxidation (Mash and Wittkorn 2016). MCs-LA and -LF had little or no reaction with chlorine. MCs-LR and -RR were degraded through chlorination because they reacted with chorine at arginine amino acids present in their chemical structure. MCs-LY and -YR are also reactive with chlorine as they are sharing both arginine and tyrosine residues, which are reactive with chlorine (Draper et al. 2013; Mash and Wittkorn 2016; Woolbright et al. 2017; Zhang et al. 2016).

Application of prechlorination for algae-laden water as pretreatment required specific dose and contact time to minimize their effects on cell integrity, AOM release, toxin release, and chlorinated DBP formation (Wu et al. 2019). USEPA recommends avoiding pre-oxidation to inhibit the release of cyanobacterial toxins.

Chlorination is one of the typical drinking water disinfection processes. The behavior of microcystins during chlorination has been studied by Merel and their research group (Merel, Clément, and Thomas 2010). Based on their study, pH and chlorine dose affect

the efficiency of the process. Oxidant nature was found to be effective as well. Oxidation of toxins with chloramine was weaker than chlorine. MC-LR was efficiently altered by chlorination. However, six different byproducts were introduced into the system. Byproducts were including dihydroxy-microcystin, monochloro-microcystin, monochloro-hydroxy-microcystin, monochloro-dihydroxy-microcystin, dichloro-dihydroxy-microcystin, and trichloro-hydroxy-microcystin. (Merel et al. 2010).

Chlorine can improve the coagulation of cyanobacteria; however, potentially can lyse the cyanobacterial cells and release toxic metabolites. The released toxin can be degraded by chlorine as well. Release and degradation of microcystin toxins under chlorination have been investigated in a previous study. The cell lysis occurred at a chlorine dose of 7 - 29 mg min/L that is a standard dose for the disinfection process. The release of the intracellular toxin was three times faster than its degradation by chlorine. The pH, chlorine exposure, and the presence of cyanobacterial cells were affecting the degradation of extracellular microcystin (Daly, Ho, and Brookes 2007).

UV and Ozone: UV irradiation followed by the ozonation process was utilized to remove spiked MC-LR from filtered water from a water treatment plant in Harbin, China. The concentration of MC-LR spiked in the water was 100 μg/L. The average light intensity on the surface of the solution was 2.6 mW/cm$_2$, and a 10 W low-pressure UV lamp was used as a UV irradiation source (Liu et al. 2010). Ozonation process alone (1.0 mg/L O_3 over 5 min) was able to remove 50% of MC-LR from filtrate water. However, the same process was able almost completely to remove MC-LR from Milli Q water. This difference between two removal efficiencies might be due to the direct reaction of ozone

with dissolved substances in water or ozone decomposition and hydroxyl radicals production that results in immediate reactions with solutes (Liu et al. 2010). The sequential use of UV for 5 min and 0.2 mg/L ozone for 5 min removed the toxin to lower than 1 μg/L (>99%). Increasing ozone dose to 0.5 mg/L resulted in 0.1 μg/L final concentration of MC-LR. The results of this study showed that the sequential use of UV and ozone is more effective than the implementation of UV or ozone alone or integrated application of ozone and UV (Liu et al. 2010).

Ozone, chlorine, chlorine dioxide, and permanganate: Oxidative elimination of MC-LR from natural waters using ozone, chlorine, and permanganate has been studied. In a study, oxidants were applied to water from a eutrophic Swiss lake (Lake Greifensee), and the effects of a natural matrix on toxin oxidation and byproduct formation were investigated. Based on the results of this study, permanganate, chlorine, and ozone were able to oxidize MC-LR. The concentration of required permanganate for complete removal of MC-LR was 1.5 mg/L, 3 mg/L of chlorine was able to almost complete MC-LR oxidation, and around 95% oxidation of MC-LR was achieved by 0.25 mg/L O_3. The formation of trihalomethanes (THMs) in the treated water limited the application of high-chlorine doses (Rodríguez et al. 2007).

Ozone has shown effective results for the degradation of microcystins. Required dose and contact time depend on the quality of water, namely, dissolved organic carbon concentration and character, and alkalinity (Rositano et al. 2001). Based on the results of a study, MCs-LR and -LA were destroyed entirely after 5 min and residual ozone concentration of 0.5 – 0.7 mg/L. The results showed that the destruction of both toxins

happens under common ozonation conditions before granular activated carbon filtration (Rositano et al. 2001).

Two different water treatment plants in Switzerland and Germany were investigated to verify the efficiency of systems to remove MCs. Radioactive protein phosphatase assay, Adda-ELISA, and HPLC methods were utilized to evaluate the treatment systems. Lake Zurich DWTP was following the treatment steps, including preozonation (1.0 mg/L), rapid sand filtration (pumice/quartz sand), intermediate ozonation (0.5 mg/L), activated carbon filtration (GAC, quartz sand), and slow sand filtration. This plant was efficiently removing both cyanobacterial cells and toxins. The treatment processes at Wahnbachtal Dam DWTP were flocculation (0.8 mg $Al_2(SO_4)_3$/L), sedimentation, quartz sand filtration, and chlorination of pipeline system (0.15–0.2 mg/L). After flocculation and sand filtration, extracellular toxin concentration was the same as raw water (15 ± 16 ng MC-LR equiv./L), and only traces of intracellular microcystin toxin were detectable (Hoeger, Hitzfeld, and Dietrich 2005).

2.2.3. Adsorption

The addition of powdered activated carbon (Cook and Newcombe 2008) and granular activated carbon (He et al. 2016) to the treatment process can enhance cyanotoxin removal. However, it is more capable of cell removal and ineffective to remove soluble toxins, and toxin residuals often remain (Afzal et al. 2010; He et al. 2016). Activated carbon also has a limited life and considerably increases treatment costs (Senogles et al. 2001). Besides, activated carbon and membrane technologies just transfer algal toxins from the treated water to the solid phase or concentrated streams with no degradation (Sichel, Garcia, and Andre 2011).

2.2.4. Biodegradation

Biodegradation of algal toxins is very uncommon. However, there are studies on *Proteobacteria* and *Actinobacteria* to degrade microcystins compounds using gene homologs (Chen et al. 2010; Yan et al. 2012). MC-LR concentration of 40 mg/L was completely biodegraded in 1 hour by *Sphingopyxis* (Yan et al. 2012), and *Stenotrophomonas* effectively degraded MCs-LR and RR from lake water (Chen et al. 2010). These studies are bench-scale studies, and the degrees of success in the biodegradation processes need future research to understand the biodegradation pathway and define compatible species for each type of algal toxins. There are limited studies on the useful genes of bacterial strains that involve in biodegradation, and therefore, there are rare homologs for identified genes that result in challenging sequencing analysis.

2.2.5. Membrane

New pressure-driven membrane filtration, microfiltration, nanofiltration, and reverse osmosis can effectively remove MC-LR from drinking water through size exclusion (Eke et al. 2018). Natural organic matter (NOM) is always challenging membrane-based technologies, and algal organic matter is not an exception. In membrane-based technologies, algal organic matter is problematic by narrowing and blocking pores and the formation of a loose cake layer (Sillanpää, Ncibi, and Matilainen 2018). Another negative point regarding the use of a membrane is that removal of algal toxins with small molecular weight like anatoxin-a (MW 165) is not efficient (Hall et al. 2000; Hitzfeld, Hoger, and Dietrich 2000). Also, as mentioned before, membrane technologies just transfer algal toxins from the drinking water to concentrate with no degradation (Sichel et al. 2011).

2.2.6. Advanced Oxidation Processes

Oxidation technology has functional removal capacities for a broad spectrum of emerging contaminants (Sichel et al. 2011). Advanced oxidation processes (AOPs) have received growing attention among different water treatment technologies in the last decade (Duan et al. 2018; Rizzo et al. 2018; Yin, Ling, and Shang 2018). Integrated disinfection methods such as UV/chlorine (Duan et al. 2018), UV-LEDs/chlorine (Yin et al. 2018), and UV/ H_2O_2 (Keen et al. 2016; Keen and Linden 2013) showed positive effects on persistent and emerging contaminants. Besides, alternative oxidation processes using UV/peracetic acid (Rizzo et al. 2018) and electrochemical generation of H_2O_2 (Chen et al. 2018) have been recently considered as potentially effective treatment methods. AOPs have been evaluated for microcystins and other algal toxins removal (Afzal et al. 2010; He et al. 2016; Senogles et al. 2001; Song et al. 2006).

Research has been conducted on the treatment of most common MCs in water (MCs-LR, -RR, -YR, and -LA) using four different methods: direct photolysis of MCs using UV, UV/H_2O_2, UV/$S_2O_8^{2-}$, and UV/HSO_5^-. Direct UV irradiation showed limited photolysis of MCs. At the same initial oxidant concentration, UV/$S_2O_8^{2-}$ and UV/H_2O_2 showed the highest and the least efficiency, respectively (He et al. 2015). At the same condition, MC-LR removal using UV/H_2O_2 was faster than other MCs, which suggests the quicker reaction of MC-LR with hydroxyl radical (He et al. 2015).

Moreover, electrochemical processes are gaining increasing attention recently as next-generation technologies. Electrochemical methods generate hydroxyl radicals and other reactive species capable of removing a variety of water contaminants and organic substances (Radjenovic and Sedlak 2015). The problem connected with electrolysis is

that the electrodes are consumed during the process (Tran et al. 2012), and the anode is very expensive. Also, to have a higher removal efficiency of contaminants, catalytic oxidation is used that accelerates the corrosion of electrodes (Drogui et al. 2001; Martínez-Huitle and Brillas 2008). Considering the promising potential of AOPs to mitigate the concentration of algal toxins in drinking water, further research is required to develop AOP technologies to be appropriate for full-scale treatment. Moreover, assessment of these processes in terms of disinfection byproducts formation is essential, as some studies indicate that AOP may increase disinfection byproduct formation (Dotson et al. 2010; Remucal and Manley 2016).

Based on the studies summarized in this section, oxidation of various compounds by AOP can lead to their detoxification and increased biodegradation. Current research presented in this dissertation is focused on understanding and application of UV/Cl_2 and UV/H_2O_2 as two common and practical AOPs among water treatment methods to remove algal toxins, including MCs-LR, -RR, and YR while minimizing the formation of DBPs and toxic transformation products of microcystins. This research contributes to protecting the environment and public health by assessment of AOPs to remove algal toxins, understanding the mechanism of their removal, and the contribution of operational factors to enhance AOPs.

2.3.Toxicity Assays for the Detection of Microcystins

Cyanotoxins include two groups of cytotoxins and biotoxins. Biotoxins are toxic substances with biological origin that can cause a broad adverse effect that includes attacking red blood cells and nervous system and tissue destruction. Cytotoxins are toxic substances that target individual cells. Microcystins are biotoxins with cytotoxic

activities. Biotoxins have very harmful health effects and are comprehensively studied (Carmichael and An 1999).

Biological, physicochemical, and biochemical methods have been utilized to detect biotoxins. Biological methods use small animals such as mice, fish, invertebrates and microbes. Physicochemical methods are chromatographic methods such as high-performance liquid chromatography, electrospray ionization mass spectrometry and nuclear magnetic resonance that are sensitive within the range of ppb to ppt. Biochemical processes are as sensitive as physiochemical methods but faster (Carmichael and An 1999). Biochemical methods are discussed in the following paragraphs in detail.

Biochemical methods include immunoassays such as enzyme-linked immunosorbent assay (ELISA) and enzyme assays such as inhibition of protein phosphatase 2A (PP2A) (Carmichael and An 1999; He et al. 2016). Biochemical methods are attracting increased attention compared with the physicochemical method because biochemical methods are simple to run, cost-effective, and sensitive (Carmichael and An 1999). In one study, the toxicity of certain microcystins was assessed using both ELISA and PP2A assays. PP2A was more sensitive than ELISA (Ikehara et al. 2008).

ELISA is a quantitative and sensitive MCs detection method in water samples (He et al. 2016; Zeck et al. 2001). This method is based on the recognition of MCs (Adda)-DM (direct monoclonal) and their congeners by a monoclonal antibody (Zeck et al. 2001). In a sample containing microcystins, a microcystin-horseradish peroxidase competes for the binding sites of anti-microcystins antibodies in solution. Then, anti-microcystins antibodies are bound by a second antibody immobilized. After washing the samples and

the addition of the substrate solution, a blue color signal is generated. The intensity of the color decreases proportionally with the increase of microcystins (Zeck et al. 2001).

PP2A is an essential serine/threonine phosphatase that plays a vital role in the regulation of a wide range of cellular processes (Song et al. 2006). Microcystins are potent inhibitors of PP2A, thus leading to downstream proteins hyperphosphorylation, which may be related to their toxicity and tumor promotion activity (Liu and Sun 2015). Microcystin forms covalent bonds to the catalytic subunit of protein phosphatase 2A (PP2A) that is irreversible and noncompetitive. A higher concentration of MCs inhibits more PP2A (Carmichael and An 1999). Protein phosphatase will dephosphorylate the substrate. Protein phosphatase activity on the fluorescent substrate can be determined by measuring the fluorescence intensity. The higher the fluorescence intensity, the lower the MCs concentration.

Genotoxicity of formed products can be determined using the Ames II assay to assess if new modes of toxicity were introduced through UV/H_2O_2 and UV/Cl_2 processes (Kitis 2004). Ames II test is a modified microplate format of Ames test and consists of a mix of Salmonella strains that capture different types of mutations (base pair mutation and frameshift). Ames test genotoxicity assay uses various mutant strains of Salmonella carrying mutations. Reverse mutation happens by exposure of these bacteria to mutagenic agents under specific conditions (Maron and Ames 1983). Microorganisms having these strains are unable to produce histidine (histidine auxotroph Salmonella). The organism's ability to produce histidine after reverse mutation is measured by the resulting pH change using a color indicator (Martijn 2015).

2.4. Disinfection By-products and Advanced Oxidation Process

The exposure of aqueous chlorine (HOCl/OCl-, pK_a = 7.5) to UV irradiation in the UV/Cl_2 process starts a chain of reaction. These reactions are shown in Eq. 1 to Eq. 4 and the parenthesis indicate pH-dependent speciation. Hydroxyl radicals and chlorine radicals are the main intermediates, and chloride, chlorate, and oxygen are the final products of these reactions (Zhao et al. 2011). Hydroxyl radicals and chlorine radicals enabled UV/Cl_2 to serve as effective disinfection and advanced oxidation process that controls pathogens and micropollutants (P. Sun et al. 2016; Zhao et al. 2011). Depending on the water matrix, formation of chlorination by-products would be possible. By-products formed in early stages may be decomposed by hydroxyl radicals in further reactions (Cerreta et al. 2019).

$$HOCl(OCl^-) + h\vartheta \rightarrow HO^{\cdot}(O^{\cdot -}) + Cl^{\cdot} \quad \text{(Eq. 1)}$$

$$HO^{\cdot} + HOCl(OCl^-) \rightarrow OCl^{\cdot} + H_2O(OH^-) \quad \text{(Eq. 2)}$$

$$Cl^{\cdot} + HOCl(OCl^-) \rightarrow OCl^{\cdot} + HCl(Cl^-) \quad \text{(Eq. 3)}$$

$$2OCl^{\cdot} \rightarrow Cl_2O_2 \rightarrow products \quad \text{(Eq. 4)}$$

The presence of bromide in water resources treated by UV/Cl_2 leads to bromine formation and incorporate in bromine-containing THMs formation (Zhang et al. 2011). NOM in natural water is a precursor of DBPs. NOM may react with free halogen species and their radicals under UV irradiation and form DBPs that are similar to DBPs formed under chlorination in the dark (Zhang et al. 2011). In the presence of algal organic matter, less germicidal organic chloramines were produced during the chlorination, and more nitrogenous DBPs were formed during chloramination (Fang, Yang, et al. 2010). Based on previous studies, chlorination and chloramination of algal matter can produce a lower concentration of carbonaceous DBPs such as HAA (Fang, Yang, et al. 2010). In general,

the high nitrogen content of algal organic matter decreases the effectiveness of the disinfection process and increases the formation of nitrogenous DBPs (Zhang et al. 2011).

There are fewer studies on UV/H_2O_2 and DBPs formation compared to UV/Cl_2. A water matrix containing NOM mainly produces biodegradable compounds rather than harmful DBPs (Martijn 2015). In a study on degradation of iopamidol by UV/persulfate, UV/chlorine, and UV/H_2O_2, two DBPs, iodoform, and monoiodacetic acid, were detected (Zhao et al. 2019). UV/chlorine had the least DBPs formation (Zhao et al. 2019). UV/H_2O_2 advanced oxidation has the potential to degrade many trace organic compounds in drinking water (Dotson et al. 2010). However, following hydrogen peroxide quenching with chlorine and post-chlorination can increase the regulated DBPs formation (Dotson et al. 2010).

UV/H_2O_2 can mineralize DOM and decrease total chromophoric DOM and apparent molecular weight (Dotson et al. 2010). The relationship of chlorine decay and THMs formation to NOM size has been studied on Mississippi River water (Gang, Clevenger, and Banerji 2003). The results showed that total THM formation in fractionated NOM was a function of chlorine consumption. The less molecular weight of the fractions resulted in the higher total THM yield coefficients from 31 to 42 µg-total THM/mg-Cl_2 (Gang et al. 2003). In another research, the AOM of *microcystin aeruginosa* was characterized, and the relationship of intracellular organic matter (IOM) and extracellular organic matter (EOM) molecular weight distribution and formation of DBPs were assessed (Li et al. 2012). The results of this study showed that the formation potentials of chloroform, chloroacetic acid, and nitrosodimethylamine were 21.46, 68.29, and 0.0096 µg/mg C for IOM, and 32.44, 54.58 and 0.0189 µg/mg C for EOM (Li et al. 2012).

Based on the studies summarized in this section, the assessment of treatment methods based on DBPs formation was essential and the conditions can be optimized to avoid forming additional DBPs. Four THMs, nine HAAs, and N-Nitrosodimethylamine (NDMA) were studied in this project.

2.5. Problem Statement

Algal blooms in water resources are a critical and everyday global issue and are rapidly progressing. HABs have socioeconomic and ecological costs that affect drinking water, water quality, food web resilience, and habitats (Carmichael and Boyer 2016). The adverse health impact of cyanotoxins in water supply has been first published in 1878 (Francis 1878). HAB risk is directly influenced by nutrients (Carmichael and Boyer 2016; Gobler et al. 2016). Discharge of nutrients in the watersheds resulted in the detection of algal toxins such as microcystins in water resources (Carmichael and Boyer 2016; Gobler et al. 2016). HABs are increasing globally due to higher density population and climate change, and the regions where the environment has changed more because of agriculture and development HABs are more prevalent (Carmichael and Boyer 2016).

In September 2013, Carroll Township, Ohio, was the first public water utility in the United States to release a ‘do not drink’ advisory because microcystin equivalent exceeded 1 mg/L in finished water. Approximately 2200 residents of Carroll Township were impacted by this HAB event (Bajracharya et al. 2019). Later in August 2014, the City of Toledo, Ohio, issued a “Do Not Drink” advisory due to microcystin breakthroughs in their finished water. This HAB event lasted for three days and impacted over 400,000 residents and businesses (Bajracharya et al. 2019; Carmichael and Boyer 2016).

The treatment of microcystins is challenging since they are highly persistent, widely distributed, and require new treatment options. The peptide ring of microcystins appears to be somewhat resistant to treatment (Chae et al. 2019). In recent years, AOPs showed promising results in the removal of refractory contaminants in water treatment (Nihemaiti, Permala, and Croué 2020). Among many of the AOPs being tested in various studies, UV/Cl_2 and UV/H_2O_2 processes have attracted attention. UV/H_2O_2 is one of the most commonly used AOP at full scale that is widely commercially available and has the potential to decrease the concentration of many trace organic pollutants (Dotson et al. 2010). UV/Cl_2 process is more effective than UV or chlorination alone in the removal of micropollutants (Sharma et al. 2019) and is feasible for application on full-scale at DWTPs (Dotson et al. 2010). UV/Cl_2 process is also considered to be easier to operate than UV/H_2O_2 because plant operators are more familiar and comfortable with Cl_2 than with many other chemicals used in AOPs, and Cl_2 is easily measured, unlike H_2O_2.

Recent studies are showing the susceptibility MC-LR to UV/Cl_2 process (Duan et al. 2018; Sun et al. 2018; Zhang et al. 2016). Also, there are limited studies on the removal of MC-LR in synthetic and natural water samples using UV/H_2O_2 (He et al. 2012; Moon et al. 2017). There has been no comprehensive and comparative study that would assess DBPs and transformation products for both UV/Cl_2 and UV/H_2O_2 processes tested alongside.

This project is developing technical solutions to the problem by using UV/Cl_2, and UV/H_2O_2 advanced oxidation as effective water treatment technologies. This project is dedicated to expanding knowledge on novel AOP options to get comprehensive results to inform utilities on the methods to use UV/H_2O_2 and UV/Cl_2 efficiently. Invention and

evaluation of the alternative treatment technologies are necessary to address water infrastructure needs. This project seeks those alternatives by exploring the potential of novel AOPs to remove MCs-LR, -RR, and -YR. The optimized version of both UV/H_2O_2 and UV/Cl_2 systems can significantly contribute to water purification by offering a solution for utilities dealing with water resources contaminated by microcystins while achieving disinfection at the same time.

This project provides comparative information that is essential for the utilities making decisions on the best technology for their source water. Also, this work would provide a fundamental understanding of how these two processes interact with algal toxins and the background matrix, especially with respect to formation of harmful substances, such as transformation products and DBPs. This work significantly contributes to both practical and fundamental base of knowledge about UV/H_2O_2 and UV/Cl_2 processes.

2.6. Research Goals

Understanding and evaluating novel treatment methods can be a key to be able to provide clean and satisfactory water to the customers. In this regard, the goal of this research is to 1) assess UV/H_2O_2 and UV/Cl_2 AOPs in terms of algal toxins removal (microcystin variants LR, RR, and YR were studied); 2) investigate the possible introduction of new modes of toxicity to the system (genotoxicity) or formation of products that retain the toxicity of the parent toxin; 3) determination of the effect of UV/H_2O_2 and UV/Cl_2 AOPs on the formation of disinfection byproducts, including unregulated nitrosamine NDMA; and 4) study the effect of water matrix, specifically nitrate and algal DOM, which co-occur with algal toxins, on the toxin removal efficiency

of the processes, the formation of toxic transformation products, and the formation of DBPs.

2.7. Research Tasks

The following tasks were completed to achieve the goals of this project,

1) LC-MS/MS Method Development to measure MCs
2) Investigating the efficiency of UV/H_2O_2 and UV/Cl_2 for MCs-LR, -RR and -YR removal with and without additional nitrate and/ or algal DOM
3) Determination of toxicity of transformation products during UV/H_2O_2 and UV/Cl_2 processes and the effect of water matrix
4) Identification of the structural changes to the toxins using LC/MS-MS
5) Evaluate the effect of UV/H_2O_2 and UV/Cl_2 and water matrix on DBPs formation

These tasks are based on the hypotheses that UV/H_2O_2 and UV/Cl_2 AOPs can be optimized to detoxify algal toxins and minimize the formation of additional disinfection byproducts.

CHAPTER 3. MATERIALS AND METHODS

3.1. Sample Collection and Water Matrices

The samples were collected from Mount Holly DWTP, where no powdered activated carbon (PAC) and preoxidization were utilized (both of which could have altered the nature of the DOM and affected the DBP formation experiments). The water samples were collected in December when no background algal blooms were present. The water in Mount Holly DWTP goes through coagulation, sedimentation, filtration, and disinfection (chlorine) processes. The water sample was collected before the disinfection unit so that it represents the location where the actual AOP would take place. Water samples were filtered through 0.45 µm Mixed cellulose ester filter that has very low extractable, which was experimentally confirmed (Appendix A1), and is naturally hydrophilic. The filters were prewashed using 1000 mL ultrapure water based on the results of preliminary tests for leaching by running some ultrapure water through it and measuring TOC/TN content before and after filtration (Karanfil, Erdogan, and Schlautman 2003). A mixed cellulose ester filter was selected based on TOC and TN leaching results (Appendix A1). The filters were prewashed and were not affecting the nitrogen content of water samples. Also, 0.45 µm filters remove most of the bacteria and prevent changes to the organic matter during storage. Polytetrafluoroethylene (PTFE) filters can be used to avoid the increase of organic matter. However, the hydrophobic characteristic of PTFE filters makes them inappropriate to filter a large volume of water. The filtered water sample was stored at 4◦C for future use. The characteristics of the water sample can be found in Table 2.

Table 2. Characteristics of Water Sample

Characteristics	NO_3-N	NO_2-N	TN	TKN	NH_3-N	TON	TOC	Br
Water (mg/L)	0.473	0.013	0.6	0.114	ND	0.114	0.6334	0.105

Water matrix was augmented with additional components in some of the experiments (specifically, intracellular algal DOM and nitrate) to consider the effect of background matrix on treatment efficiency and byproducts forming. Non-toxin-producing *Microcystis* algae was cultured in the lab, and intracellular algal dissolved organic matter (DOM) were extracted based on the method in section 3.2. Furthermore, the toxins were spiked to the matrices, as described in section 3.3. Water matrices for toxicity analysis and DBPs analysis are listed in Table 3.

Table 3. Water Matrices

Toxicity Analysis	**DBPs Analysis**
Toxin	Background
Toxin + NO_3- (20 mg/L as N)	NO_3-
Toxin + Algal DOM (3 mg/L as C)	Algal DOM
Toxin+ NO_3-+ Algal DOM	NO_3-+ Algal DOM

Water samples were spiked with 100 μg/L of MC-LR, 60 μg/L of MC-RR, and 100 μg/L of MC-YR, separately. For MC- LR, 100 μg/L was spiked to represent a worst-case situation that is when surface water is treated by coagulation and sand filtration and the amount of spiked MCs-RR and -YR was based on their possibility of occurrence in water compared to MC-LR and their LC-MS/MS detection limit. Spike levels were within the range of highest average concentrations detected in the summer in surface water resources (Xiaowei Liu et al. 2010).

3.2. Algae Culture, Extraction, and Characterization

Blue-green algae culture of *Microcystis sp.* was obtained from Carolina Biological Supply Company. *Microcystis sp.* was cultivated until the stationary growth phase in 125 mL flasks containing 100 mL BG11 media (Gibco, Thermo Fisher Scientific, US) that is optimized for the growth and maintenance of Cyanobacteria under a fluorescent lamp with light/dark cycle of 12 h/12 h. The culture was incubated at 22◦C (Devi and Sahoo 2015; Fang, Ma, et al. 2010). BG11 media formulation is included in Appendix A2. New cultures were set up by transferring 5 mL of a stock culture into 100-mL of the fresh medium under fluorescent lights for ten days to allow the alga to grow.

Extracellular organic matter was extracted by centrifuging algal mass at 10,000 rpm for 10 min, followed by filtering the collected supernatant through a prewashed 0.45 μm cellulose acetate membrane (Karanfil et al. 2003). The organic matters in the filtrate represented EOM (Daly et al. 2007; Lee et al. 2018; Li et al. 2012)

Intracellular organic matter was extracted following these steps: First, the cells separated during the centrifugation were washed and re-suspended with 100 mL of ultrapure water three times. Next, the cells were subjected to three freeze/thaw cycles at -80◦C and 37◦C accordingly. Finally, the solution was filtered through prewashed 0.45 μm cellulose acetate membranes. The organic matter in the filtrate was intracellular organic matter (Daly et al. 2007; Lee et al. 2018; Li et al. 2012). EOM and IOM were stored in the dark at -20◦C for long term storage and 4◦C for short term storage. Figure 1 presents the steps for extracellular and intracellular organic matter extraction, and Figure 2 displays the algae culture, cell pellet, and the IOM.

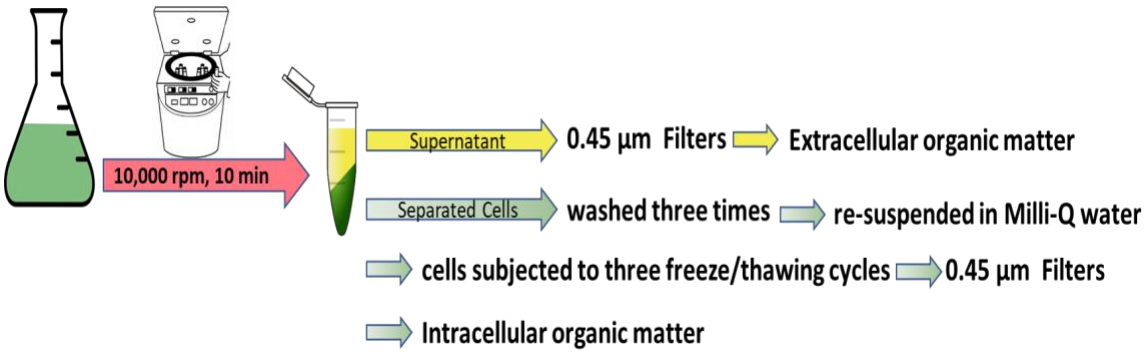

Figure 1. Extracellular and Intracellular Algae Organic Matter Extraction

Figure 2. (from left) Algae Culture, Cell Pellet, and IOM

Algal organic matter in natural waters experiencing an algal bloom is between 2 to 9.5 mg/L TOC based on previous studies (Adams et al. 2018; Deng et al. 2017; Lee et al. 2018). The EOM is not the primary source of organic matter based on literature to have a harmful adverse effect, so we continued the experiments with IOM.

The intracellular organic matter was characterized within seven days (Lee et al. 2018) to determine the carbon and nitrogen content by measuring the following parameters: nitrate (NO_3-N), nitrite (NO_2-N), total nitrogen (TN), total Kjeldahl nitrogen (TKN), ammonia (NH_3-N), total organic nitrogen (TON), total organic carbon (TOC). Nitrate,

nitrite, TN and ammonia were measured using Hach kits and TKN was calculated. TOC was measured using a Shimadzu TOC-LCPN instrument based on method 5310B of the Standard Methods for the Examination of Water and Wastewater published by American Public Health Association in 2017 (23rd Edition). These characteristics were selected based on previous studies on algal organic matter and its effect on DBPs formation and taste and odor of water (Goslan et al. 2017; Henderson et al. 2008; Li et al. 2012). Table 4 includes the characteristics of IOM.

Table 4. Characteristics of IOM

Characteristics	**NO_3-N**	**NO_2-N**	**TN**	**TKN**	**NH_3-N**	**TON**	**TOC**
Concentration (mg/L)	0.328	0.024	14	13.648	0.13	13.518	33.63

3.3.LC-MS/MS Analysis Microcystins Toxins and Their Byproducts

Water samples were spiked with 100 µg/L of MCs-LR, 60 µg/L of MCs-RR, and 100 µg/L of MCs-YR. The concentrations of toxins are at least 20 times more than the detection limit of the LC-MS/MS method to make sure that the residual toxins after treatment would be higher than the detection limit. MCs standards at 10 µg/mL were obtained from Eurofins Abraxis (Abraxis, PA, USA). Figure 3 shows the chemical structure of target microcystins (Renner, Botch-jones, and Mallet 2019).

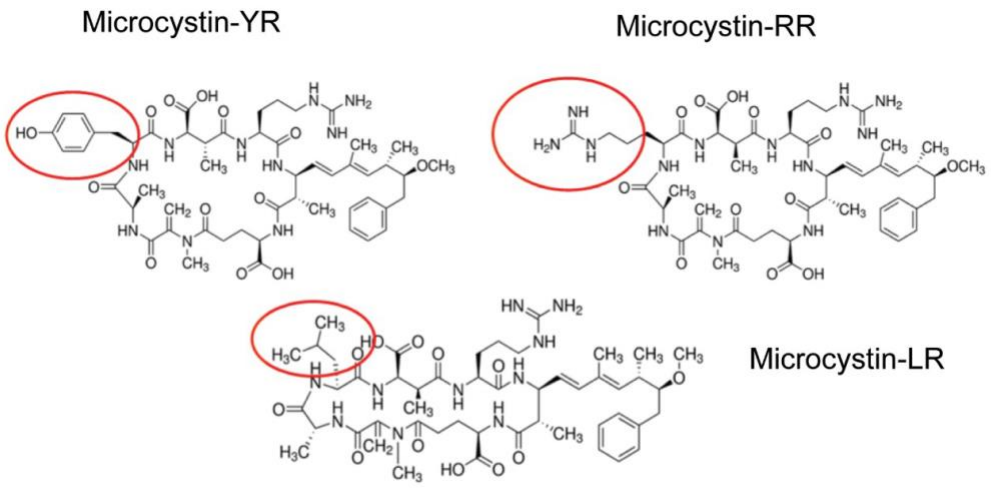

Figure 3. Chemical Structure of Target Microcystins; Variable Amino Acids including Tyrosine in MC-YR, Arginine in MC-RR, and Leucine in MC-LR are Circled

Samples were analyzed to determine the concentration of the parent compound remaining at each level of treatment and toxic product formation. Liquid chromatography with tandem mass spectrometry detector (LC/MS-MS) was used, which consisted of a Thermo Scientific Accela LC System and Velos pro-dual-pressure linear ion trap mass spectrometer and a C18 column (ZORBAX rapid resolution, Stable Bond, 80Å C18, 3.0 x 100 mm, 3.5 µm, p/n 861954-302). The column temperature was 50°C. Microcystins were evaluated using EPA method 544. Gradient mobile phase of 0.1% formic acid + 5 mM ammonium formate in water (Solvent A) and 80:20 Acetonitrile/Isopropanol (solvent B) was performed. The linear gradient elution condition is shown in Table 5. Before the linear gradient, the first minute of the run at 20% Solvent B was routed to waste to avoid instrument damage from samples and added buffers and quenching agents. After the linear gradient, the column was flushed with 100% Solvent B for 1 minute, then allowed to equilibrate to 20% Solvent B over 5 minutes (Table 5). The solvent flow rate of 0.6 mL/min was used, and the sample injection volume was 10 µL. All solvents were HPLC grade or higher.

Table 5. Linear Gradient Elution Conditions

Time (min)	%B
0	20
4.0	30
6.0	100
9.0	100
10.0	20
15.0	20

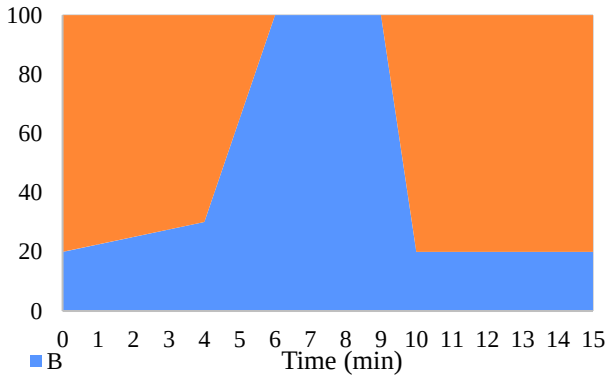

Table 6 presents the molecular formula and molecular weight of MCs. MCs were analyzed using positive electrospray ionization (ESI) MS in full–scan mode to allow the analysis of the degradation byproducts. Table 7 shows the precursor ions and the targeted full-scan MS/MS. The collision energy of 35 eV was provided by nitrogen gas with a flow rate of 0.2 mL/min. The blank and standard solutions containing methanol and MCs stock solution were examined using MS analysis with a full scan. The standard curves of LC-MS/MS for MCs are displayed in Figure 4.

Table 6. Chemical Properties of MCs

Toxins	CAS no.	Molecular Formula	First Variable Residue (X)	Second Variable Residue (Z)
MC–LR	101043-37-2	$C_{49}H_{74}N_{10}O_{12}$	Leucine	Arginine
MC–RR	111755-37-4	$C_{49}H_{75}N_{13}O_{12}$	Arginine	Arginine
MC–YR	101064-48-6	$C_{52}H_{72}N_{10}O_{13}$	Tyrosine	Arginine

Table 7. MCs Mass Spectrometry Information

Toxins	Precursor Ion	MW (g/mol)	Precursor Ion (m/z)	Targeted Full-Scan (MS/MS)
MC–LR	$[M+H]^+$	994.549	995.6	[m/z 285-1100]
MC–RR	$[M+2H]^{2+}$	1037.566	520.1	[m/z 150-1100]
MC–YR	$[M+H]^+$	1044.528	1045.5	[m/z 285-1100]

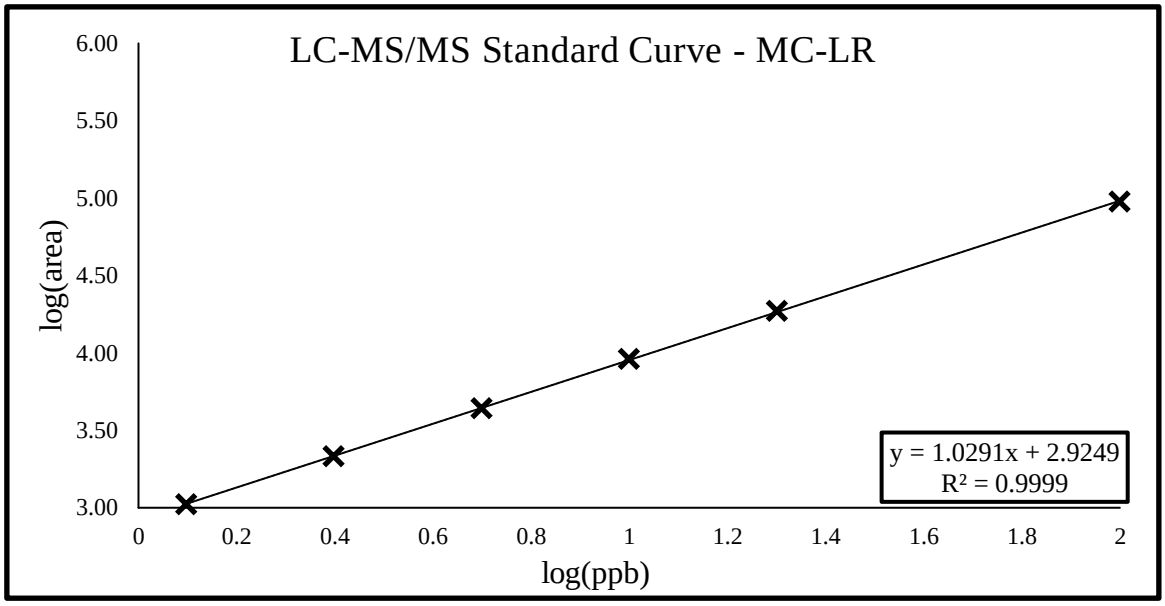

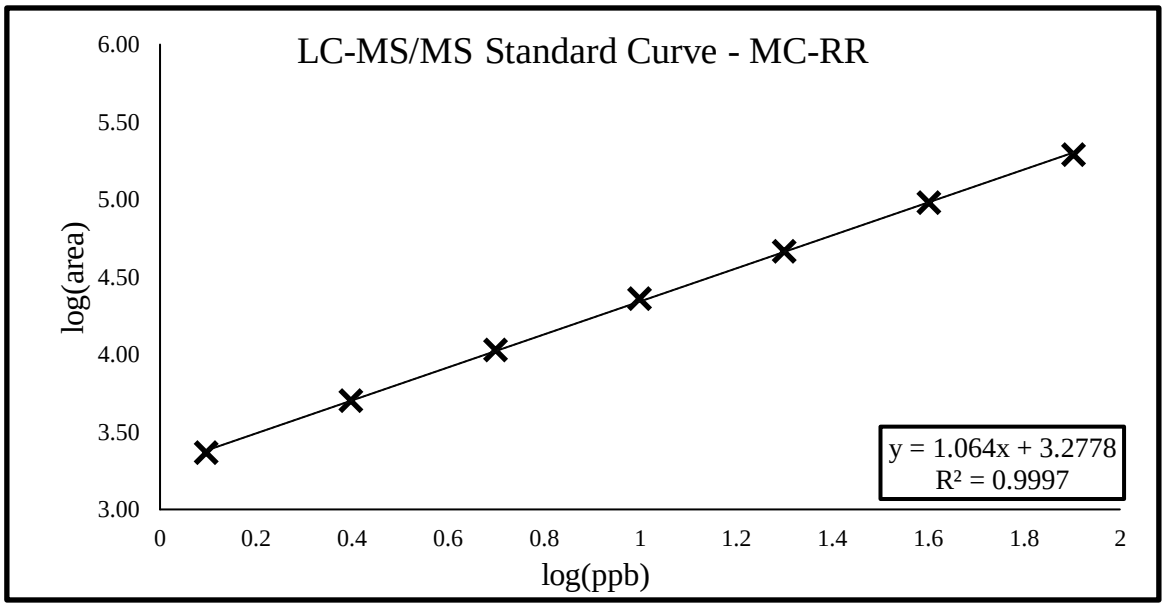

Figure 4. Standard Curves of LC-MS/MS for MCs

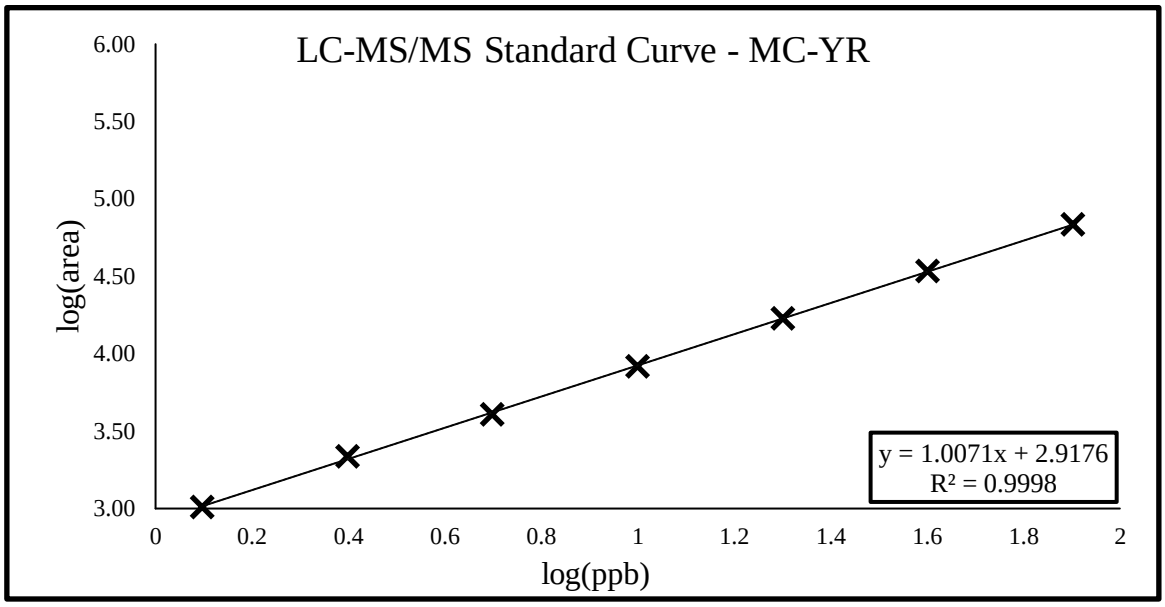

Figure 4. (Cont'd) Standard Curves of LC-MS/MS for MCs

3.4. UV/H_2O_2 and UV/Cl_2 Oxidation Treatment of Algal Toxins

H_2O_2 30% w/w, chlorine 10 to 15% solution of sodium hypochlorite, and ascorbic acid were purchased from Sigma-Aldrich (St. Louis, MO). Ascorbic acid was used to quench Cl_2 and is suitable for the analysis of DBPs (Kristiana et al. 2014). Chlorine was quenched immediately by collecting a sample into a vial containing ascorbic acid at a 150% of stoichiometric concentration to assure that there was no residual chlorine. H_2O_2 was quenched with bovine serum albumin (BSA) (Sigma Aldrich, >96%) which is a suitable quenching agent for toxicity and LC-MS/MS analysis (Keen, Dotson, and Linden 2013). The effective concentration of bovine catalase was found based on previous studies (Keen et al. 2013; Liu et al. 2003) and preliminary tests. Bovine catalase of 0.2 mg/L was effectively quenching the H_2O_2 at both ranges of AOPs utilized in this study in less than 10 min with no effect on DBP formation in the uniform formation condition (UFC) test. To evaluate the contribution of H_2O_2 to the effectiveness of the UV/H_2O_2, the concentration of H_2O_2 was measured in the mixture using triiodide method (Klassen,

Marchington, and McGowan 1994). For this method, ammonium molybdate, potassium iodide, and potassium hydrogen phthalate were obtained from Sigma-Aldrich (St. Louis, MO). In UV/Cl_2 process, chlorine was measured using *N*, *N*-diethyl-p-phenylenediamine (DPD) Hach powder pillows.

AOP experiments were conducted on a bench scale using a quasi-collimated beam apparatus equipped with a 1 kW medium pressure mercury lamp (Ace Glass). AOP experiments were performed at the ambient pH of the water matrix (6.8). The UV doses for the MCs AOPs were within the range of full-scale UV doses used in AOPs at drinking water treatment plants (up to 500-2000 mJ/cm^2) using a medium pressure (MP) mercury vapor lamp. In addition, MC-LR AOPs was repeated using low pressure (LP) mercury vapor lamps to test chlorine efficiency at the range of disinfection dose (up to 30 mJ/cm^2).

The UV setup had two openings for beam collimation; however, the beam is never truly collimated, since some dispersion remains in the beam. Petri Factor was incorporated in the calculations, accounting for the UV irradiance distribution over the sample surface due to the beam dispersion. UV dose determination and bench-scale setup were based on Bolton and Linden's (2003) study (Figure 5).

Figure 6 shows the schematic of experimental matrices. Sixteen different batches were prepared for each of the three toxins which included different matrices and chlorine or hydrogen peroxide concentrations. Each batch was treated under five UV doses and all experiments were performed in triplicate to determine the statistical significance of the results. Therefore, 720 (16 batches × 5 UV doses × 3 MCs × 3 replicates) samples were collected. Each sample was analyzed for toxin removal using LC-MS/MS and for hepatotoxicity using assays. In addition, 16 batches including different water matrices

and chlorine, or hydrogen peroxide concentration were treated under three UV doses for DBPs analysis. These experiments have been performed in triplicate and three samples were collected for each run for THMs, HAAs, and NDMA analysis. Hence, total of 432 (16 batches × 3 UV doses × 3 DBPs × 3 replicates) samples were extracted for DBPs analysis.

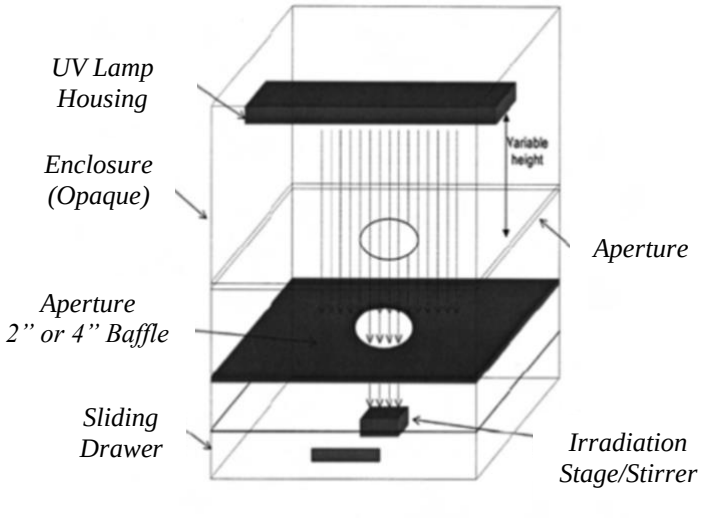

Figure 5. Bench-Scale Setup for Conducting UV Experiments (Bolton and Linden 2003)

1	2	3
Water Matrix	**UV-AOPs**	**Analysis**
Toxin	5 mg/L H_2O_2	Toxicity Analysis:
Toxin + NO_3^-	10 mg/L H_2O_2	MCs Removal
Toxin + Algal DOM	2 mg/L Cl_2	Genotoxicity
Toxin + NO_3^- + Algal DOM	4 mg/L Cl_2 (5 Doses of UV)	Hepatotoxicity
Background	5 mg/L H_2O_2	DBP Analysis:
NO_3^-	10 mg/L H_2O_2	Haloacetic Acids (HAAs)
Algal DOM	2 mg/L Cl_2	Trihalomethanes (THMs)
NO_3^- + Algal DOM	4 mg/L Cl_2 (3 Doses of UV)	N-Nitrosodimethylamine (NDMA)

Figure 6. Schematic of the Experimental Matrix

3.5. Toxicity Analysis

Toxicity assays include toxicity specific to the toxin (hepatotoxicity) and genotoxicity to measure if new modes of toxicity have been formed through the treatment process. Hepatotoxicity assay includes total toxicity, so it will show if more toxin has been produced in the system other than what was spiked initially and if toxins are transformed into each other (Schmidt, Wilhelm, and Boyer 2014).

3.5.1. Protein Phosphatase Inhibition Analysis (Hepatotoxicity)

Figure 7 is showing the workflow of PP2A assay. The buffer solution containing the assay components except the fluorescent substrate was prepared (Table 8), considering 96 wells (reactions) and excess reactions. The mixture and fluorescent substrate were pre-warmed at 37◦C. The clear, flat-bottom, and sterile 96-wells plate (200 µL wells) (Qiagen) was prepared by adding 70 µL of buffer solution, 120 µL of the fluorescent substrate, and ten µL of different samples including treated sample, untreated sample and background water matrix. The kinetics and endpoints were read after one h using Tecan Genios microplate reader with a fluorescence detector at 360 nm excitation and 465 nm emission. Negative control was a sample with no toxin, and growth kinetics in control wells equals 100% enzyme activity reference. The activity was calculated by linear regression of the reaction curves to give slope/min (Mountfort, Holland, and Sprosen 2005).

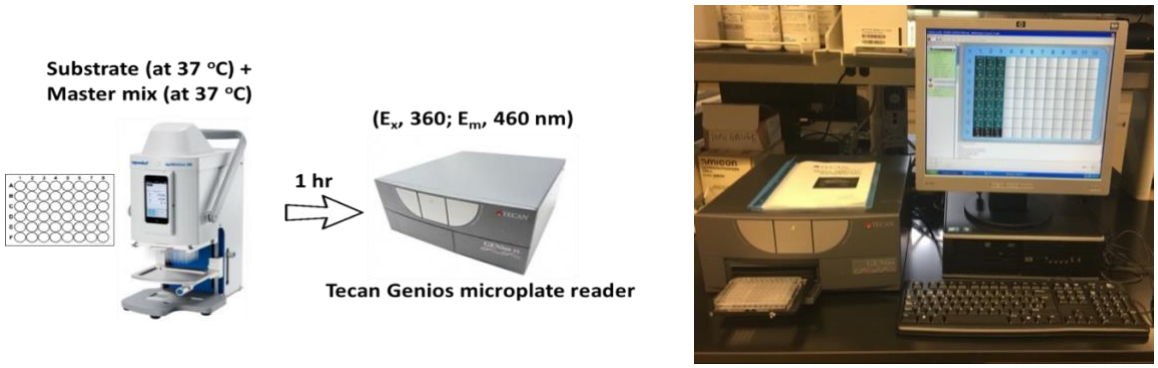

Figure 7. PP2A Test Workflow

Table 8. PP2A Assay Mixture

Components	**Amount**
50 mM Tris buffer (pH 7.0) and 0.1 mM $CaCl_2$	50 µL
Enzyme (0.02 U/assay, final concentration, 1.5 nM)	10 µL
40 mM $NiCl_2$	5 µL
5 mL of BSA (1 mg /mL of distilled water)	5 µL
Sample (treated, untreated sample or matrix blank)	10 µL
1.7 mM fluorescent substrate (4-methylumbelliferyl phosphate)	120 µL
Total	**200 µL**

To prepare 0.1 L of Tris buffer (1 M, pH 7.0), first, 80 mL of distilled water was measured in a suitable container. Second, 12.114 g of Tris base was added to the solution. Then the pH was adjusted to 7.0 using HCl. Finally, distilled water was added until the volume is 0.1 L. Figure 8 is showing the PP2A standard curves for MC-LR, -RR, and -YR.

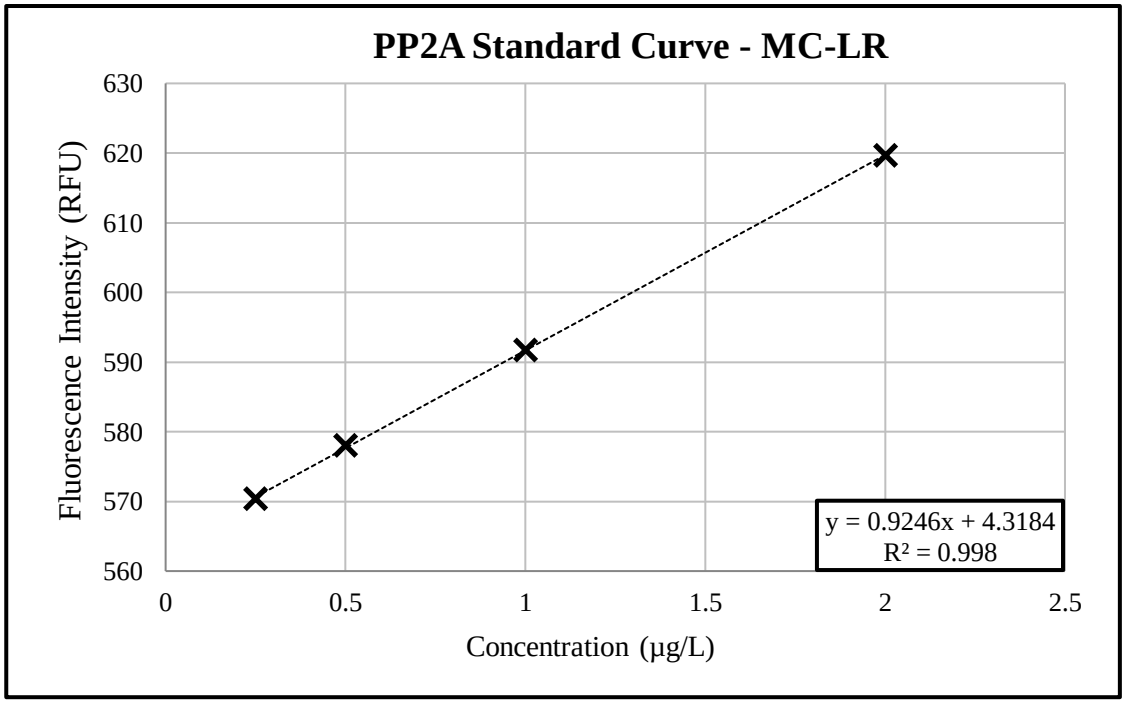

(a)

Figure 8. PP2A Standard Curve for MCs: (a) MC-LR, (b) MC-RR, and (c) MC-YR

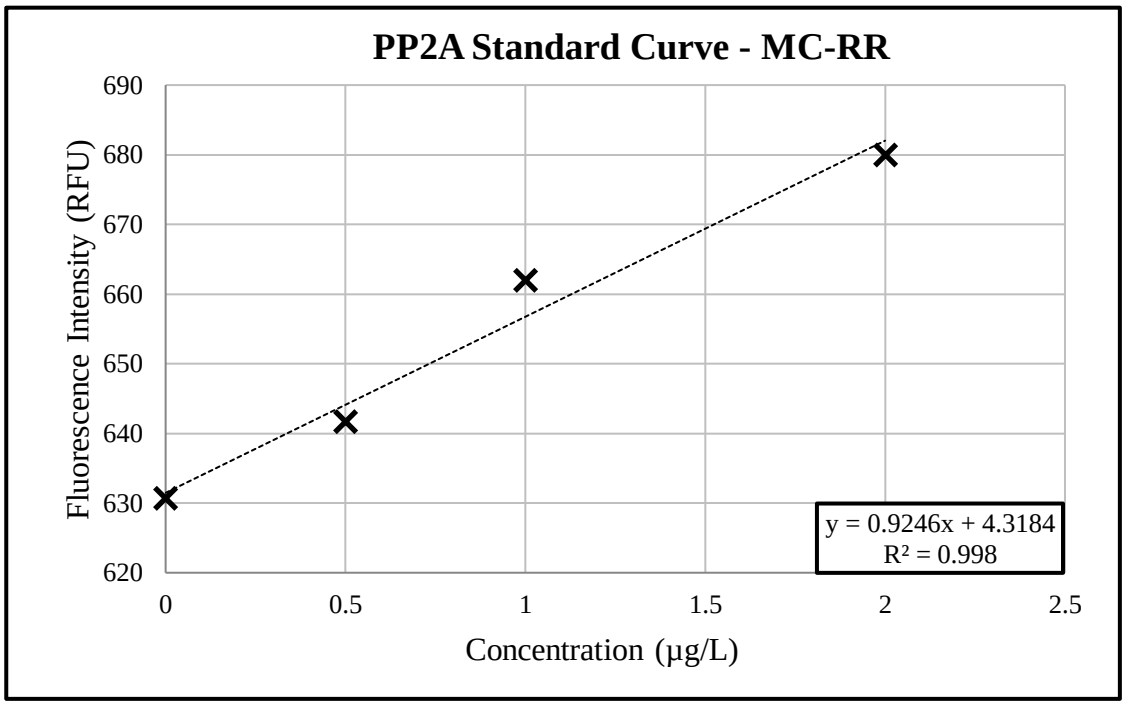

(b)

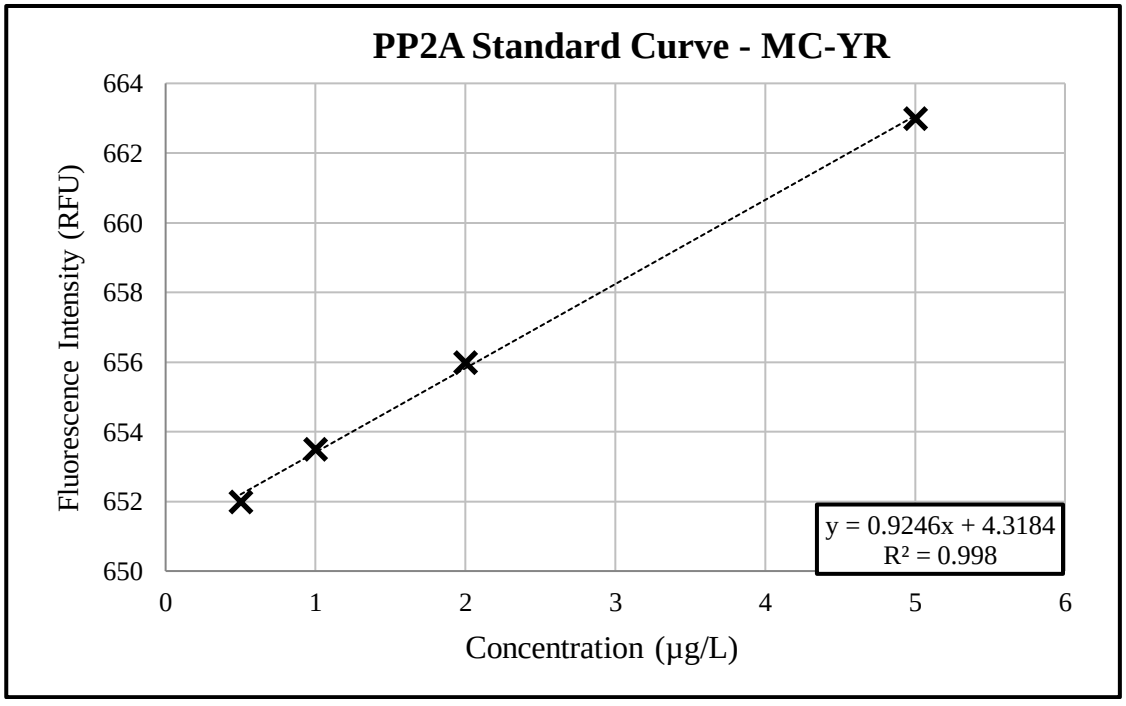

(c)

Figure **8**. (Cont'd) PP2A Standard Curve for MCs: (a) MC-LR, (b) MC-RR, and (c) MC-YR

3.5.2. Ames II (Genotoxicity)

For Ames test, each sample was tested in six concentrations in triplicate and one positive and one negative control. EPA suggested strains of TA98 and TA100 for algal toxin risk assessment using the Ames method (USEPA 2015). Genotypes of the TA98 and TA100 Salmonella typhimurium strains are shown in Table 9 (Kamber et al. 2009). Salmonella typhimurium strains were stored at -20ºC for long-term storage.

Table 9. Genotypes of the TA98 and TA100 Salmonella Typhimurium Strains

Strain	Mutation	Type	Target	Cell Wall	Repair	pKM101
TA98	hisD3052	Frameshifts	GCGCGCGC	rfa	uvrB	yes
TA100	hisG46	Base-pair subst.	GGG	rfa	uvrB	yes

Ames Modified ISO kits were purchased form EPBI (Environmental Bio-Detection Products Inc.) to run Ames II tests for the parent compounds. First, reagent V (commercial name) was added to nutrient broth bottle and immediately transferred to bacterial (*TA100*) bottle. The bottle was shaken and incubated at 37°C overnight for initial bacterial growth. The next morning bacterial vial was observed for turbidity. The bacteria were diluted to optical density of 0.07 measured at a wavelength of 600 nm (OD600 = 0.07). Then, exposure media was prepared according to Table 10 and final solution was mixed well. The volume of 200 µL of master exposure mix was added to a 24-well plate. The chemical 4-nitroquinoline-1-oxide (4NQO), that is carcinogenic and mutagenic quinoline, was used as positive control mutagen. The amount of 50 µL of 4NQO was added into wells A4 and A5 assigned as positive control wells (Figure 9). The wells were mixed using reinjecting solution through pipette repeatedly. Well A6 was left as a blank and no sample or reagent was added to this well. Next, 1600 µL of undiluted sample as added to wells B1 to B3 serving as the most concentrated sample. Six different

concentrations of sample including one undiluted and five dilutions were added in the 24 well plate in triplicate. Sterilized water was added to bring final volume of all wells to 1800 µL. Finally, 200 µL of diluted *TA100* was added to all wells except A6 that was the reagent control. Wells A1 to A3 that served as negative controls contained the bacteria. The final volume of each well was 2 mL. The exposure plate was incubated at 37° for 100 minutes without shaking.

Table 10. Master Exposure Mix (5.0 ml per experiment)

Reagent	Volume (mL)
Exposure Medium Concentrate	4.15
40% D-glucose	0.30
D-biotin	0.05
L-Histidine	0.50
Total	**5.00**

Near to the incubation time completion, the reversion solution was prepared. Master reversion mix was prepared based on Table 11. Reversion solution tubes were prepared by adding 800 µL of reversion mix and 7.8 ml of sterile water to each tube. When the 100 min incubation of exposure plate was complete, 1.6 mL of exposed bacterial solution in each well of the 24-well plate was transferred into the reversion tubes.

Table 11. Master Reversion Mix

Reagent	Volume (mL)
40% D-glucose	2.30
Bromocresol Purple	3.50
D-biotin	4.65
0X Reversion Solution	11.65
Total	**22.1**

The volume of 200 µL of bacteria-reversion mix in each tube was distributed into 48 wells of a 96-well plate using a multichannel pipette. All 96-well plates were incubated at 37°C without shaking for two days to allow revertant bacteria to grow. Mutagenicity was measured by a color change from purple to yellow caused by pH drop due to bacterial metabolism. Figure 9 shows an overview of the experiment.

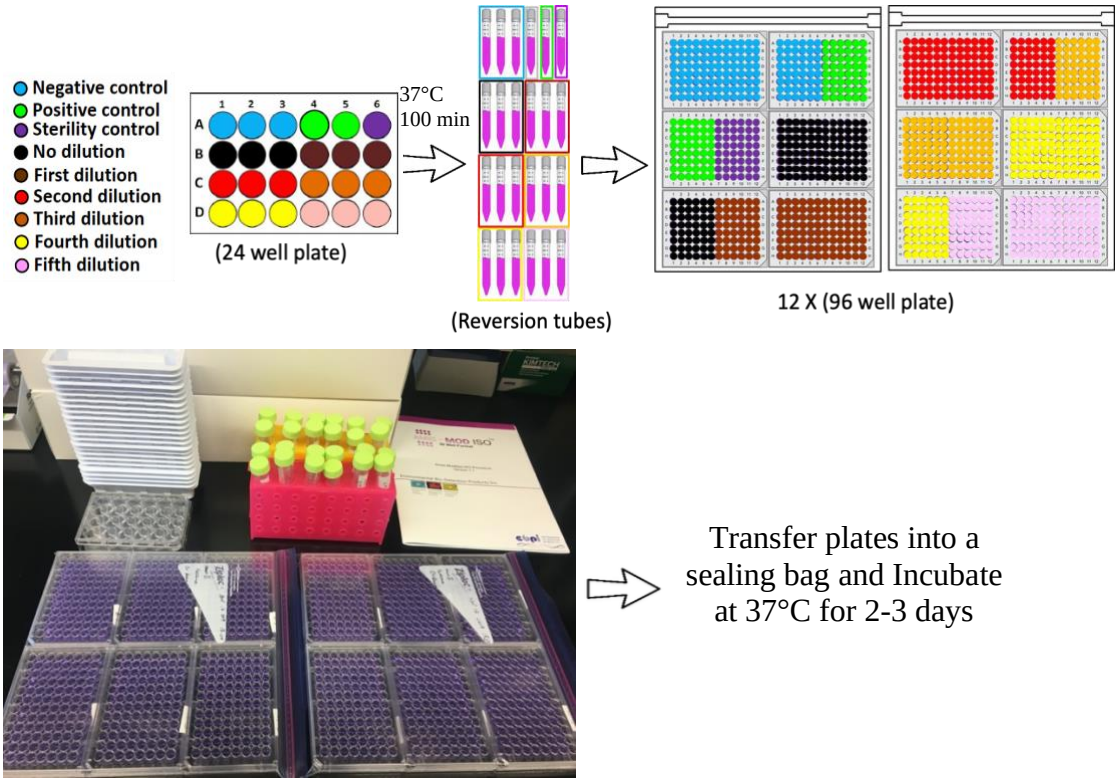

Figure 9. Overview of the Ames Experiment (EBPI)

3.6. Disinfection By-products Analysis

Samples were prepared under uniform formation condition (UFC) (Summers et al. 1996) to analyze disinfection byproducts. Residual chlorine was measured using a Hach DPD powder pillow test that is based on USEPA Method 8167 and 8021 and residual chlorine was quenched using ascorbic acid. Three groups of disinfection byproducts were studied. Four regulated trihalomethanes (THMs) and nine regulated haloacetic acids (HAAs) were

analyzed based on EPA method 551.1 (Hodgeson et al. 1995), and EPA method 552.3 (Domino et al. 2003) accordingly. These methods were further optimized based on a journal publication (Liu et al. 2013). One nitrosamine (*N*–Nitrosodimethylamine, or NDMA) was from the third group of DBPs analyzed and was measured based on a modified EPA method 521 using solid-phase extraction (Munch and Bassett 2004), followed by the LC-MS/MS method developed by Zhao and her research group (Zhao et al. 2006).

A six-year review document on DBPs was prepared by the USEPA, and among different nitrosamines in drinking water, NDMA was being detected most frequently (USEPA 2016). All of the other nitrosamines were either absent or at very low levels in most of the samples. Therefore, NDMA formation was selected for evaluation in this study.

3.6.1. Uniform Formation Conditions

Samples were prepared under uniform formation conditions (UFC) to analyze disinfection byproducts (Summers et al. 1996). UFC results can be used to directly compare DBPs formation during treatment and assess the effect of different components of the treatment method (Summers et al. 1996). Based on the UFC standard operating procedure, each sample was dosed with borate buffer and hypochlorite buffer, and the pH was adjusted to 8.0 ± 0.2. Residual chlorine was 1.0 ± 0.4 mg/L, and the incubation time was 24 hrs in the dark at 20.0 ± 1.0◦C (Summers et al. 1996).

A preliminary test has been conducted to determine the 24-hrs chlorine demand of each water matrix and chlorine dose accordingly to achieve 1.0 ± 0.4 mg/L of residual chlorine after 24 hrs. In this, test three chlorine dosages were dosed based on Cl_2:TOC ratios of 1.2:1, 1.8:1, and 2.5:1. At the end of the chlorine exposure, residual chlorine was

measured with Hach DPD test and quenched with ascorbic acid. From the results of these tests, the chlorine dose for UFC was selected to yield a 24-h residual of 1.0 mg/L free chlorine.

Cl_2-to-TOC dosage of 2.5:1 worked best with the residual chlorine after 24 h of 1.16 and 0.93 mg/L for water samples with additional algal DOM and water sample without added DOM accordingly. Table 12 is showing the results of UFC preliminary dosing tests.

Table 12. Uniform Formation Condition Preliminary Tests

Sample	**Cl_2:TOC Ratios**	**24-h Chlorine mg/L**
Matrix without algal DOM	1.2	0.32
	1.8	0.74
	2.5	**1.16**
Matrix with algal DOM	1.2	0.02
	1.8	0.24
	2.5	**0.93**

All bottles and glassware were precleaned using a programmable dishwasher that included the following steps; rinse three times with warm tap, rinse three times with deionized water, place in acid bath, rinse with tap water followed by DI water.

3.6.2. Trihalomethanes Analysis

THMs were analyzed based on EPA method 551.1 (Hodgeson et al. 1995). This method was optimized by Liu and their research group (Liu et al. 2013). The liquid-liquid extraction method was used to extract the THMs as follows: First, 3.0 mL MTBE (methyl tert-butyl ether) and 4 g Na_2SO_4 was added to 50 mL of the water sample. Next, the mixture was extracted for 11 min by shaking vigorously. Then, the vial was inverted for five minutes and allowed the water and MTBE phases to separate. After that, 1 mL of the

MTBE phase was transferred to an autosampler vial. Finally, 10 µL of 4-bromofluorobenzene as an internal standard was added to the vials and vials were stored at -20◦C for confirmation analysis (Liu et al. 2013).

Gas chromatography – electron capture detector (GC-ECD) analysis was performed using Shimadzu-QP2010 GC (Shimadzu, Japan) that was equipped with a split/split-less injector and an electron capture detector (ECD, ^{63}Ni). The analysis was done using split-less mode with the injector temperature at 230◦C. Helium and nitrogen were used as the carrier and makeup gas at a flow rate of 1.4 mL/min and 30 mL/min, respectively. THMs were separated on fused silica DB-1301 capillary column (30 m length, 0.25 mm inner diameter, and 1 µm film thickness with a temperature range between -20◦C and 280-300◦C) (Agilent Technologies, Palo Alto, CA, USA). The oven temperature was maintained at 35◦C for 15 min, and then programmed at 25◦C/min to 145◦C and held for 3 min, and finally 35◦C/min to 240◦C which was held for 5 min. The temperature of the detector was held at 260◦C (Hodgeson et al. 1995; Liu et al. 2013).

The concentration of THM4 standard solution (Cat. No. 30036 - Restek, PA, US) was 200 µg/mL for each THM. The linearity range of the GC-ECD analysis was 0.01–100 mg/L for THM4. Table 13 is showing four THMs targeted in this study. Figure 10-A to D is showing the standard curve of each THM compound.

Table 13. THM4 in Standard Solution

Compound	Compound abv	CAS	Concentration	RT (min)
Bromodichloromethane	BDCM	(75-27-4)	200 µg/mL	11.54
Bromoform	BF	(75-25-2)	200 µg/mL	22.44
Chloroform	CF	(67-66-3)	200 µg/mL	28.63
Dibromochloromethane	DBCM	(124-48-1)	200 µg/mL	31.38

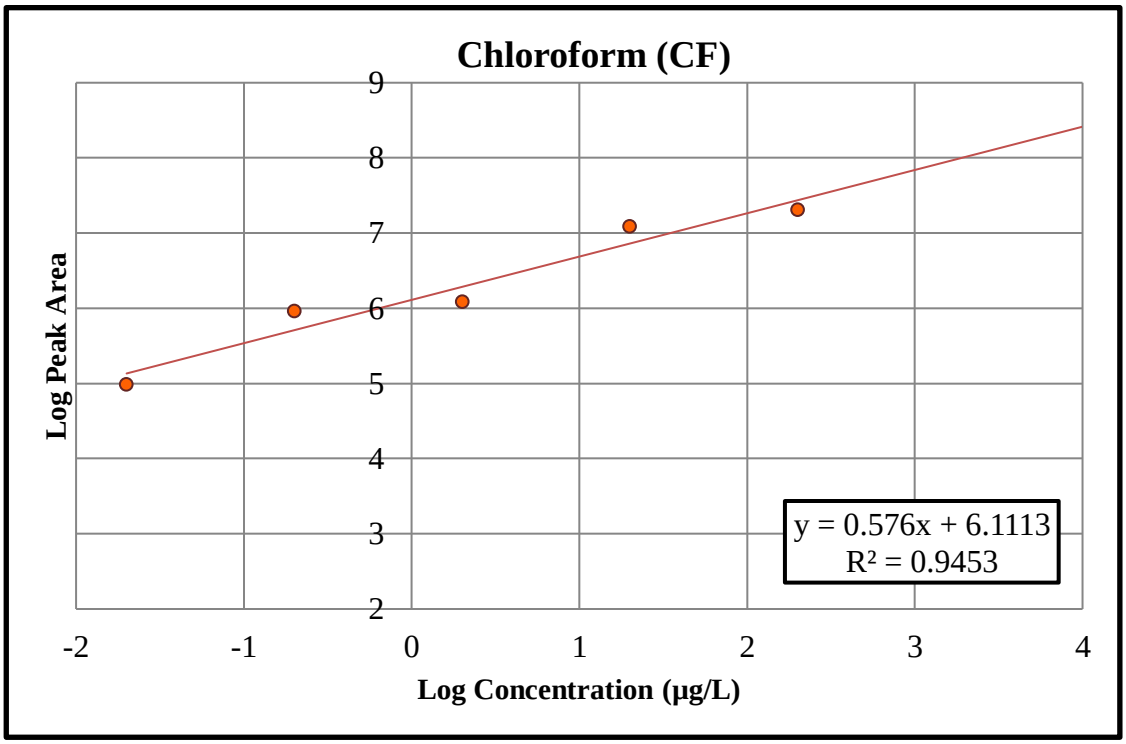

(a)

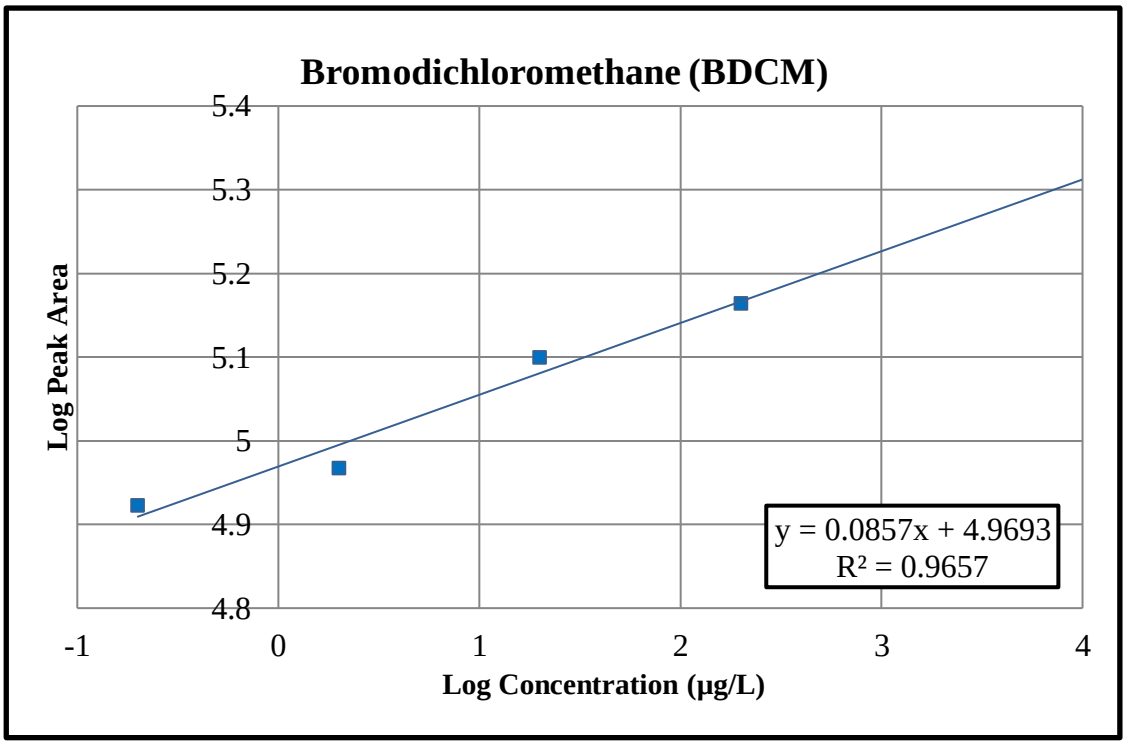

(b)

Figure 10. GC-ECD Standard Curves of THMs: (a) Chloroform, (b) Bromodichloromethane

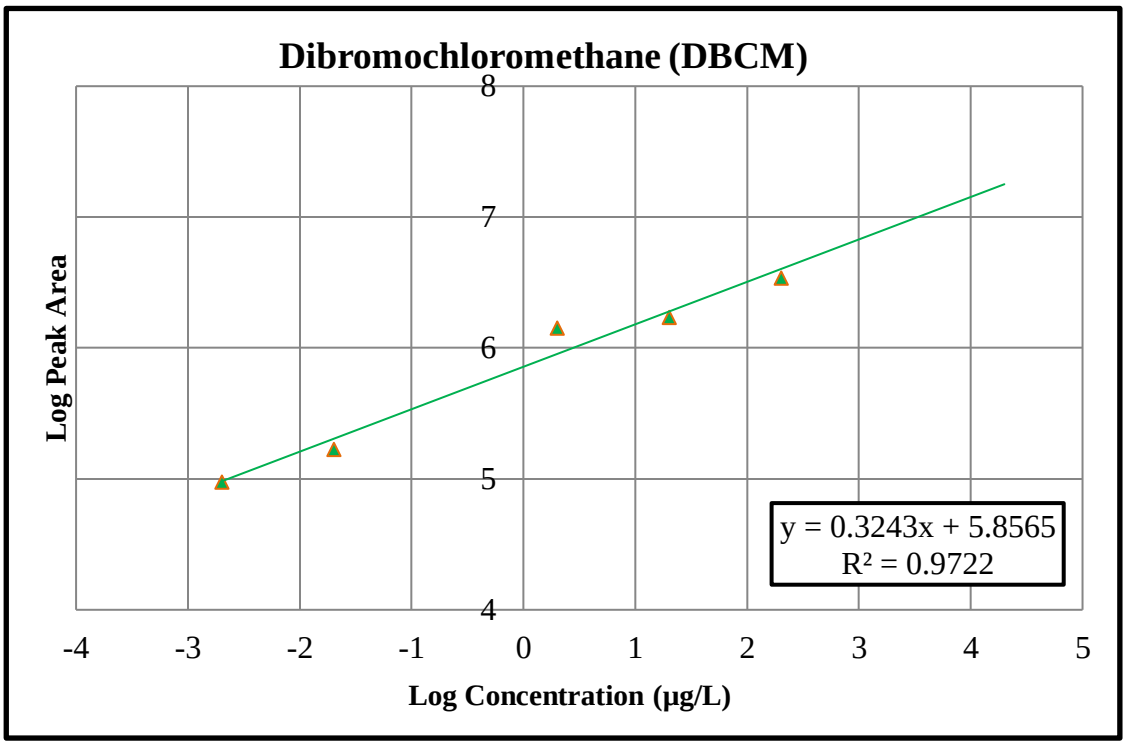

(c)

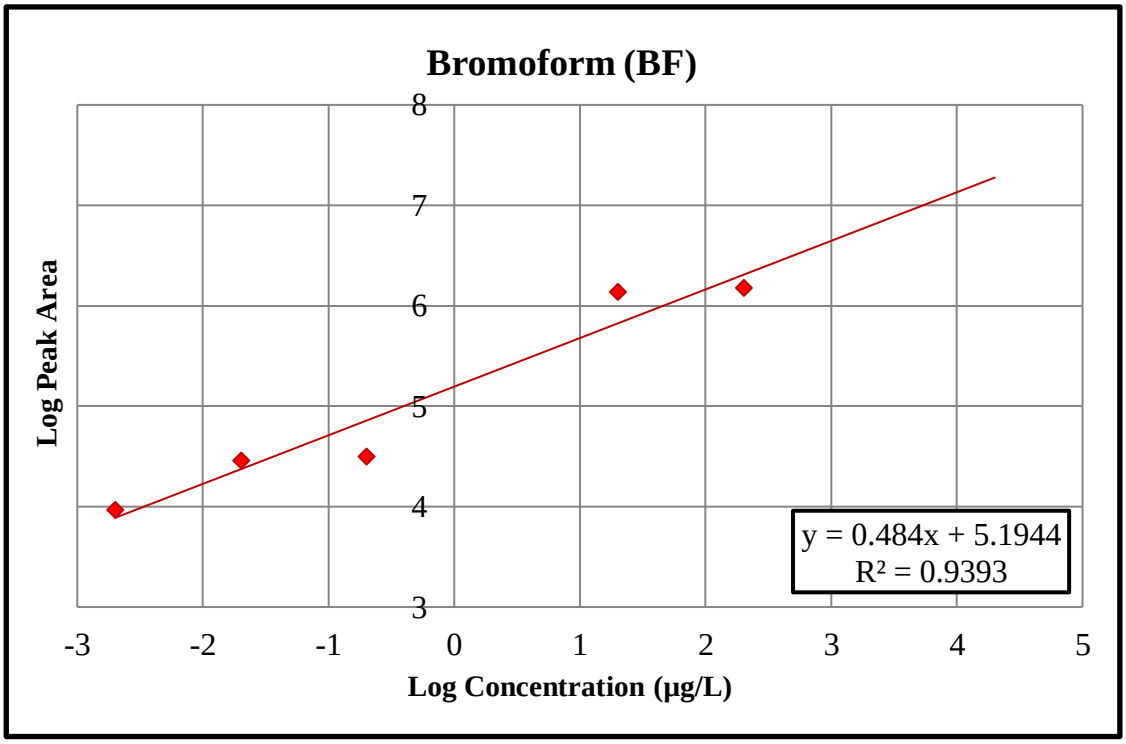

(d)

Figure 10. (Cont'd) GC-ECD Standard Curves of THMs: (c) Dibromochloromethane, and (d) Bromoform

3.6.3. Haloacetic Acids Analysis

HAAs were analyzed based on EPA method 552.3 (Domino et al. 2003). This method was optimized by Liu and their research group (Liu et al. 2013). The liquid-liquid extraction method was used to extract the THMs as follows: First, 40 mL of the water sample was transferred to a precleaned 60-mL glass vial with a PTFE-lined screw cap using a clean, graduated cylinder for each sample. Next, 2 mL concentrated sulfuric acid (97% ACS grade), and 16 g of Na_2SO_4 was added to the water sample, and the water sample was shaken vigorously by hand until all Na_2SO_4 was dissolved. Next, 3.0 mL of MTBE with internal standard (120 mg/L of 1-2dibromopropane) was added. Next, the sample was shaken vigorously for 14 min, and the phases were allowed to separate for 5 mins. Then the 2 mL of the upper MTBE layer was transferred to a 15 mL graduated conical centrifuge tube, and 1 mL of 15% acidic methanol was added to each tube. To prepare 15% acidic methanol, 5 mL of sulfuric acid was added to 60 mL of methanol contained in a 100 mL volumetric flask that was placed in a cooling bath. The solution was mixed and diluted to 100 mL with methanol. After sealing, the tubes were placed in a water bath at 40°C and heated for 160 min. Then the tubes were removed from the water bath and cooled to room temperature. After that, 8.5 mL of a 129 g/L Na_2SO_4 solution was added to each centrifuge tube, and the lower layer was discarded. Finally, 1 mL of saturated $NaHCO_3$ solution was added, and the upper ether layer was transferred to an autosampler vial and was stored at -20°C for confirmation analysis (Liu et al. 2013). To prepare saturated $NaHCO_3$, sodium bicarbonate was added to 100 mL of water and the

solution was mixed periodically until a small amount of undissolved sodium bicarbonate remained despite further mixing.

GC-ECD analysis of HAAs was the same as THMs except as noted below (section 3.6.2.). For HAAs analysis, the SH-Rtx-1701 capillary column (30 m length, 0.25 mm inner diameter, and 1 µm film thickness with a temperature range of -20 to 270/280◦C) (Shimadzu, Japan) was used. The oven temperature was maintained at 40◦C for 10 min, and then programmed at 10◦C/min to 85◦C, and finally 30◦C/min to 205◦C which was held for 5 min. HAAs were analyzed by ECD held at 260◦C. (Domino et al. 2003; Liu et al. 2013).

The HAA9 standard solution was purchased from Restek (Cat. No. 31646, PA, US). Table 14 is showing nine HAAs that were targeted in this study. The linearity range of GC-ECD analysis was 0.01–150 mg/L for HAA9. Figure 11-A to I shows the standard curve of each THM compound.

Table 14. HAA9 in Standard Solution

Compound	Compound abv	CAS	Concentration
Bromochloroacetic acid	BCAA	(5589-96-8)	400 µg/mL
Bromodichloroacetic acid	BDCAA	(71133-14-7)	400 µg/mL
Chlorodibromoacetic acid	CDBAA	(5278-95-5)	1000 µg/mL
Dibromoacetic acid	DBAA	(631-64-1)	200 µg/mL
Dichloroacetic acid	DCAA	(79-43-6)	600 µg/mL
Monobromoacetic acid	MBAA	(79-08-3)	400 µg/mL
Monochloroacetic acid	MCAA	(79-11-8)	600 µg/mL
Tribromoacetic acid	TBAA	(75-96-7)	2000 µg/mL
Trichloroacetic acid	TCAA	(76-03-9)	200 µg/mL

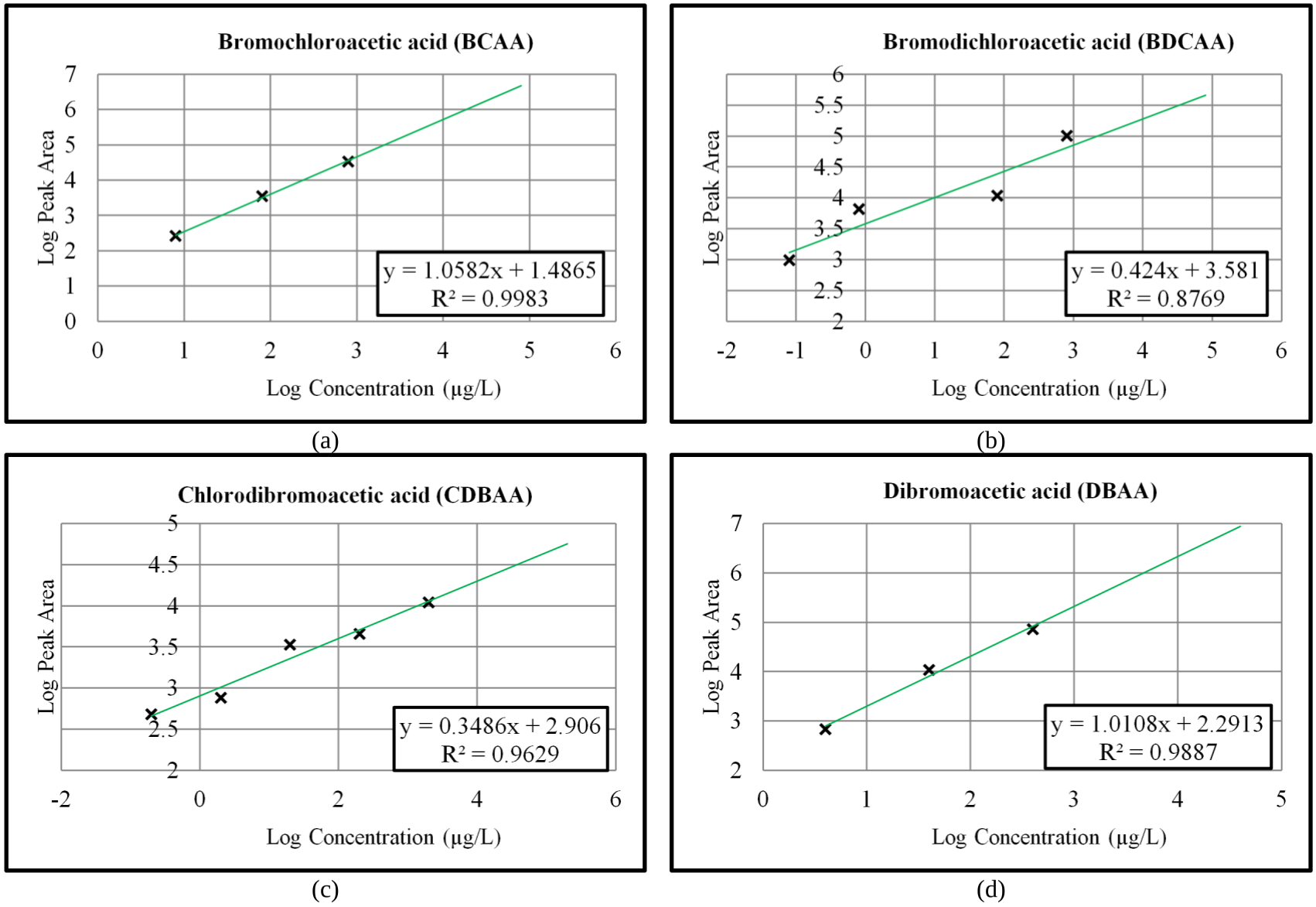

Figure 11. GC-ECD Standard Curves for HAAs

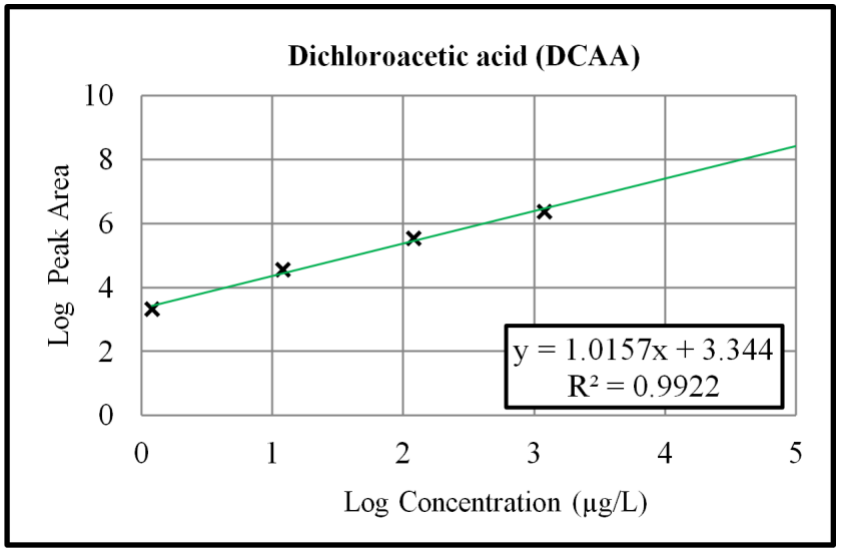

(e)

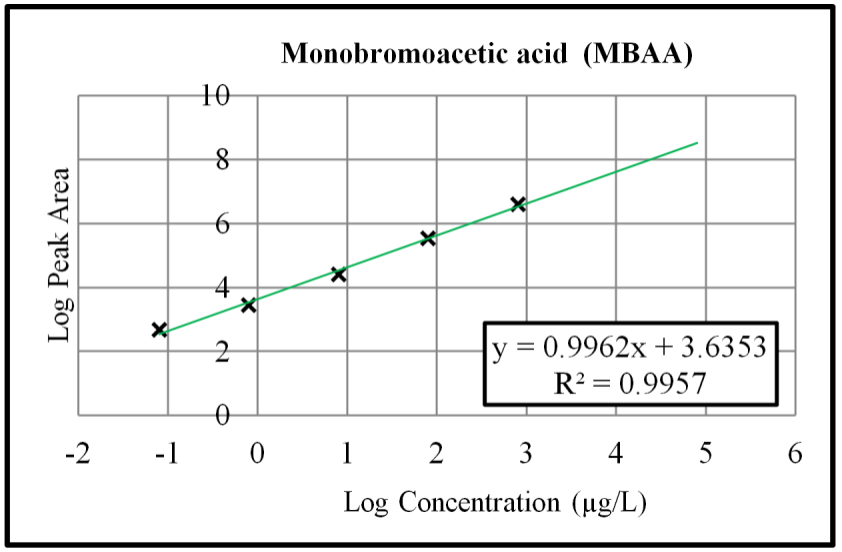

(f)

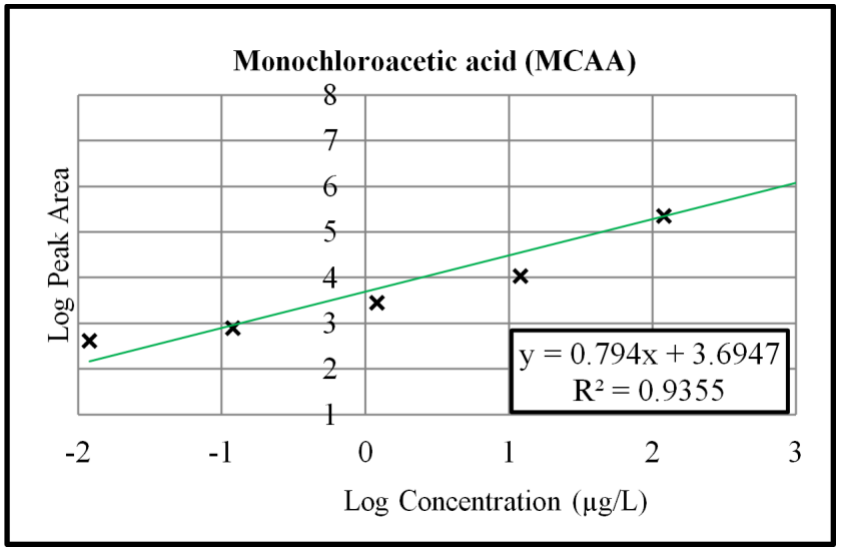

(g)

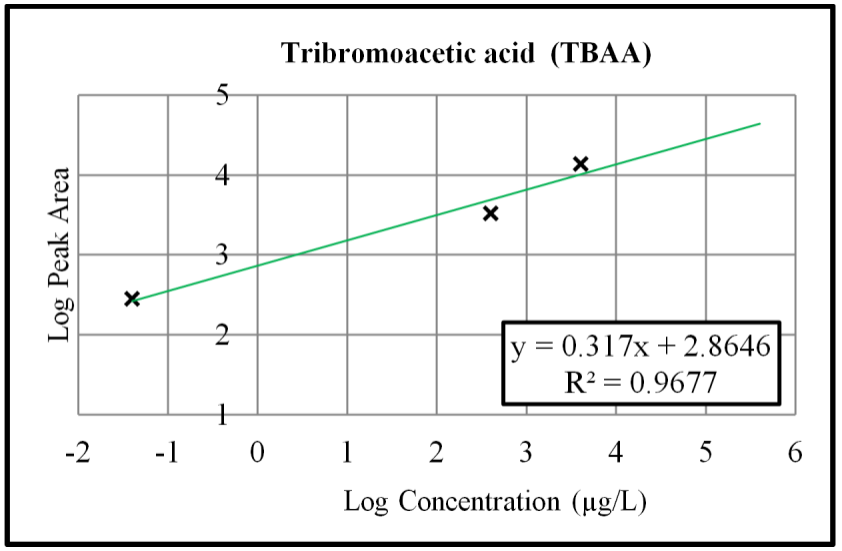

(h)

Figure 11. (Cont'd) GC-ECD Standard Curves for HAAs

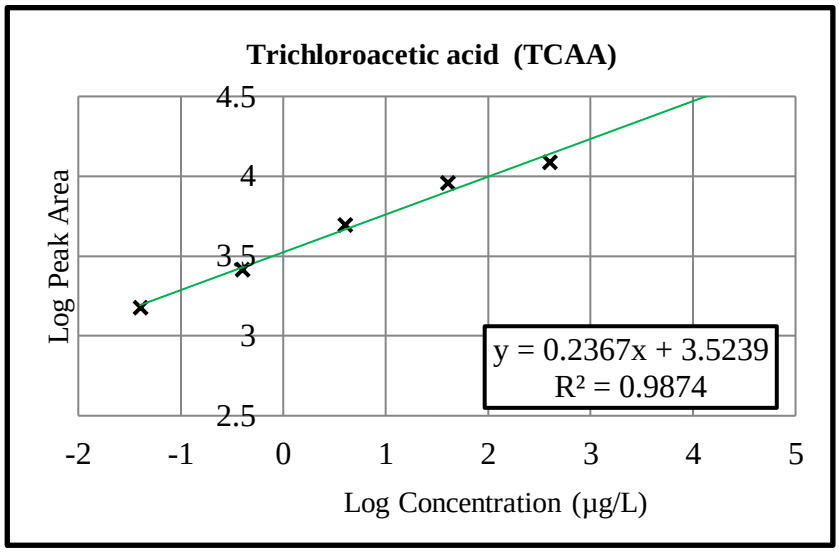

Figure 11. (Cont'd) GC-ECD Standard Curves for HAAs

3.6.4. Nitrosamines Analysis

Different researchers working on NDMA have utilized gas chromatography-mass spectrometry (GC/MS) method combined with electron impact or chemical ionization and GC with thermal energy analyzer (Zhao et al. 2006). One of the drawbacks of the mentioned methods is that they are limited to the analysis of volatile and thermally stable compounds. Also, they do not provide structural information for the identification of unknown DBPs or labile nitrosamines (Zhao et al. 2006). LC-MS method has attracted attention to measure THMs and NDMA (Wang et al. 2012; Zhao et al. 2006). The LC-MS/MS enabled the measurement of nine nitrosamines with a detection limit of 3.1 ng/L of NDMA (Zhao et al. 2006). That study suggested the method including solid-phase extraction (SPE), liquid chromatography (LC) separation, and tandem quadrupole linear ion trap mass spectrometry (MS/MS) detection that resulted in the detection of both thermally stable and unstable nitrosamines (Zhao et al. 2006).

As NDMA is a potential carcinogen for humans and animals, all safety precautions must be strictly adhered to handle these compounds, and proper safety procedures should

follow waste disposal. The solid-phase extraction (SPE) method using Supelclean™ Coconut Charcoal SPE Tube was utilized to extract the NDMA. The SPE packing material was polypropylene with a bed weight of 2 g and a volume of 6 mL. Charcoal bonding was the active group. The vacuum system (-30 kPa) was used to draw the water sample through the cartridge. The following steps were applied to obtain extracts. First, the SPE cartridges were initially rinsed with 15 mL each of hexane and dichloromethane, and the residual organic solvents were removed under vacuum. Next, the cartridges were then conditioned with 15 mL of methanol and 15 mL of water. Next, 0.5 g of sodium bicarbonate was added to 250 mL of the water sample (pH 8). Then, 25 µL of NDMA-d6 with a concentration of 400 µg/L was spiked into the sample to obtain a final concentration of 40 ng/L. Then, the sample was passed through the SPE cartridge at a flow rate of 3-5 mL/min. After that, the analyte adsorbed on the SPE cartridge was eluted using 15 mL of dichloromethane and was collected in 15 mL tubes and concentrated down to 1 mL under vacuum. Finally, the eluent was transferred to an autosampler vial and was stored at -20◦C for confirmation analysis (Charrois et al. 2004; Zhao et al. 2006). The internal standard NDPA-d14 (100 µL of 200 µg/L) was added to the extract (final concentration of 40 ng/L) before the LC-MS/MS analysis. As blank NDMA-free water was extracted to ensure all reagents were NDMA-free. A stock solution of 1000 µg/mL and a set of calibration standard solutions of 0.001 to 1000 µg/mL were prepared in methanol and stored in 4ºC. Working solutions of 5 to 200 µg/L in 1:1 methanol/water was freshly prepared before LC-MS/MS (Zhao et al. 2006). 100 mg NDMA standard was purchased from Sigma-Aldrich (Cat. No. 48552, Missouri, US).

Agilent 6400 series triple quadrupole LC-MS/MS system was used with positive electrospray ionization combined with the multiple-reaction monitoring (MRM) mode. The mobile phase was 10 mM ammonium acetate and 0.01% acetic acid in water (solvent A) and 100% methanol (solvent B) (Zhao et al. 2006). The solvents were HPLC-grade or higher. The eluent flow rate was 0.3 mL/min. The solvent gradient program included 60% of solvent B for 1 min. The gradient was increasing from 60% to 90% of solvent B over 5 min. Then returned back to 60% of solvent B over 0.1 min. Finally, the gradient was returned to the initial conditions by a 13-min re-equilibration before the next sample injection. Injection volume was 100 µL.

The column was a ZORBAX Eclipse XDB-C8 capillary column 4.6×150 mm, 3.5 µm (Agilent Technologies, Palo Alto, CA, USA). MassHunter Quantitation software was used for quantification and the worklist containing all the sample types and calibration level was set up. The peaks of standards and extracted samples were monitored automatically and results were reproducible. MS/MS parameters including collision energy and cell accelerator voltage are shown in Table 15. Gas flow rate was 10 L/min at 350◦C.

Table 15. Optimized LC-MS/MS Condition for NDMA Detection

Compounds	Parent Ion (m/z) $[M+H]^+$	Product Ion (m/z) $[M+H]^+$	Collision Energy (eV)	Cell Accelerator Voltage
NDMA	75	43	15	4
NDMA-d6	81	46	25	4
NDPA-d14	145	97	25	4

Figure 12 presents the LC-MS/MS calibration curve for NDMA. LC-MS/MS analysis was linear in the whole range of 0.001–1000 µg/L for NDMA.

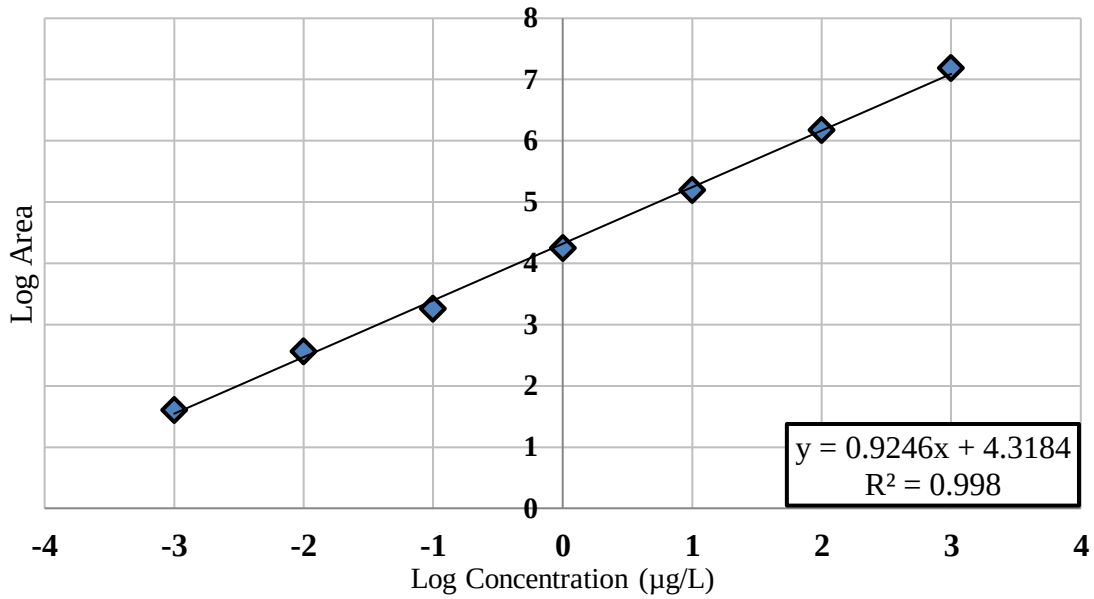

Figure 12. LC-MS/MS Calibration Curve for NDMA

3.6.5. t-Test Analysis

Two-Sample t-Tests has been performed in Excel to evaluate the significance of any differences in DBP formation between the samples. Two-sample t-tests compared the means of two groups specifically. The results of the t-test determine whether two group means are different. Null hypothesis is that the means of two group are equal. If the t-statistic value is smaller than -t-critical or higher than +t-critical then the null hypothesis is rejected. Rejecting the null hypothesis means that the results are statistically significantly different and failing to reject the null hypothesis means that the results are not significantly different. In all cases the t-test provides p-values as well. The smaller the p-value means that the evidence to reject the null hypothesis is stronger. A p-value of less than 0.05 is statistically significant.

CHAPTER 4. RESULTS AND DISCUSSIONS

4.1. Comparison of UV/H_2O_2 and UV/Cl_2 AOPs for Algal Toxins Removal

UV/Cl_2 and UV/H_2O_2 were assessed as practical treatment methods to treat MCs in water with minimum DBPs formation and toxicity risk. Algal toxins were tested in background water matrix from a drinking water treatment plant as well as in samples with elevated nitrate and/or AOM. Microcystis algae cultured in the lab for extraction of AOM was not toxic, and MCs were spiked to the matrix one at a time. Each toxin was tested separately because PP2A toxicity assay defines the total toxicity of samples, and a mixture of two or more toxins cannot be adequately assessed. Furthermore, co-occurrence of two or more microcystin- producing genera in the water sample is less than 38% (Loftin et al. 2016).

Water matrices were dosed with oxidants and collected before and after the UV irradiation for LC-MS/MS analysis, as described in the method section. As discussed earlier, the UV doses for the MCs AOPs were within the range of full-scale UV doses used in AOPs at drinking water treatment plants (up to 500-2000 mJ/cm_2) using MP mercury vapor lamps. UV setup was adjusted to reflect the residence time of a full-scale process in order of minutes.

Figures 13 to 15 show the degradation of MCs-LR, -RR, and -YR as a function of UV dose in the presence of 5 and 10 mg/L of H_2O_2 and 2 and 4 mg/L of Cl_2 and different types of water matrices. Each toxin included 16 different batches of samples including different matrices and treatment methods that were conducted with controls and blanks.

In the background matrix, UV/Cl_2 performed much better than UV/H_2O_2 for MC-LR, while the opposite was observed for MC-YR. Both processes were approximately equally effective for MC-RR. While UV/H_2O_2 and UV/Cl_2 processes were effective in oxidizing all microcystin variants, including LR, RR, and YR, UV/Cl_2 provided additional oxidation for MC-LR that can be because of added benefit of the direct chlorine reaction. Table 16 shows the removal efficiency of different treatment methods under 500 and 2000 mJ/cm_2.

The presence of nitrate resulted in additional hydroxyl radicals and resulted in similar performance for the two AOP processes as radical reactions were prevalent over direct reactions with Cl_2. Additional AOM in the matrix not only scavenged the radicals, but it also reacted with Cl_2, which reduced the effectiveness of both processes considerably. The results are consistent with other studies that show that the presence of DOM decreases the removal efficiency in UV/Cl_2 and demonstrate its impact as background scavenger of both radicals and oxidant (Sichel et al. 2011). The presence of AOM negatively affects the removal rate when AOPs are utilized to degrade micropollutants because of the high reactivity of AOM with HO• (Lee et al. 2018; Martijn 2015). The effect of DOM as a hydroxyl radical scavenger was observed for all three MCs. The low degradation of MCs in the presence of AOM indicates high HO• scavenging by organic matter since microcystins toxins compete with organic matter for the reaction with HO•.

Table 16. Removal Efficiency (%) of MC-LR, -RR, -YR UV/H_2O_2 and UV/Cl_2

Matrix	Oxidant Dose	MC-LR		MC-RR		MC-YR	
		UV = 500 mJ/cm2	UV = 2000 mJ/cm2	UV = 500 mJ/cm2	UV = 2000 mJ/cm2	UV = 500 mJ/cm2	UV = 2000 mJ/cm2
Background	H_2O_2 = 5 mg/L	4.56	23.06	75.39	95.12	81.40	99.36
	H_2O_2 = 10 mg/L	11.75	26.92	70.21	88.08	83.65	96.60
	Cl_2 = 2 mg/L	50.79	76.39	81.19	94.60	20.38	52.77
	Cl_2 = 4 mg/L	70.18	77.93	76.19	93.70	7.00	43.21
Nitrate = 20 mg/L	H_2O_2 = 5 mg/L	8.43	30.75	89.49	97.20	80.18	93.33
	H_2O_2 = 10 mg/L	10.84	36.05	85.06	96.08	86.85	92.13
	Cl_2 = 2 mg/L	18.26	75.26	90.08	95.77	83.71	90.83
	Cl_2 = 4 mg/L	10.30	71.48	27.51	99.68	78.58	85.00
DOM = 3 mg/L	H_2O_2 = 5 mg/L	6.02	25.78	15.55	33.75	77.78	86.11
	H_2O_2 = 10 mg/L	14.60	74.74	17.60	53.17	83.28	93.38
	Cl_2 = 2 mg/L	12.51	25.77	11.25	44.11	52.15	73.53
	Cl_2 = 4 mg/L	5.99	40.80	6.90	23.32	95.26	98.17
DOM = 3 mg/L, and Nitrate = 20 mg/L	H_2O_2 = 5 mg/L	6.29	13.48	5.17	23.20	5.87	21.72
	H_2O_2 = 10 mg/L	15.88	23.22	4.17	17.50	17.96	43.41
	Cl_2 = 2 mg/L	11.58	38.18	7.80	26.03	28.92	97.93
	Cl_2 = 4 mg/L	12.78	62.02	9.29	28.79	52.01	98.21

The origin, nature, and composition of AOM affect the observed *pseudo*-first order constant for the reaction between HO· and AOM. The second-order rate constants of

Microcystis aeruginosa extracted AOM (IOM) with HO• was determined as 4.45×10^{8} $M^{-1}.s^{-1}$ (Lee et al. 2018; Martijn 2015). However, the reaction rate constant of standard DOM with HO• was 3.6×10^{8} $M^{-1}.s^{-1}$ (Westerhoff et al. 1999) showing that the scavenging potential of AOM is higher than DOM standards.

When both AOM and nitrate are present in the matrix the positive effect of nitrate in generating more hydroxyl radicals was suppressed by AOM scavenging of the radicals, especially in UV/H_2O_2 process.

MC-LR degradation rate under direct UV photolysis is independent of UV irradiance (He et al. 2012). For instance, in a study on degradation of MC-LR, the UV photolysis rate was $(3.65 \pm 0.21) \times 10^{-3}$ cm^2/mJ under 0.27 mW/cm^2 and $(3.57 \pm 0.18) \times 10^{-3}$ cm^2/mJ under 0.46 mW/cm^2 UV dose (He et al. 2012).

In a study on the MC-LR degradation using UV/Cl_2 process, the reaction rate increased from 5.67×10^{-2} $M^{-1}.s^{-1}$ to 6.38×10^{-2} $M^{-1}.s^{-1}$ with chlorine dosage increasing from 1.0 to 4.0 mg/L (X. Zhang et al. 2019). The previously reported results are comparable to what was observed in this study.

Figure 13 demonstrates the degradation of MC-LR under the UV doses up to 2000 mJ/cm^2 using UV/H_2O_2 and UV/Cl_2. The result shows that UV/Cl_2 led to higher degradation compared to UV/H_2O_2 that is in line with previous studies. In a research on MC-LR degradation using these two AOPs, the k_{obs} was 4.9×10^{-3} s^{-1} under UV/Cl_2 process and k_{obs} was 1.2×10^{-3} s^{-1} under UV/H_2O_2 process when oxidant dosage was the same (45 µM) (X. Zhang et al. 2019).

Theoretical second-order rate constant of MCs with HO• can be calculated based on group contribution method (GCM). The rate constants of the presented amino acids in the

structure of MC can be combined to calculate reactivity of MCs with HO•. According to this method, the reactivity of the three variants in this study are as shown in Table 17 (He et al. 2015). The actual rate of reaction of MCs with HO• are different from the theoretical values because of the structure-reactivity relationships, steric hindrance and molecular conformation. A study carrying competition kinetic experiments determined the actual reaction rates of MCs as shown in Table 17.

Table 17. Theoretical and Actual Second-order Rate Constant of MCs with HO• (He et al. 2015)

MCs Variant	Theoretical Rate Constant	Actual Rate Constant
MC-LR	2.2×10^{10} $M^{-1}.s^{-1}$	1.13×10^{10} $M^{-1}.s^{-1}$
MC-RR	2.4×10^{10} $M^{-1}.s^{-1}$	1.45×10^{10} $M^{-1}.s^{-1}$
MC-YR	3.4×10^{10} $M^{-1}.s^{-1}$	1.63×10^{10} $M^{-1}.s^{-1}$

Based on the reaction rate of MC-LR under UV photolysis higher removal efficiency was expected at 2000 mJ/cm^2 in all matrices and treatment conditions. The removal efficiency of MC-RR and -YR under high UV dose were in line with expected values based on reaction rates. The reaction rate with hydroxyl radicals is about the same for all three toxins. But they all responded differently to treatment and the data was not fully explainable by the rate constants. The observed differences could be from the different susceptibility of toxins to direct photolysis.

MC-YR degradation was higher than MC-RR and -LR under UV/H_2O_2 process. It was expected because MC-YR is more complicated in structure, compared to other two toxins, containing a benzene ring of Tyrosine that can be rapidly oxidized by HO• radicals in UV/H_2O_2.

NOM, HCO_3^-, CO_3^{-2}, NO_2^-, and bromide ions are known as hydroxyl radical scavengers in natural waters (Keen et al. 2014; Lee et al. 2018; Watts, Rosenfeldt, and Linden 2007).

The removal of UV absorbing compounds in the pretreatment decreases the competition for UV light and reduces energy consumption by UV/H_2O_2 and UV/Cl_2. Besides, the removal of these constituents decreases the HO· scavenging. NOM and nitrate are known as the most important water constituents affecting the efficacy of the UV/H_2O_2 process by absorbing UV and scavenging HO· (Martijn 2015). Additionally, NOM reacts with radicals in UV/Cl_2 much more than it does with HO· in UV/H_2O_2. The presence of NOM reduced MC-LR degradation and the higher concentration of NOM resulted in larger inhibition (X. Zhang et al. 2019). In prior studies, the k_{obs} of MC-LR in UV/Cl_2 process was 4.9×10^{-3} s^{-1} in ultrapure water and 1.5×10^{-3} s^{-1} in presence of 10 mg/L NOM. Free chlorine was consumed by NOM and decreased the degradation rate by 65%. In addition, NOM scavenges HO·, Cl·, and ClO· radicals (X. Zhang et al. 2019).

Figure 14 shows the degradation of MC-RR under the UV doses up to 2000 mJ/cm^2. The amount of oxidant did not make much of a difference for this toxin. The reaction is therefore primarily a radical reaction, and Cl_2 seemed to play a smaller role for MC-RR compared to MC-LR. Also, the reaction for MC-RR is much faster than that for MC-LR, however, the HO· rate constants were approximately the same. The possible explanation might be greater contribution from direct photolysis for MC-RR. In addition, AOM had a major negative impact on the process efficiency and reduced the degradation efficiency of MC-RR from >90% to < 70% at the highest UV dose that was expected as described before.

Figure 15 shows the degradation of MC-YR under the UV doses up to 2000 mJ/cm^2 which is a practical limit for UV based AOPs. The same results as MC-RR were observed

and the MC-YR degradation efficiency was slightly higher compared to MC-RR that was expected based on the reported reaction rates in Table 17.

The degradation of MC-YR was increased with additional DOM compared to background samples. Photolysis of organic matter can generate reactive species, and MC-YR may be susceptible to those reactions, although those are rarely dominant reactions. This could explain the improved efficiency with the addition of DOM to the background matrix.

Comparing the results of different microcystins, as shown in Figure 13 -15, the removal efficiencies are not the same given the same matrix and treatment conditions. The reason is that the chemical structure of toxins will affect the toxins' properties (e.g. reactivity with each oxidant) and removal efficiency. The reaction of the different amino acids with hydroxyl radical follows this order: Tyrosine (Y)> Arginine (R)> Leucine (L)> Alanine (A) (He et al. 2015). The same result was observed, and the removal efficiency for MC-YR > MC-RR > MC-LR.

Comparing the results for water matrices with and without nitrate when MP lamp was used the positive effect of nitrate in the additional formation of hydroxyl radicals was noticeable. UV treatment of drinking water containing nitrate or nitrite with MP UV lamps during UV/Cl_2 and UV/H_2O_2 produce reactive nitrogen species (Z. Zhang et al. 2019). In addition, nitrate in water matrix in the presence of UV irradiation generates high quantity of hydroxyl radical that is comparable with addition of 10 mg/L of H_2O_2 in process (Keen, Love, and Linden 2012).

In addition, no significant change in MC-LR -RR and -YR degradation was observed comparing low levels and high levels of H_2O_2 concentration. The reason is that the

increased H_2O_2 does not increase the steady-state HO• proportionally. Each incremental increase in H_2O_2 results in a smaller incremental increase of HO• because of HO• scavenging properties of H_2O_2 (Lopez et al. 2003).

Eqs. 5 - 8 are showing the scavenging effect of H_2O_2 that becomes significant at higher concentrations (Buxton et al. 1988; He et al. 2012). The H_2O_2 concentration limit above which no excess degradation happens depends on system characteristics (He et al. 2012).

$$H_2O_2 + HO^{\cdot} \rightarrow H^+ + O_2^{\cdot -} + H_2O \quad \text{(Eq. 5)}$$

$$HO_2^{\cdot} + HO^{\cdot} \rightarrow H_2O + O_2 \quad \text{(Eq. 6)}$$

$$HO_2^{\cdot} + HO_2^{\cdot} \rightarrow H_2O_2 + O_2 \quad \text{(Eq. 7)}$$

$$HO^{\cdot} + HO^{\cdot} \rightarrow H_2O_2 \quad \text{(Eq. 8)}$$

Understanding of the treatment mechanism when nitrate is present in the system is complicated. The formation of HO• under the UV irradiation of nitrate is more complicated than the UV/H_2O_2 process (Keen et al. 2012; Mack and Bolton 1999). A molecule of hydrogen peroxide splits into two hydroxyl radicals after the absorption of a UV photon. However, a molecule of nitrate can form nitrite and oxygen or nitrite radical and oxygen radical after absorption of a UV photon (Eq. 9a and 9b). Nitrite radicals may react with hydroxyl radicals and form nitrate or may react with water and another nitrite radical and form further nitrite ion (Keen et al. 2012). Oxygen radical reacts with water (Eq. 10) and creates a hydroxyl radical (Buxton et al. 1988). Produced nitrite in Eq. 9a can absorb another photon and form nitric oxide radicals and oxygen radicals (Eq. 11). The oxygen radical directly reacts with water and creates a hydroxyl radical (Eq 10) and nitric oxide radical, and nitrite scavenge hydroxyl radical (Eq. 12 & 13) (Keen et al. 2012).

$$NO_3^- \rightarrow NO_2^- + {}^1/_2\, O_2 \quad \text{(Eq. 9a)}$$

$$NO_3^- \rightarrow NO_2^{\cdot} + O^{\cdot -} \quad \text{(Eq. 9b)}$$

$$O^{\cdot -} + H_2O \leftrightarrow HO^{\cdot} + OH^- \quad \text{(Eq. 10)}$$

$$NO_2^- \rightarrow NO^{\cdot} + O^{\cdot -} \quad \text{(Eq. 11)}$$

$$NO^{\cdot} + HO^{\cdot} \rightarrow HNO_2 \quad \text{(Eq. 12)}$$

$$NO_2^- + HO^{\cdot} \rightarrow NO_2^{\cdot} + OH^- \quad \text{(Eq. 13)}$$

Nitrate in the water matrix has a complicated effect. Apart from creating advanced oxidation conditions, it can have a light filtering effect. The light filtering effect of nitrate interferes with H_2O_2 absorbing under UV<240 nm (Keen et al. 2012). This effect can be observed using MP UV lamps emitting UV spectrum, including wavelengths below 240 nm.

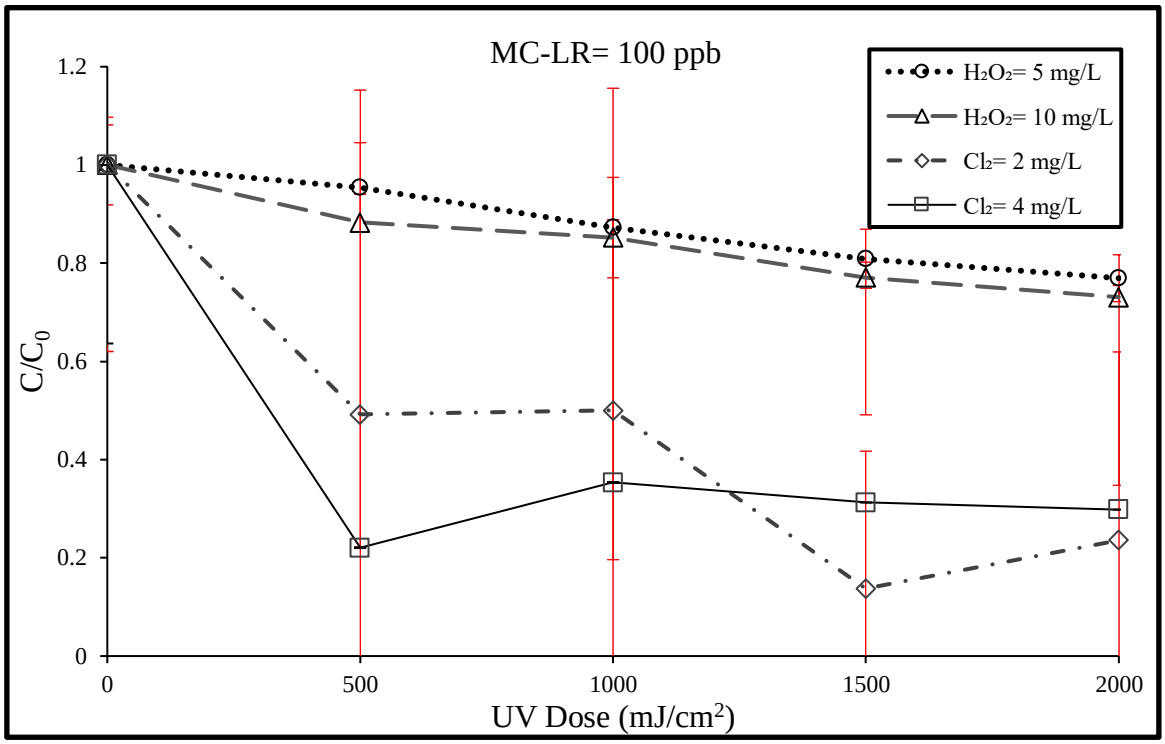

(a)

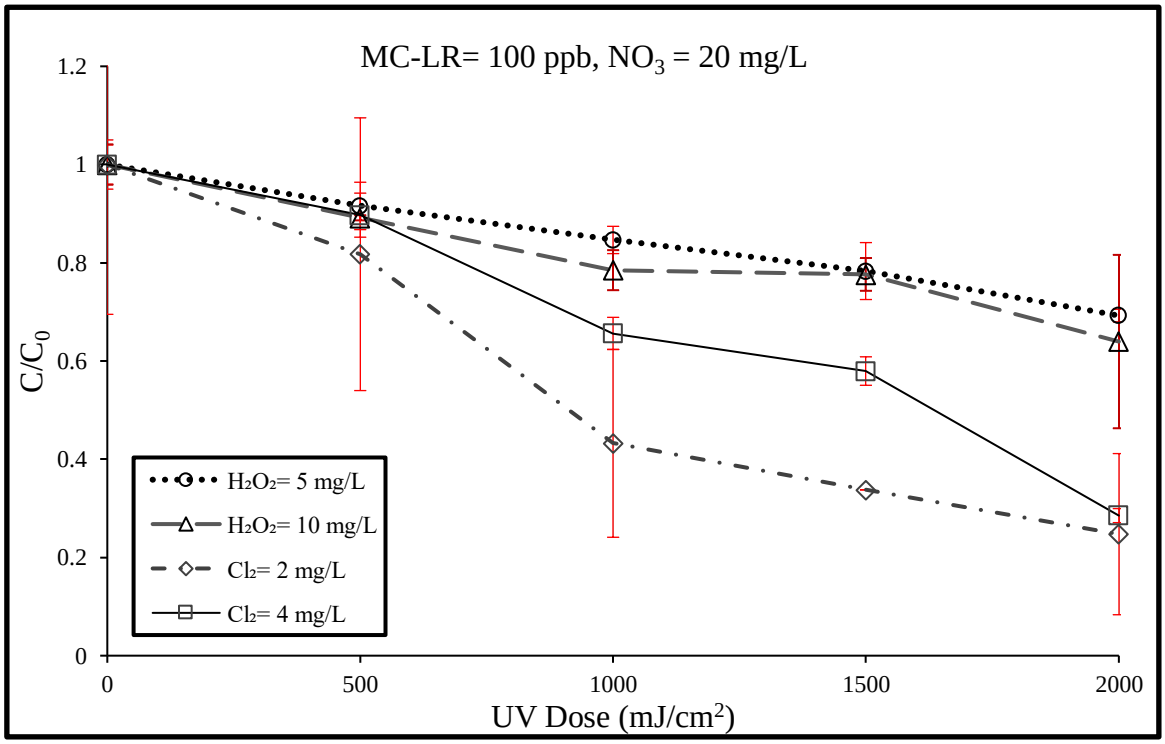

(b)

Figure 13. LC-MS/MS MC-LR under High UV Dose
Data shows the average of three replicates and the error bars are the standard deviations

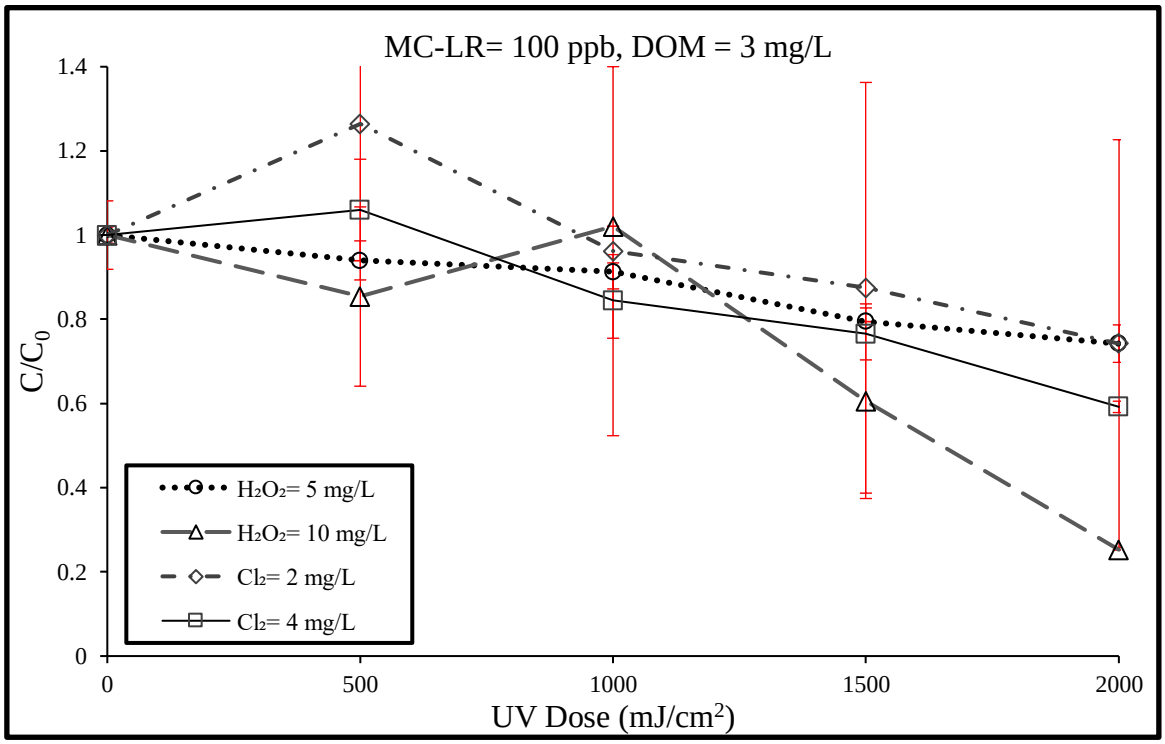

(c)

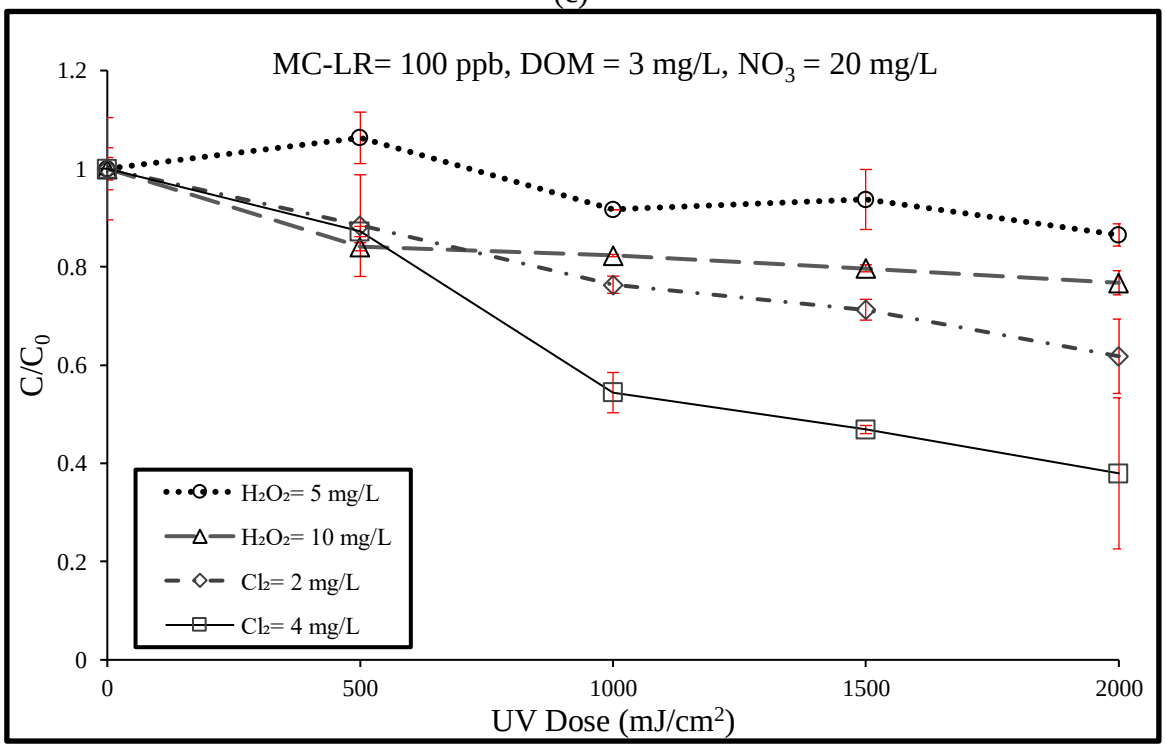

(d)

Figure 13. (Cont'd) LC-MS/MS MC-LR under High UV Dose
Data shows the average of three replicates and the error bars are the standard deviations

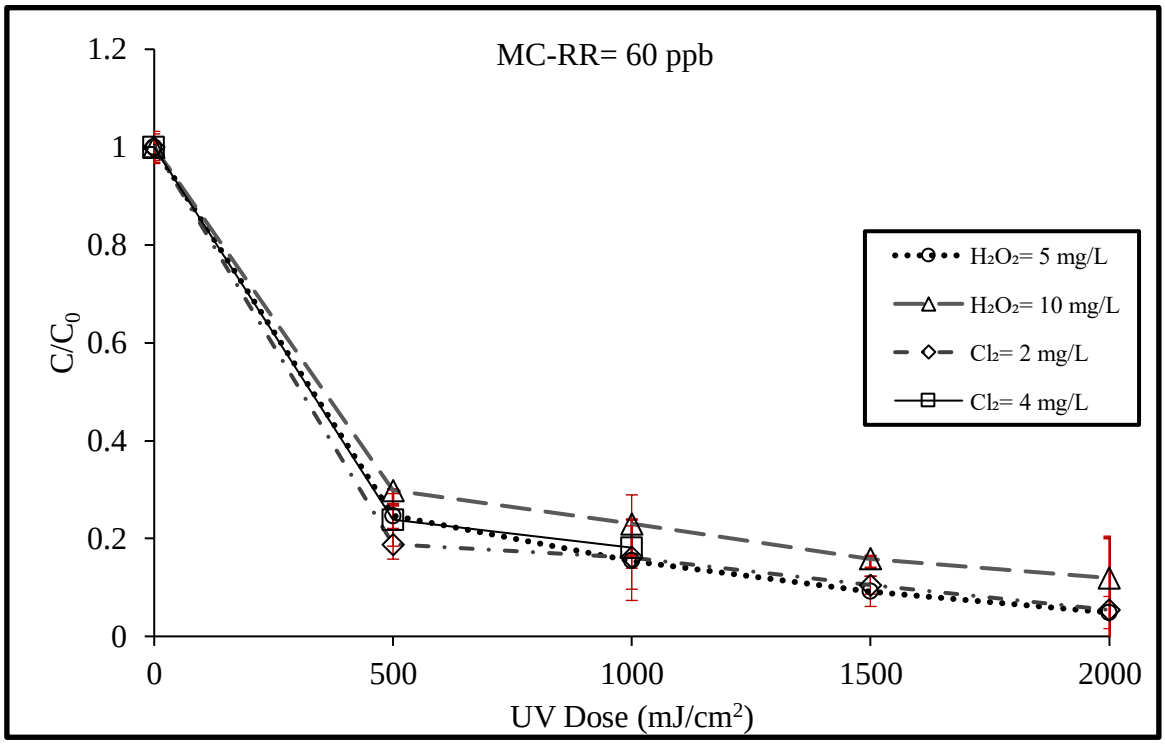

(a)

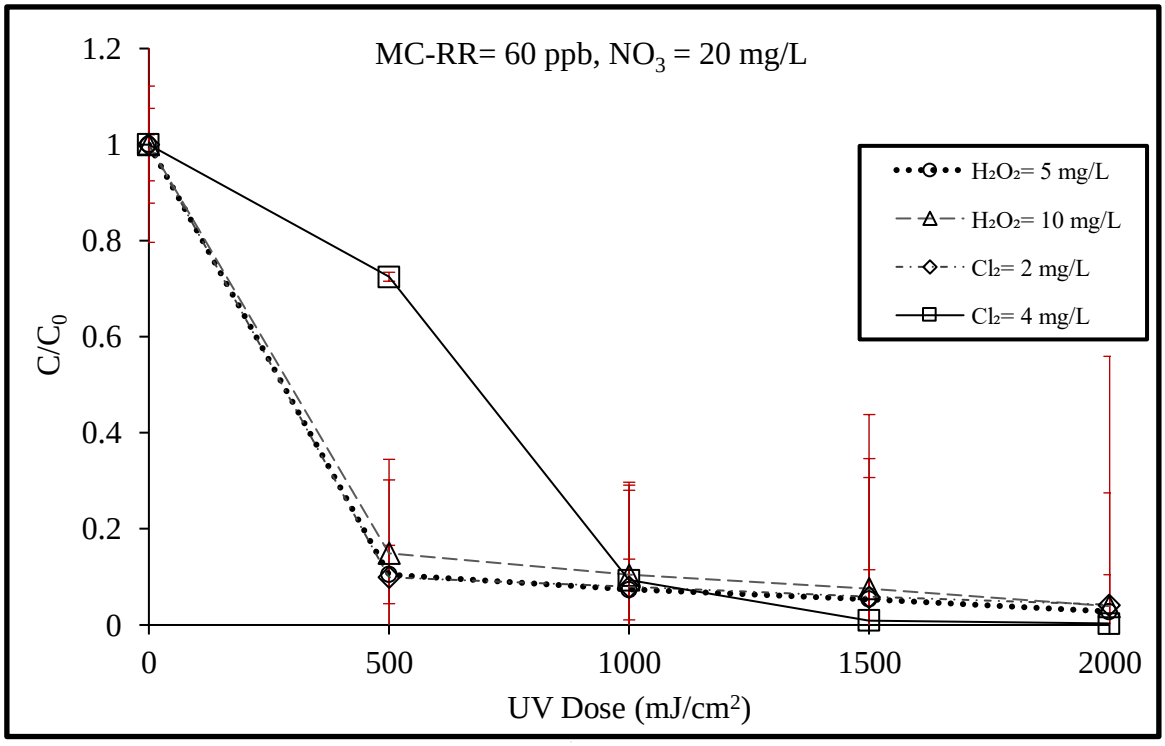

(b)

Figure 14. LC-MS/MS MC-RR under High UV Dose
Data shows the average of three replicates and the error bars are the standard deviations

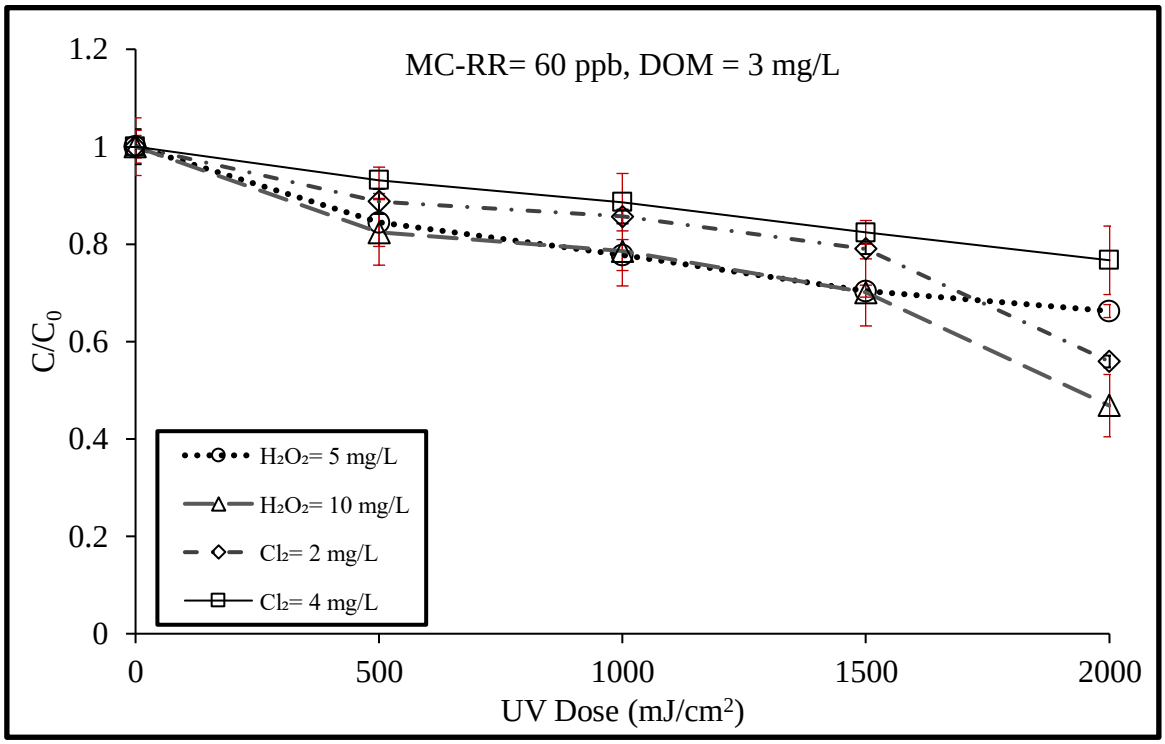

(c)

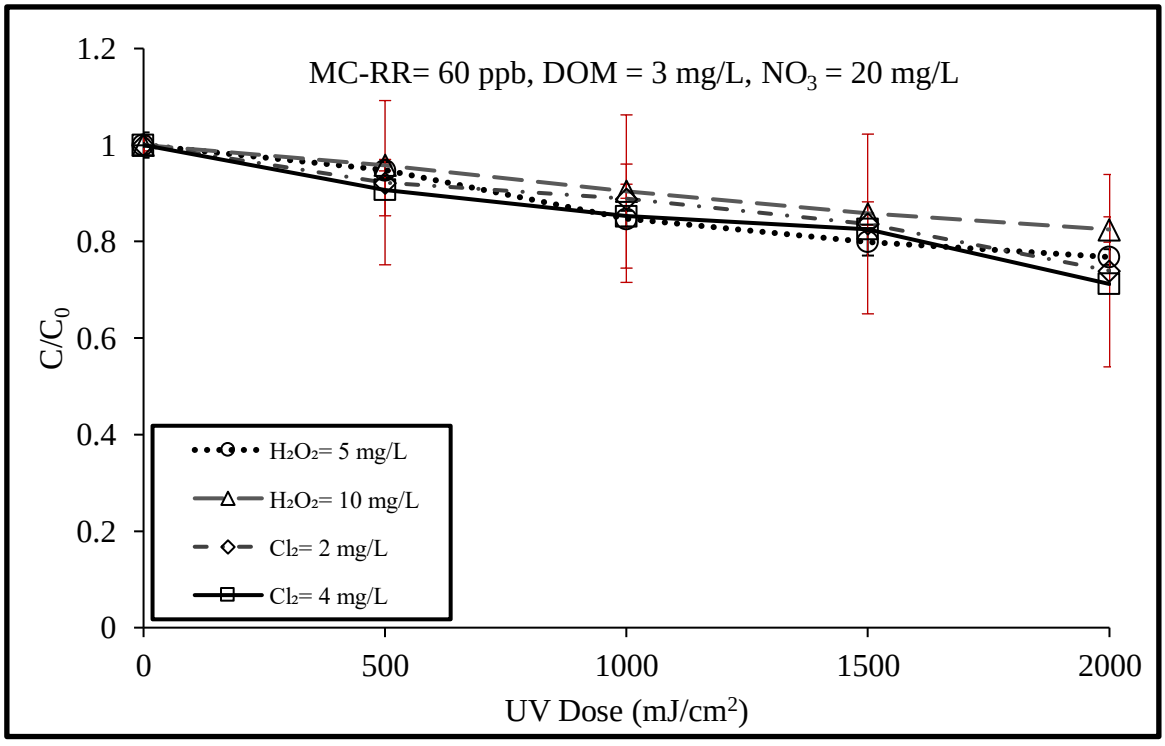

(d)

Figure 14. (Cont'd) LC-MS/MS MC-RR under High UV Dose
Data shows the average of three replicates and the error bars are the standard deviations

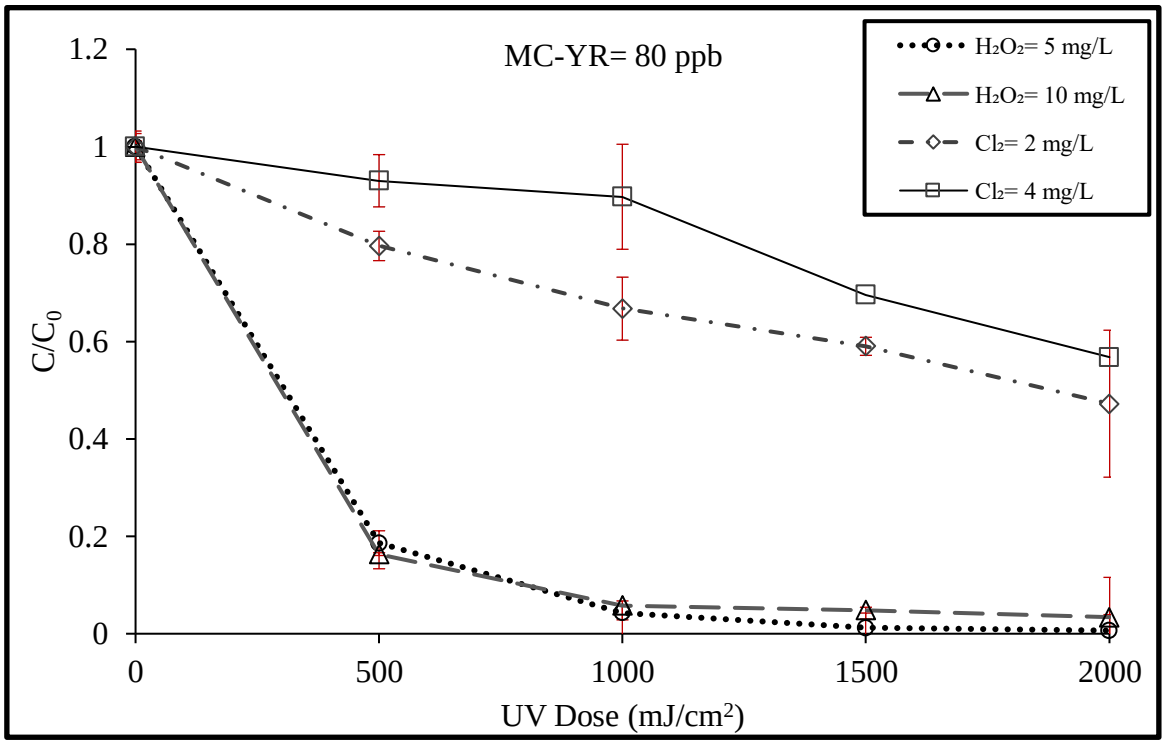

(a)

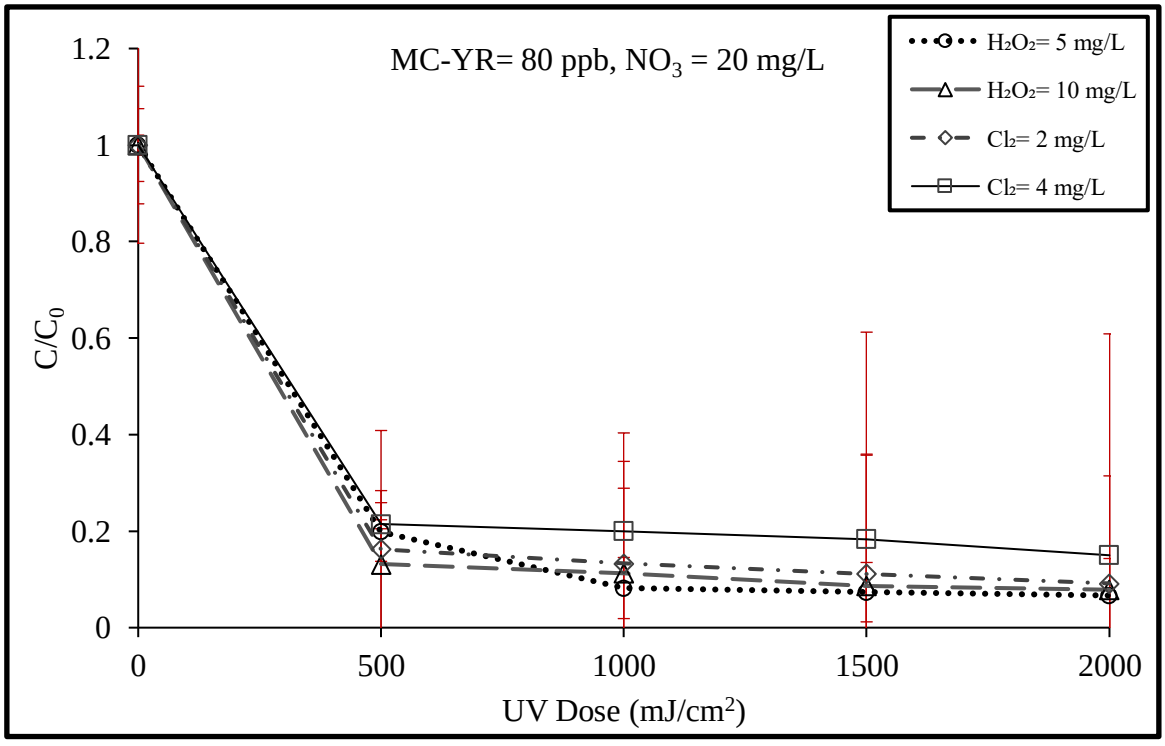

(b)

Figure 15. LC-MS/MS MC-YR under High UV Dose
Data shows the average of three replicates and the error bars are the standard deviations

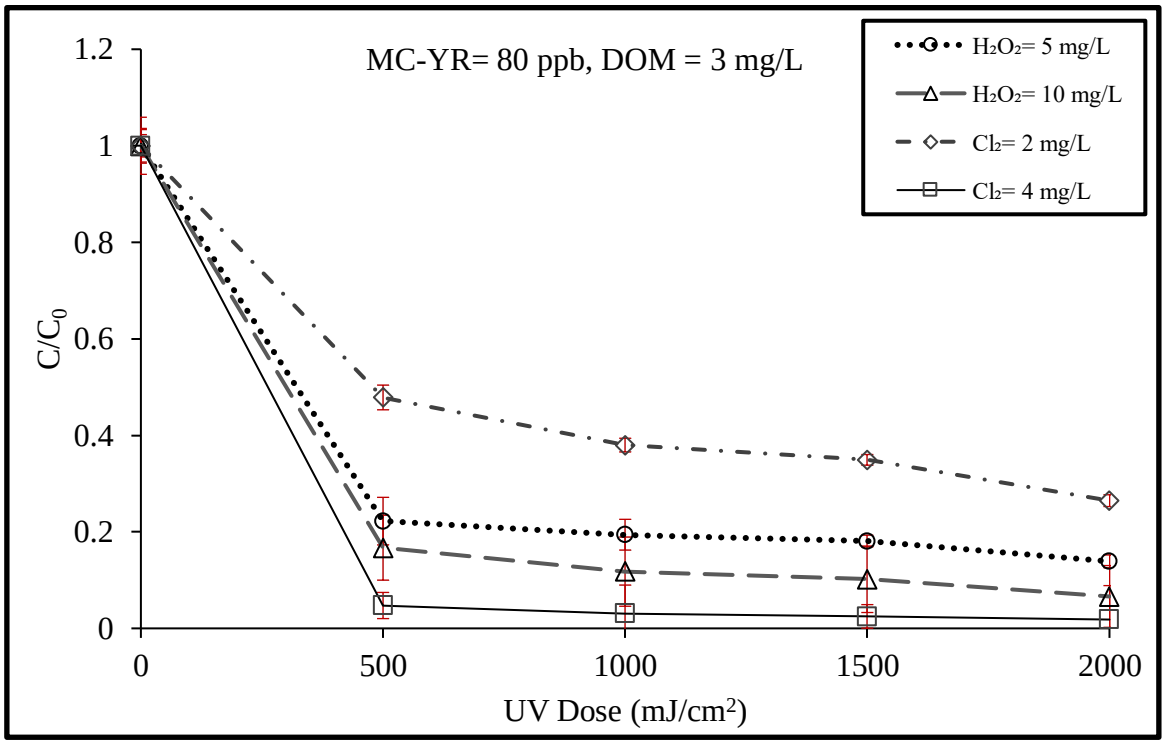

(c)

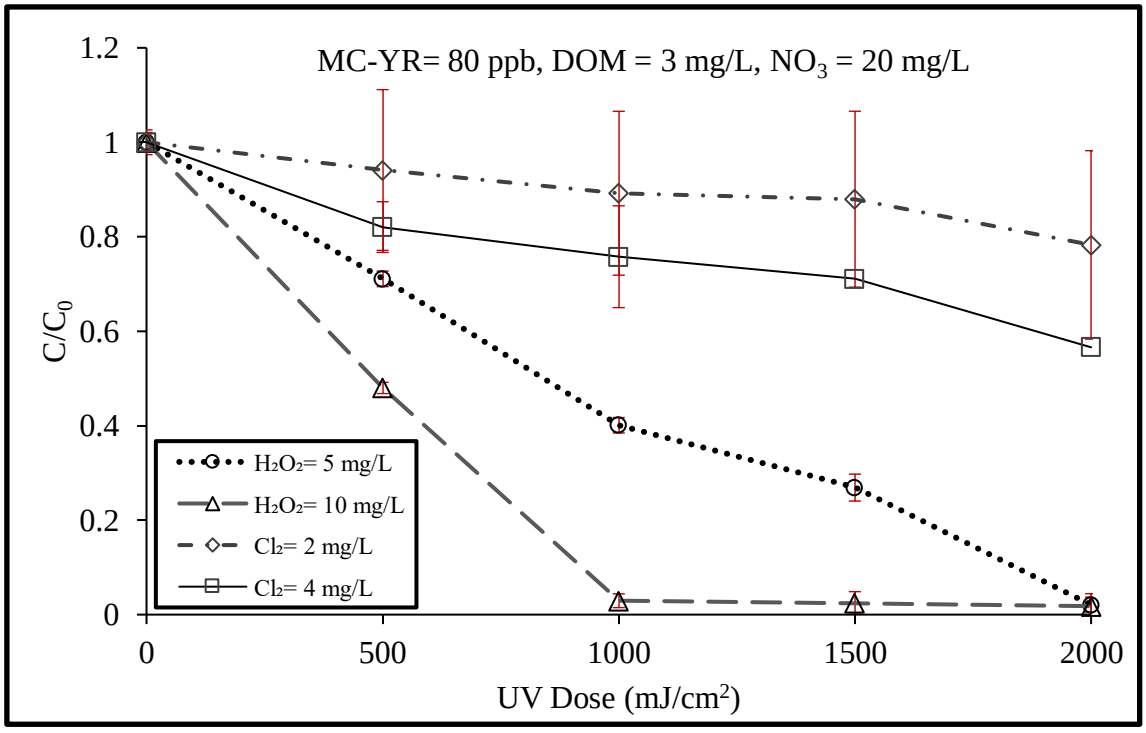

(d)

Figure 15. (Cont'd) LC-MS/MS MC-YR under High UV Dose
Data shows the average of three replicates and the error bars are the standard deviations

As discussed before, UV/Cl_2 was able to remarkably affect MCs removal and appeared to be much more effective compared to UV/H_2O_2. The efficiency of chlorine was investigated by using a lower intensity lamps but approximately the same duration of exposure to oxidants. Figure 16 shows the results of the MC-LR degradation using LP lamps and under disinfection UV dose (up to 30 mJ/cm^2). UV dose of 30 mJ/cm^2 is a commonly used disinfection dose and is too small to initiate any radical reactions.

MC-LR degradation rate under direct UV photolysis is independent of UV irradiance (He et al. 2012). For instance, in a study on degradation of MC-LR, the UV photolysis was $(3.65 \pm 0.21) \times 10^{-3}$ under 0.27 mW/cm^2 and $(3.57 \pm 0.18) \times 10^{-3}$ cm^2/mJ under 0.46 mW/cm^2 UV irradiance (He et al. 2012).

The reaction rate of MC-LR degradation with UV/H_2O_2 process at the two fluence rates has been determined in a previous study (He et al. 2012). The reaction rate of MC-LR degradation with UV/H_2O_2 process followed pseudo-first-order reaction kinetics yielding comparable fluence-based rate constants of $(3.98 \pm 0.20) \times 10^{-2}$ cm^2/mJ and $(3.47 \pm 0.13) \times 10^{-2}$ cm^2/mJ at fluence rates of 0.27 and 0.46 mW/ cm^2, respectively (He et al. 2012).

The result of this section showed that chlorine could degrade microcystins under disinfection UV dose and the addition of chlorine to existing UV disinfection process can remove microcystins. The removal efficiency of UV/Cl_2 at low UV dose derived from the effect of chlorination.

Based on the results of a study on comparison of chlorination and UV/Cl_2 process, the k_{obs} of MC-LR in UV/Cl_2 process at 4 mg/L chlorine dosage was twice of that during chlorination alone (X. Zhang et al. 2019). In mentioned study, the k_{obs} of MC-LR in

chlorination increased from 1.2×10^{-4} s^{-1} to 3.8×10^{-3} s^{-1} with chlorine dosage increasing from 1.0 to 4.0 mg/L (X. Zhang et al. 2019).

The same result have not been observed for UV/H_2O_2 under the low UV dose conditions because the hydroxyl radicals were not generated at a sufficient level at this dose, and the results primarily indicate that there is no direct oxidation of MCs by H_2O_2, unlike Cl_2 that has a pronounced direct oxidation reaction with some MCs. Also, under the LP UV lamps no possibility of creating advanced oxidation conditions was expected; however, some reaction, potentially AOP, was observed by the addition of nitrate to water.

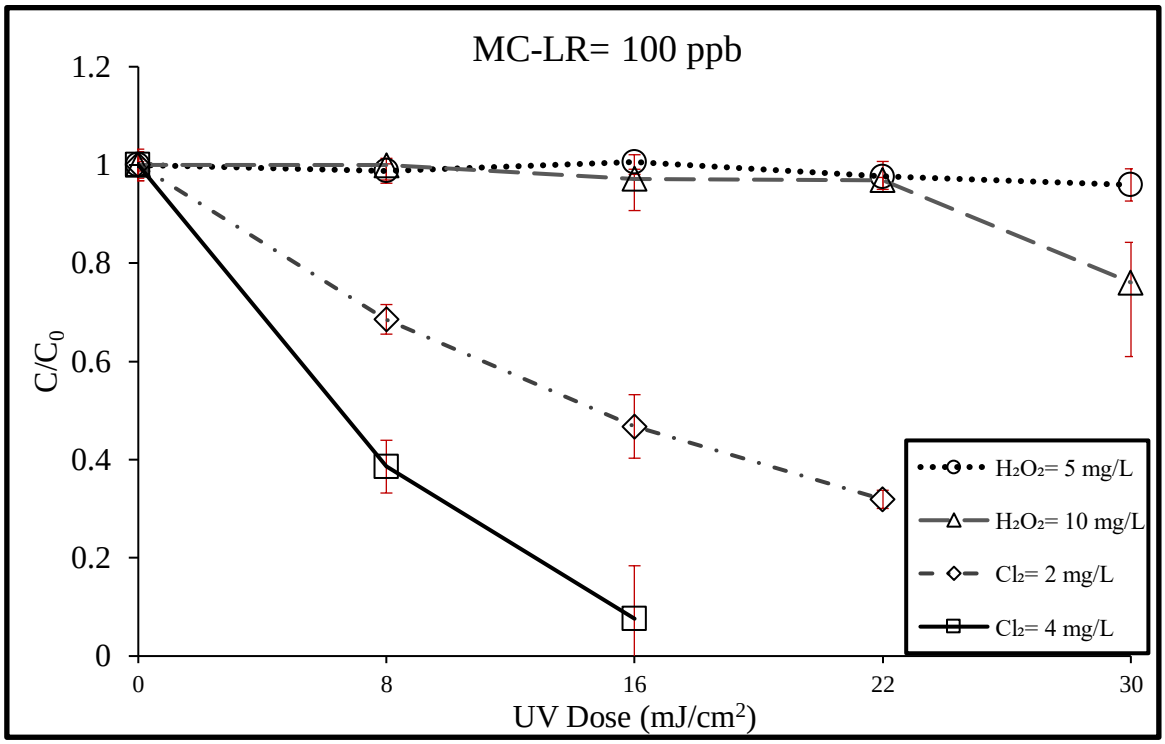

(a)

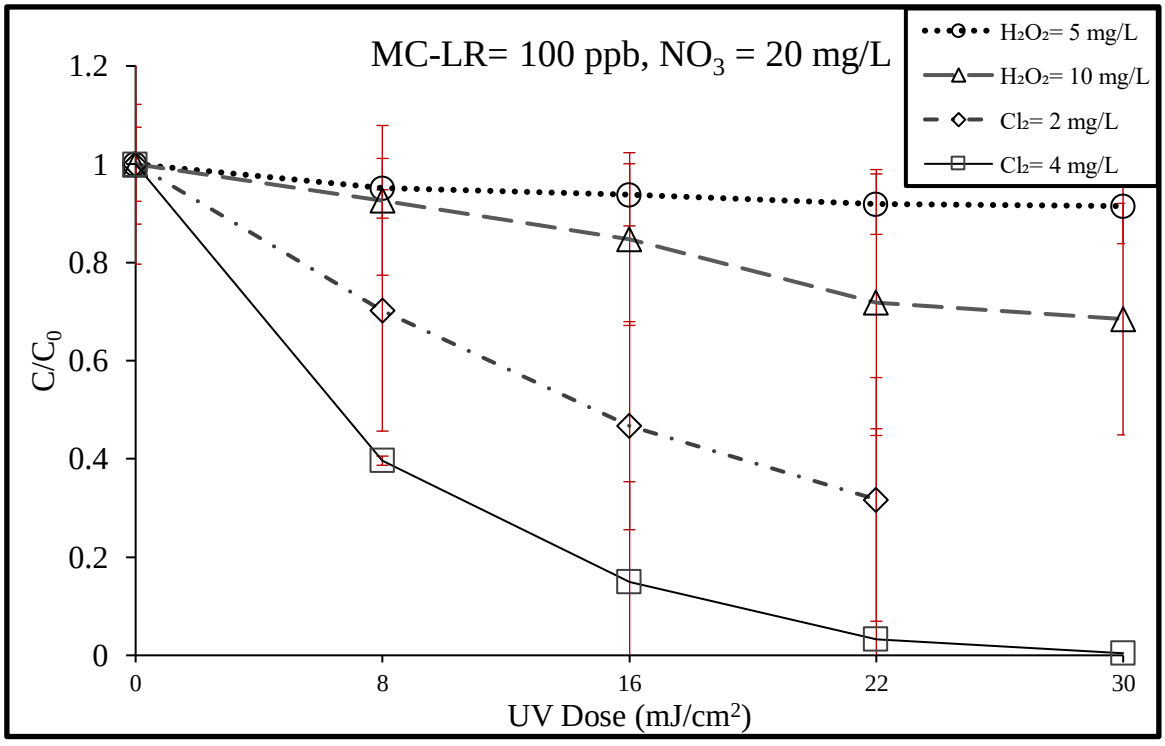

(b)

Figure 16. LC-MS/MS MC-LR under Low UV Dose
Data shows the average of three replicates and the error bars are the standard deviations

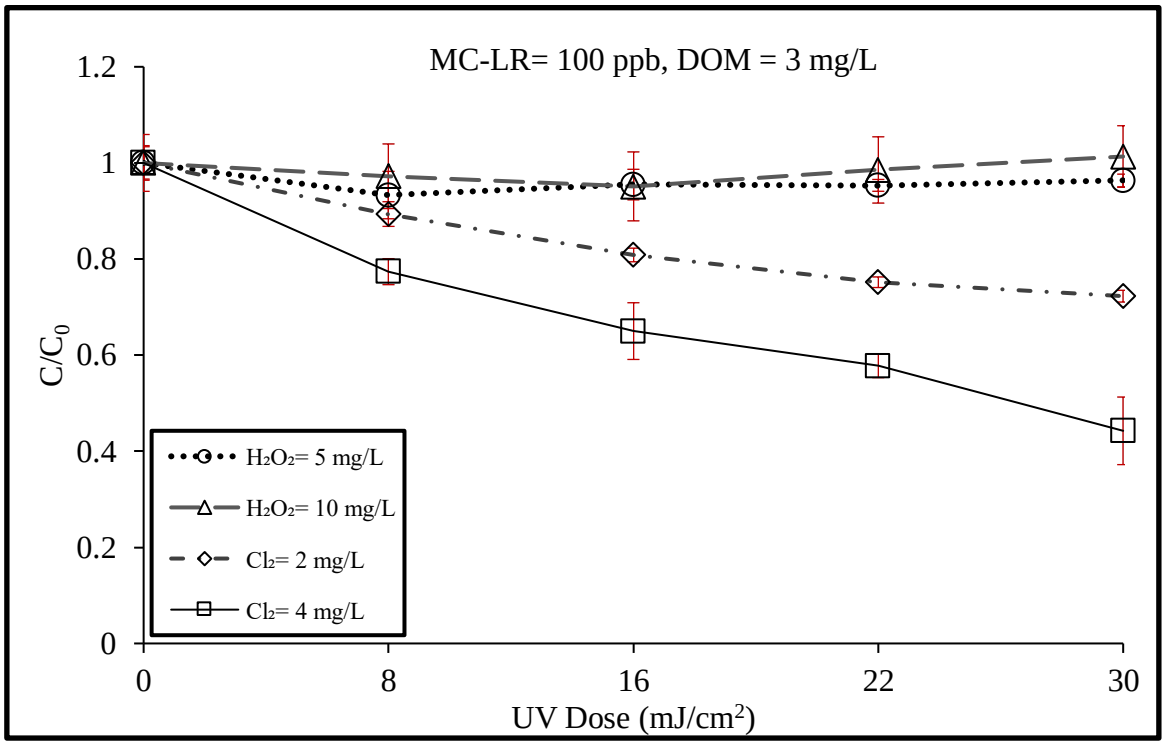

(c)

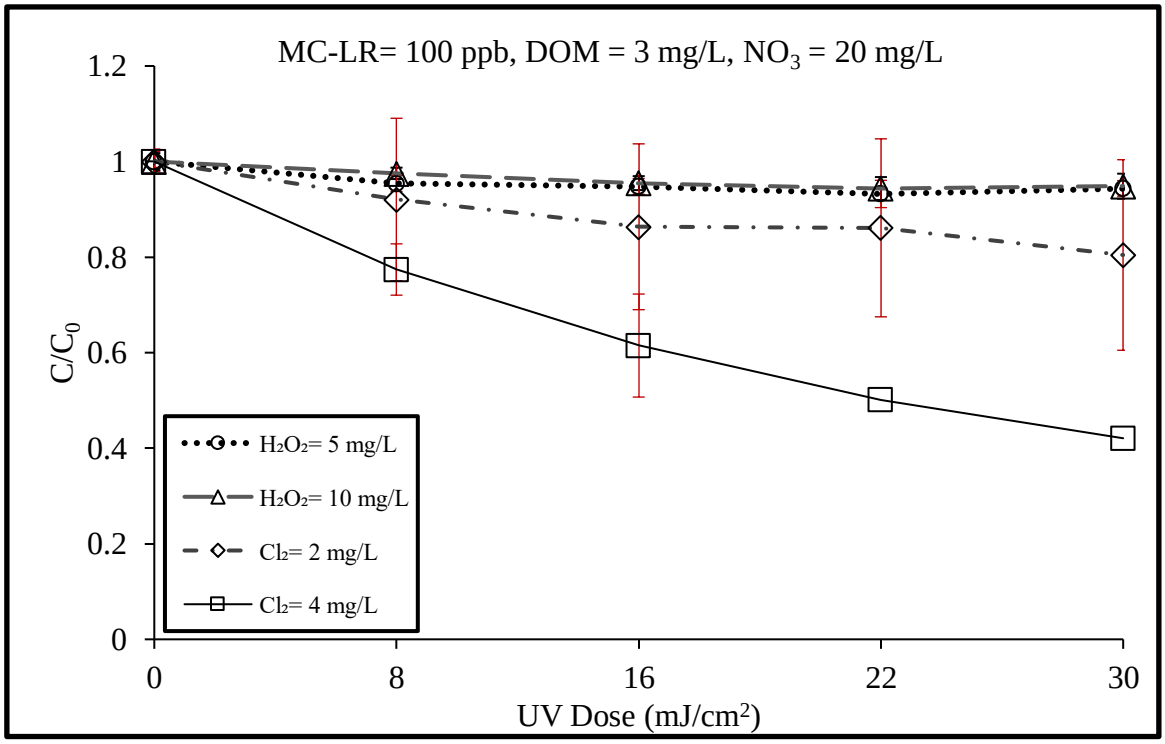

(d)

Figure 16. (Cont'd) LC-MS/MS MC-LR under Low UV Dose
Data shows the average of three replicates and the error bars are the standard deviations

4.2. Transformation Products for MC-LR Degradation during UV/Cl_2 process

Degradation byproducts of MC-LR during the UV/Cl_2 process were determined using fragmentation results obtained by LC-MS/MS for MC-LR degradation. During the UV/Cl_2 process, three main byproducts with m/z values of 796.5, 762.4, and 748.4 were formed. They are very close in retention time to the parent compound but still separate. For product analysis, a more extended gradient was required to separate the products thoroughly.

Low $[M+H]^+$ value (m/z) of < 360 was not detected by LC-MS/MS which is in line with previous studies on UV-based AOP (Merel et al. 2010; Moon et al. 2017).

As shown in Figure 17, susceptible sites to degradation and initiation of the MC-LR oxidation are diene bond, methoxy group of Adda, Arg amino acids, MeAsp Leu, Mdha Ala, and Arg-MeAsp peptide bonds (Kumar et al. 2018).

The structure of MC-LR is combined with a cyclic heptapeptide having seven amino acids. One of these amino acids is amino-9-methoxy-2,6,8-trimethyl-10-phenyl-4,6-decadienoic acid (Adda) that shows the toxicity by conjugated diene on the Adda side chain (Carmichael and An 1999). Therefore if a byproduct contains Adda functional groups, it would be biologically toxic (Sedan et al. 2015). The byproduct with m/z value of 762.4 was formed by loss of the Adda group in (C_5) with ring-opening, which presumably makes it less toxic compared to the parent compound. The methyl group that was part of the Adda group remained on m/z 762.4, but it is not expected to add toxicity to the product. Byproduct with m/z 748.4 likely forms from the product with the m/z value of 762.4, followed by the elimination of the methyl group.

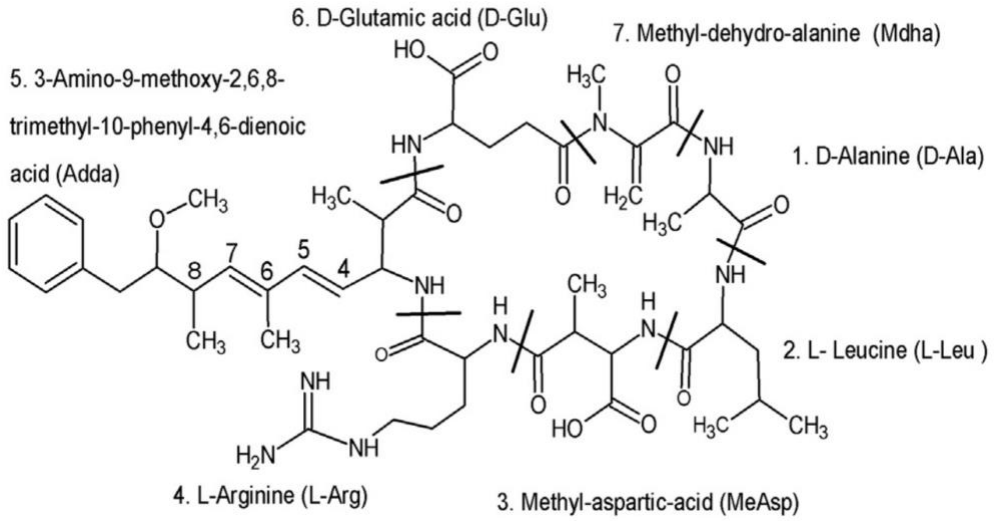

Figure 17. Susceptible Sites to Photocatalytic Degradation and Initiation of the MC-LR Oxidation (Chang et al. 2014)

The parent molecule, MC-LR, has the m/z value of 995 that is an odd number, and the products have even m/z values, which means that there was nitrogen loss from the structure and an odd number of nitrogen atoms has been lost. Chlorine prefers to attack double bonds and amines. Nitrogen atoms within the ring structure are not as accessible for chlorine attack as the ones on the external functional group. The byproduct with the m/z value of 796.5 can be formed by the bond cleavage of the C_4-C_5 bond in Adda in the MC-LR molecule (Moon et al. 2017). Hydroxyl radical is the primary reason for the ring-opening in complex MC-LR compound. (Kumar et al. 2018).

Variable amino acids in the structure of MCs can change the reaction pathway (He et al. 2015). For example, tyrosine in MC-YR results in monohydroxylation byproduct m/z 1061 formation during the UV/H_2O_2 process. However, the presence of a second arginine in MC-RR results in guanidine group loss and the absence of double bond cleavage byproducts (He et al. 2015).

Figure 18 – a shows the reactive sites observed in this study under chlorination of MC-LR in background matrix, including (1) loss of the Adda group with ring opening and methyl group remaining, (2) double bond cleavage and potential chlorination site and (3) the loss of the triamine. Figure 18 – b shows the reactive sites observed under 2000 mJ/cm^2 UV dose and Cl_2 = 4 mg/L. MC-LR degradation pathways included (1) chlorine addition, (2) Loss of Adda and triamine, (3) loss of triamine and break of double bond, and (4) loss of the benzene ring and triamine. Figure 18 – c shows the MC-LR degradation pathways under 2000 mJ/cm^2 UV dose and H_2O_2 = 10 mg/L. The structure transformation included (1) loss of Adda, (2) loss of hydrazine and Adda and nitrogen, (3) carbon-nitrogen bond cleavage.

Figure 18 – d shows MC-YR degradation pathway under 2000 mJ/cm^2 UV dose and Cl_2 = 4 mg/L that included (1) loss of the Adda, (2) loss of the Adda and triamine and double bond cleavage double bond cleavage and potential chlorination site and (3) the loss of tyrosine. Figure 18 – e shows the MC-YR degradation pathways under 2000 mJ/cm^2 UV dose and H_2O_2 = 10 mg/L. The structure transformation included (1) loss of Adda and arginine, (2) loss of rings and nitrogen.

Further study with higher concentration spikes could provide a more detailed analysis of the transformation products and pathways.

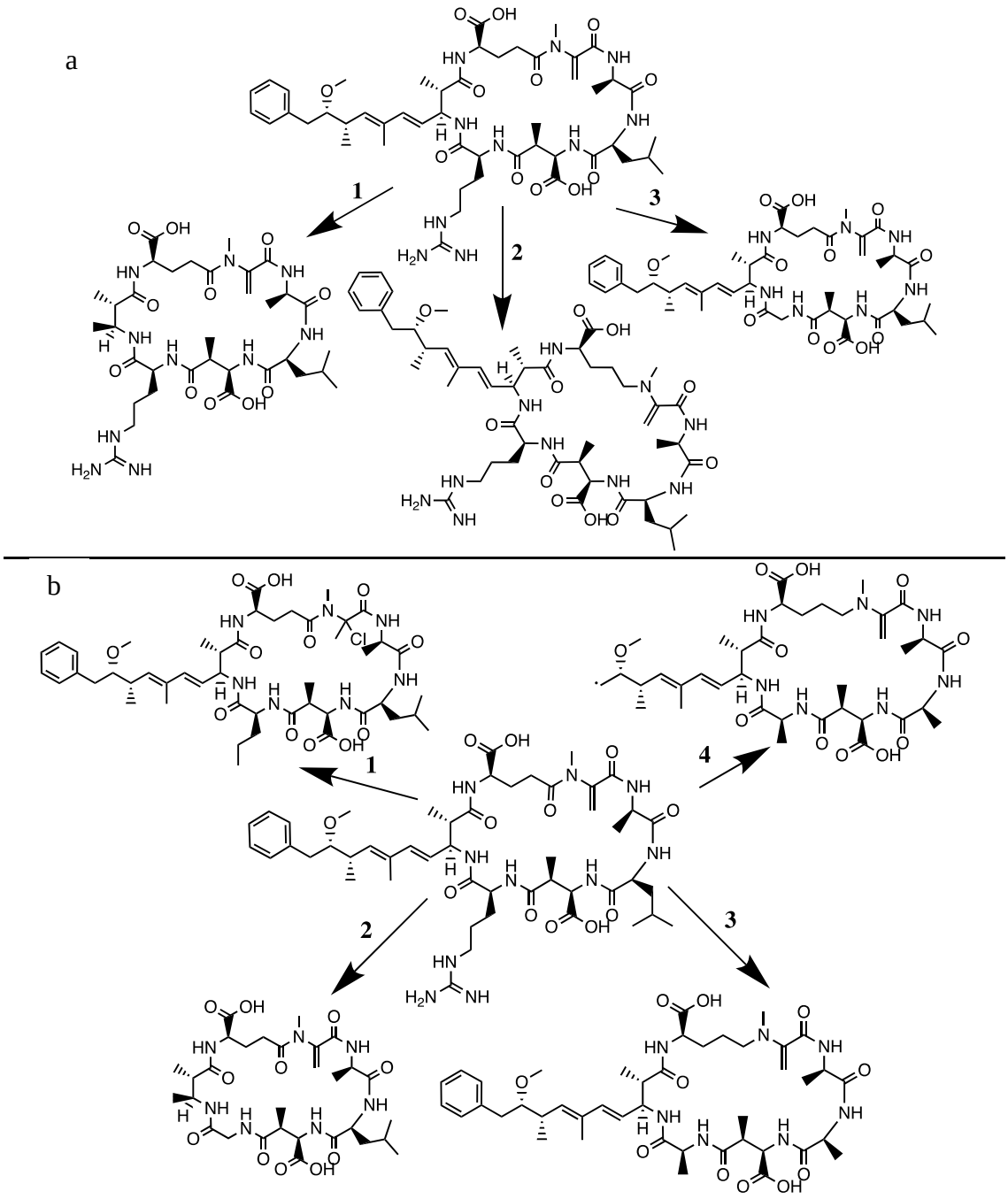

Figure 18. Structure Transformation; a) MC-LR under Cl_2= 4 mg/l, b) MC-LR under 2000 mJ/cm_2 UV Dose and Cl_2 = 4 mg/L c) MC-LR under 2000 mJ/cm_2 UV Dose and H_2O_2 = 10 mg/L, d) MC-YR under 2000 mJ/cm_2 UV Dose and Cl_2 = 4 mg/L, e) MC-YR under 2000 mJ/cm_2 UV Dose and H_2O_2 = 10 mg/L

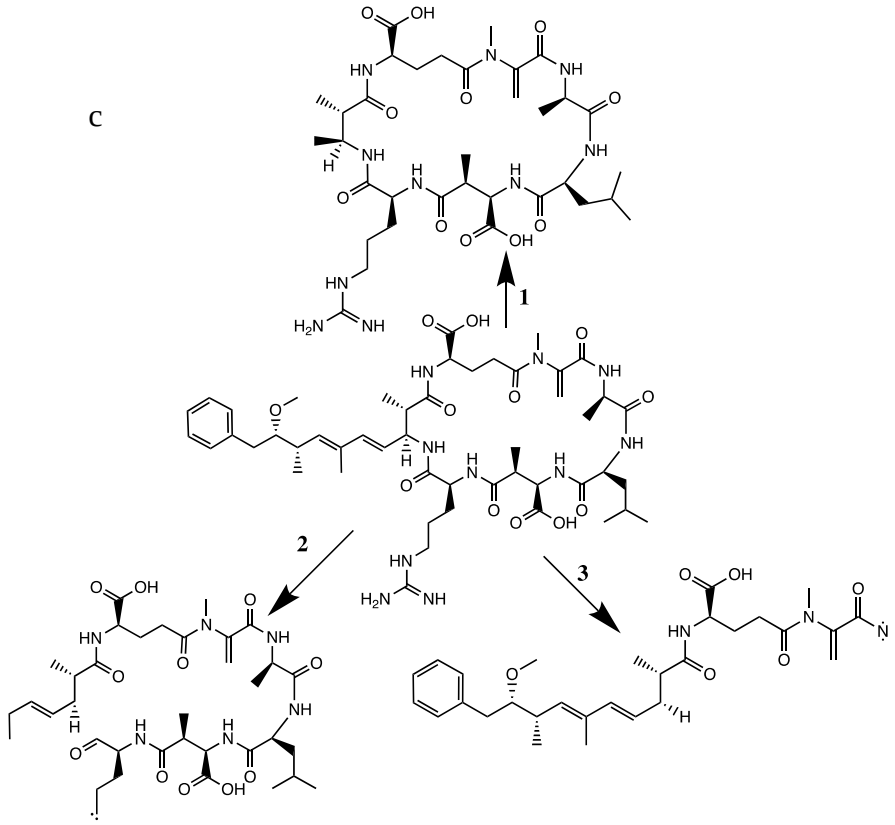

Figure18. (Cont'd) Structure Transformation; a) MC-LR under Cl_2= 4 mg/l, b) MC-LR under 2000 mJ/cm_2 UV Dose and Cl_2 = 4 mg/L c) MC-LR under 2000 mJ/cm_2 UV Dose and H_2O_2 = 10 mg/L, d) MC-YR under 2000 mJ/cm_2 UV Dose and Cl_2 = 4 mg/L, e) MC-YR under 2000 mJ/cm_2 UV Dose and H_2O_2 = 10 mg/L

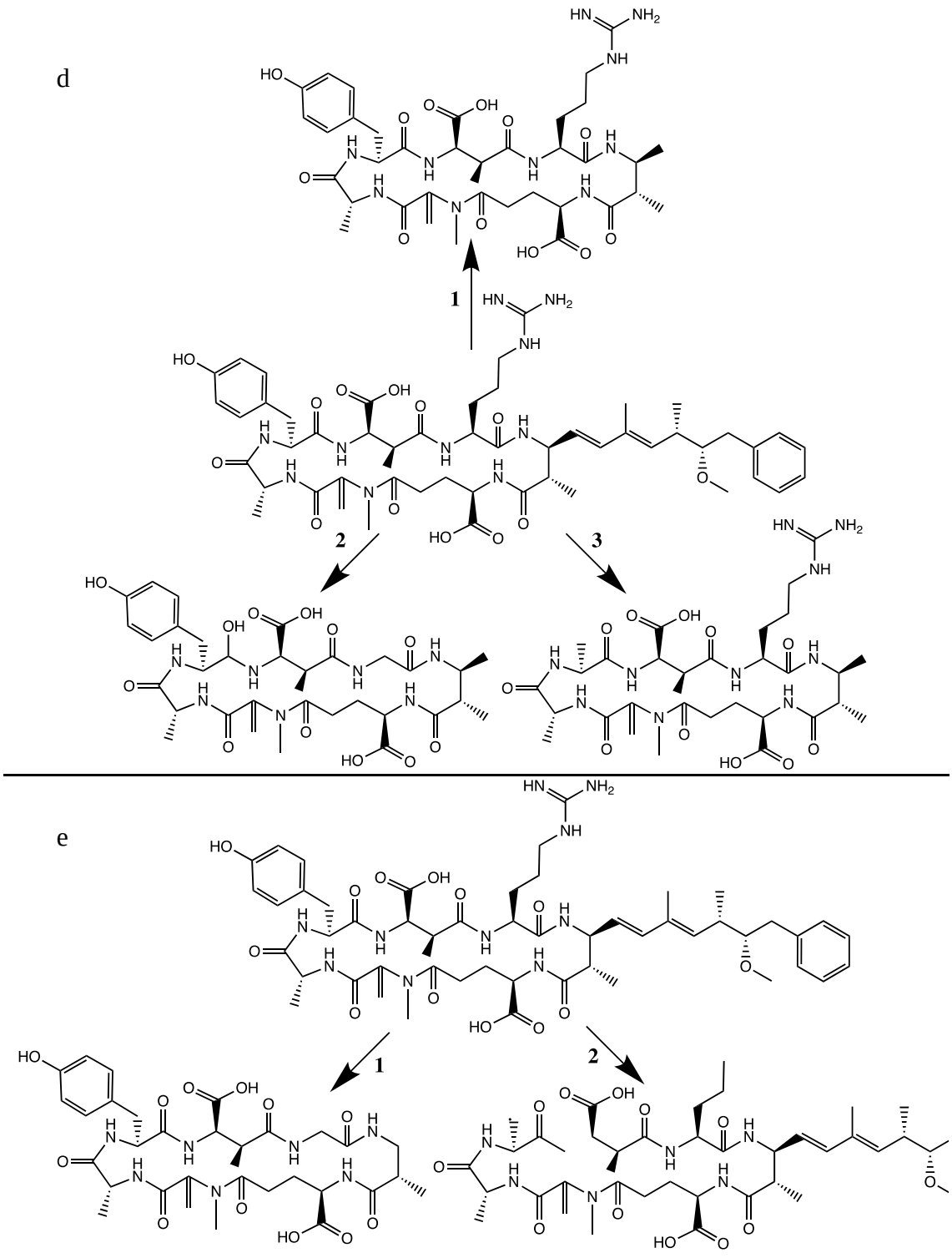

Figure18. (Cont'd) Structure Transformation; a) MC-LR under Cl_2= 4 mg/l, b) MC-LR under 2000 mJ/cm_2 UV Dose and Cl_2 = 4 mg/L c) MC-LR under 2000 mJ/cm_2 UV Dose and H_2O_2 = 10 mg/L, d) MC-YR under 2000 mJ/cm_2 UV Dose and Cl_2 = 4 mg/L, e) MC-YR under 2000 mJ/cm_2 UV Dose and H_2O_2 = 10 mg/L

4.3.Toxicity of Treated Samples

4.3.1. PP2A (Hepatotoxicity)

Cyanotoxins are mainly classified into three groups, including hepatotoxic peptides, neurotoxins, and contact irritants that are based on their significant toxicological impact (Carmichael and Boyer 2016). Hepatotoxins MCs can act as tumor promotors as they can inhibit protein phosphatases (Carmichael and Boyer 2016). Protein phosphatase inhibition assays (PP2A), ELISA (Carmichael and An 1999), LC-MS/MS (Carmichael and Boyer 2016), quantitative PCR (Lu et al. 2020), and real-time PCR (Qi et al. 2016) are useful methods to analyze hepatotoxins MCs. The following graphs (Figures 19-24) are showing the hepatotoxicity of the water samples after treatment using PP2A.

As mentioned earlier, higher concentration of toxins inhibits more PP2A and decreases the fluorescence intensity. Fluorescence intensity indicates the activity of protein phosphatase with fluorescent substrate (Carmichael and An 1999). The fluorescence intensity in relation to the MC-LR degradation was increasing by UV irradiation that indicates the positive effect of treatment on MC-LR (Figure 19). However, addition of DOM, nitrate, or both may decrease the positive effect of treatment process (Figure 19) and the reason might be that produced byproducts are more toxic than parent products.

The replacement of the second amino acid leucine in MC-LR with arginine (MC-RR) intensifies hepatotoxicity and could cause greater damage to the kidney (Atencio et al. 2008). Figure 21 shows the effect of the matrix and UV dose on hepatotoxicity of the products after MC-RR degradation. High dose of UV irradiation using MP lamp for these sets of samples resulted in a positive effect of both UV/H_2O_2 and UV/Cl_2 on hepatotoxicity of samples even when DOM or nitrate was in the matrix (Figure 21).

However, when both DOM and nitrate were in matrix (Figure 21) the hepatotoxicity of products were slightly higher than untreated sample and PP2A inhibition decreases the activity of protein phosphatase with fluorescent substrate.

The effect of matrix and UV dose during UV/H_2O_2 and UV/Cl_2 on MC-YR is shown in Figure 23 and Figure 24. Almost all of the samples were showing decrease in the fluorescence intensity after treatment and higher level of treatment resulted in higher hepatotoxicity. The only exception is when UV and Cl_2 = 4 mg/L is used for treatment of matrix containing nitrate (Figure 23 – b). Further studies are required to investigate the possible toxic products. PP2A results were not reproducible enough to draw definitive conclusions on the toxicity of the products.

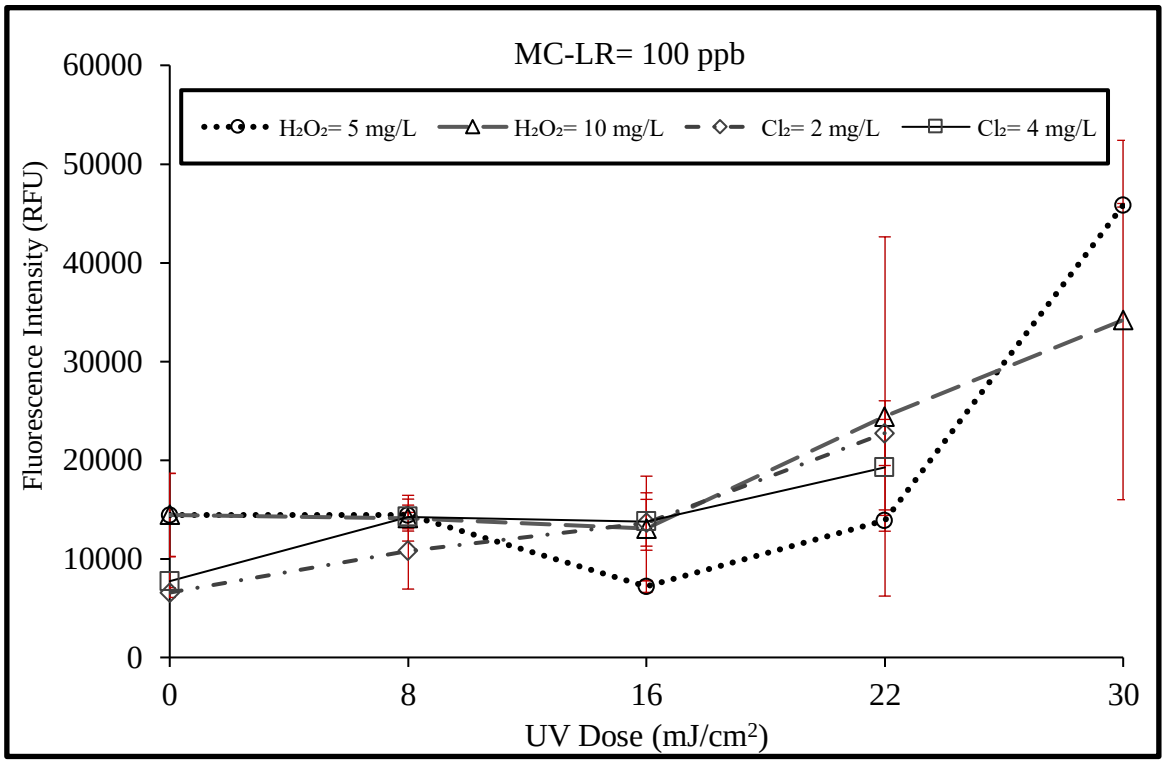

(a)

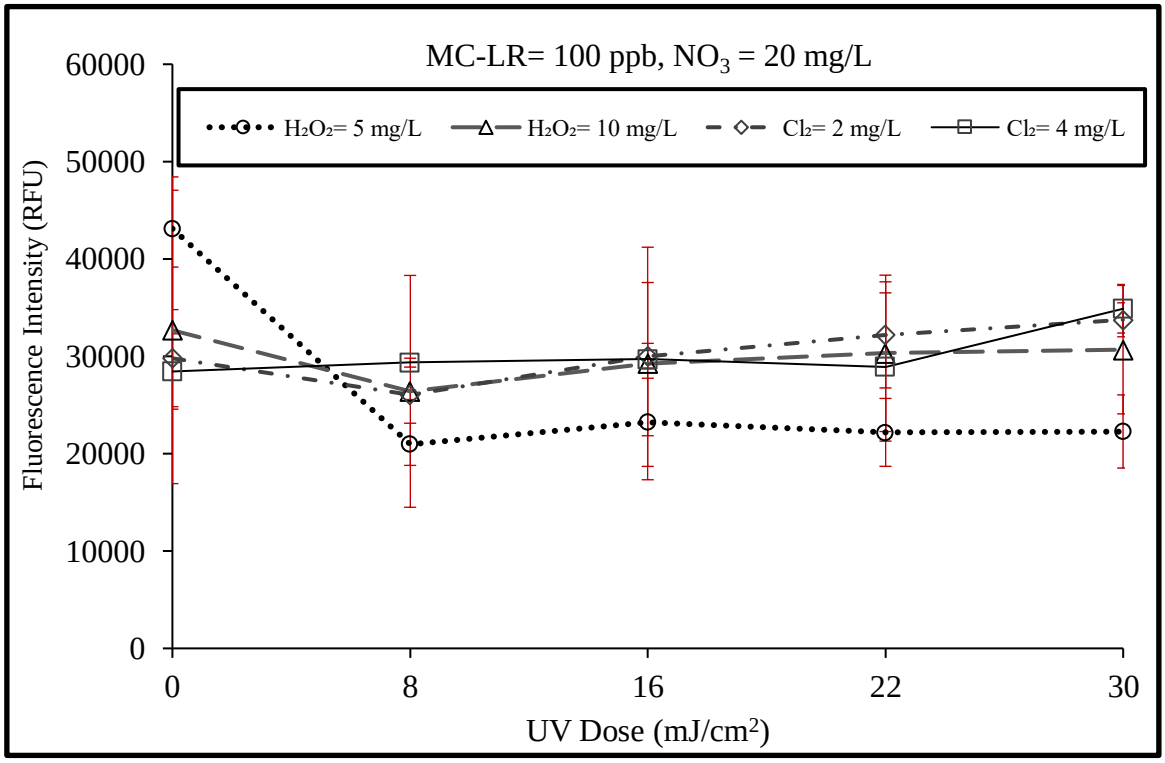

(b)

Figure 19. Effect of Matrix and UV Dose for Different Processes on Hepatotoxicity of Products after MC-LR Degradation

Data shows the average of three replicates and the error bars are the standard deviations.

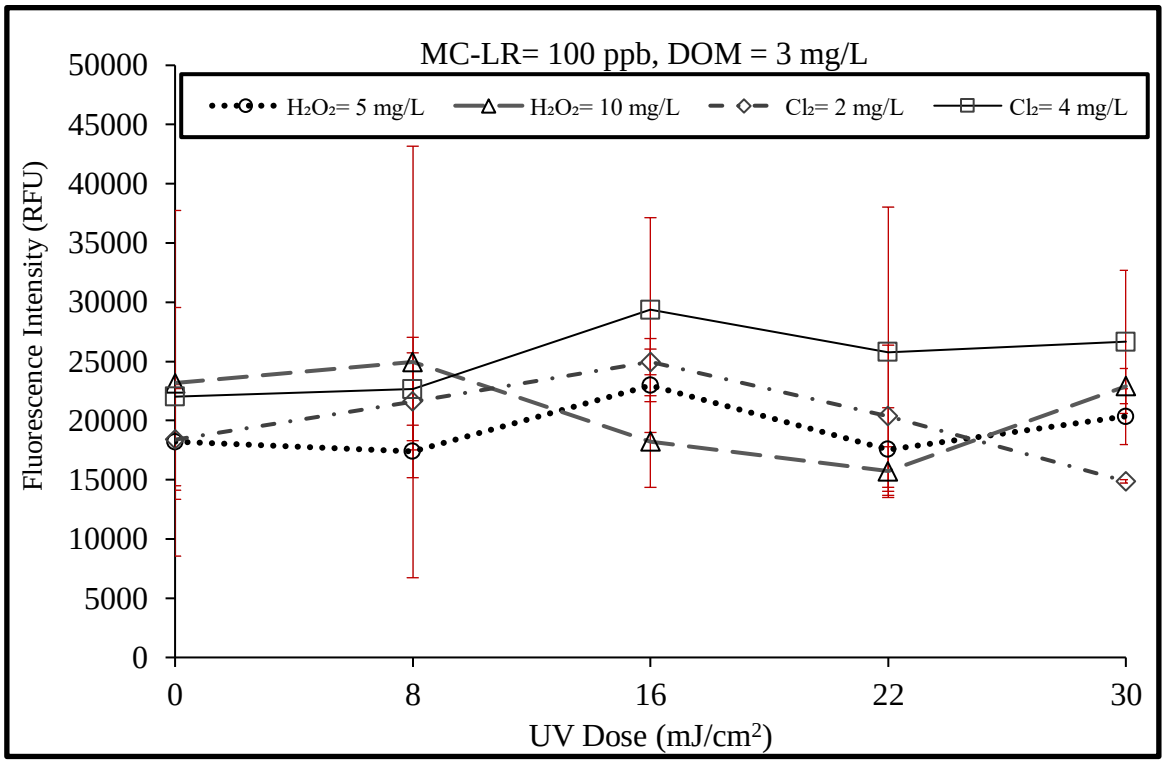

(c)

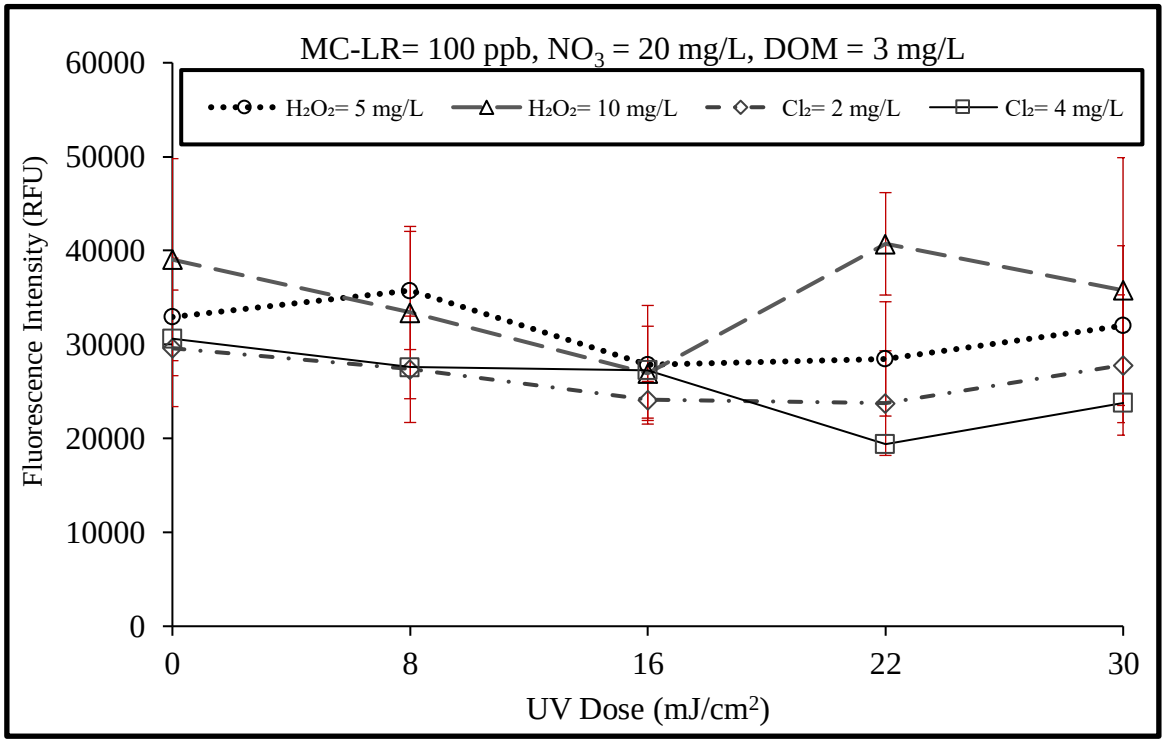

(d)

Figure 19. (Cont'd) Effect of Matrix and UV Dose for Different Processes on Hepatotoxicity of Products after MC-LR Degradation
Data shows the average of three replicates and the error bars are the standard deviations.

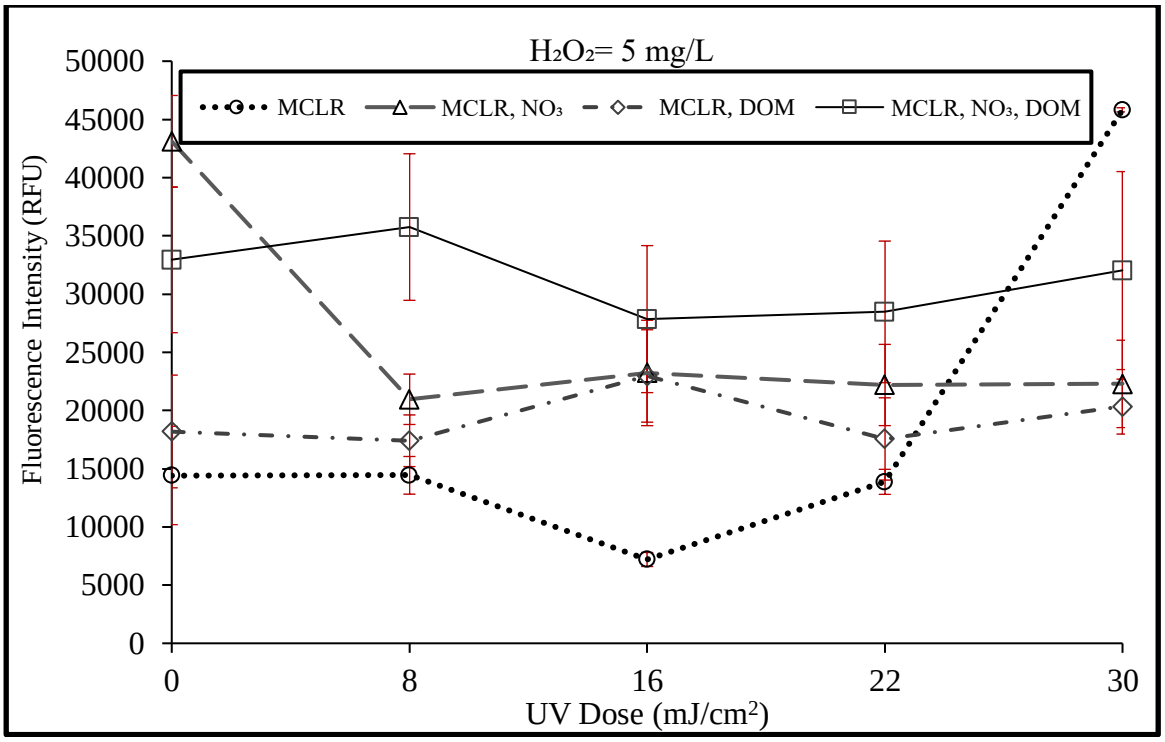

(a)

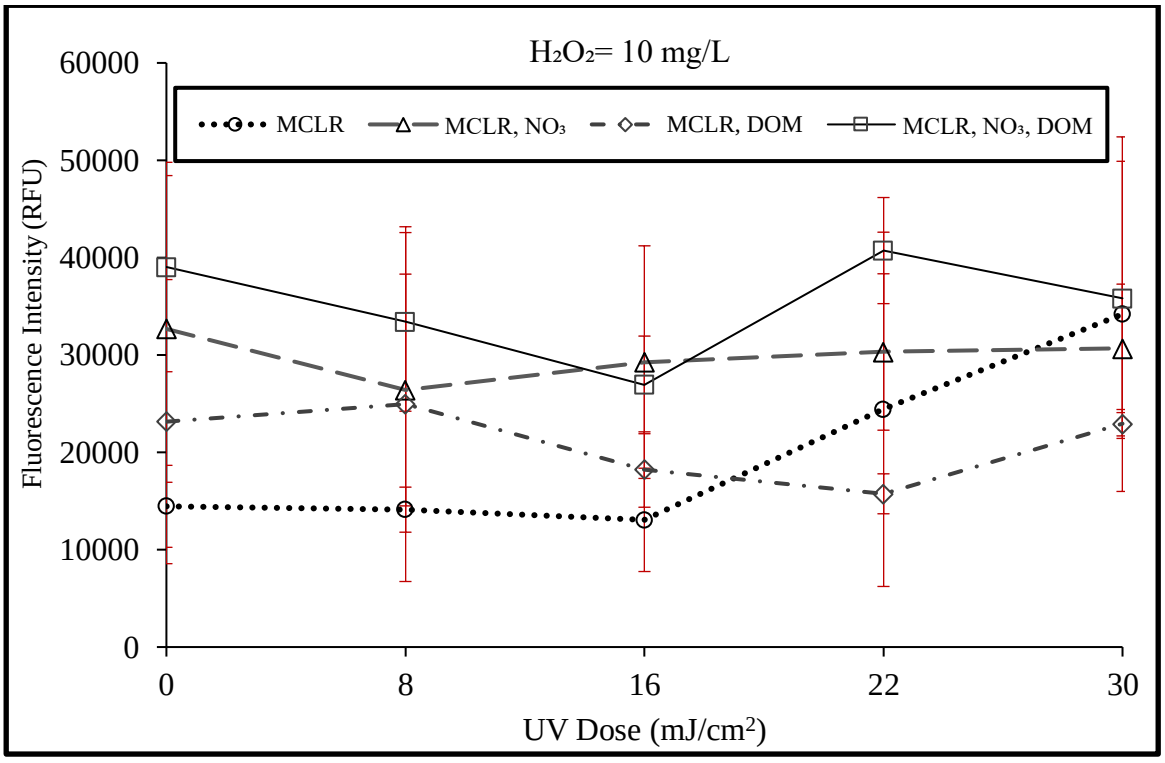

(b)

Figure 20. Effect of Processes at Given UV Dose and Matrix on Hepatotoxicity of Products after MC-LR Degradation

Data shows the average of three replicates and the error bars are the standard deviations.

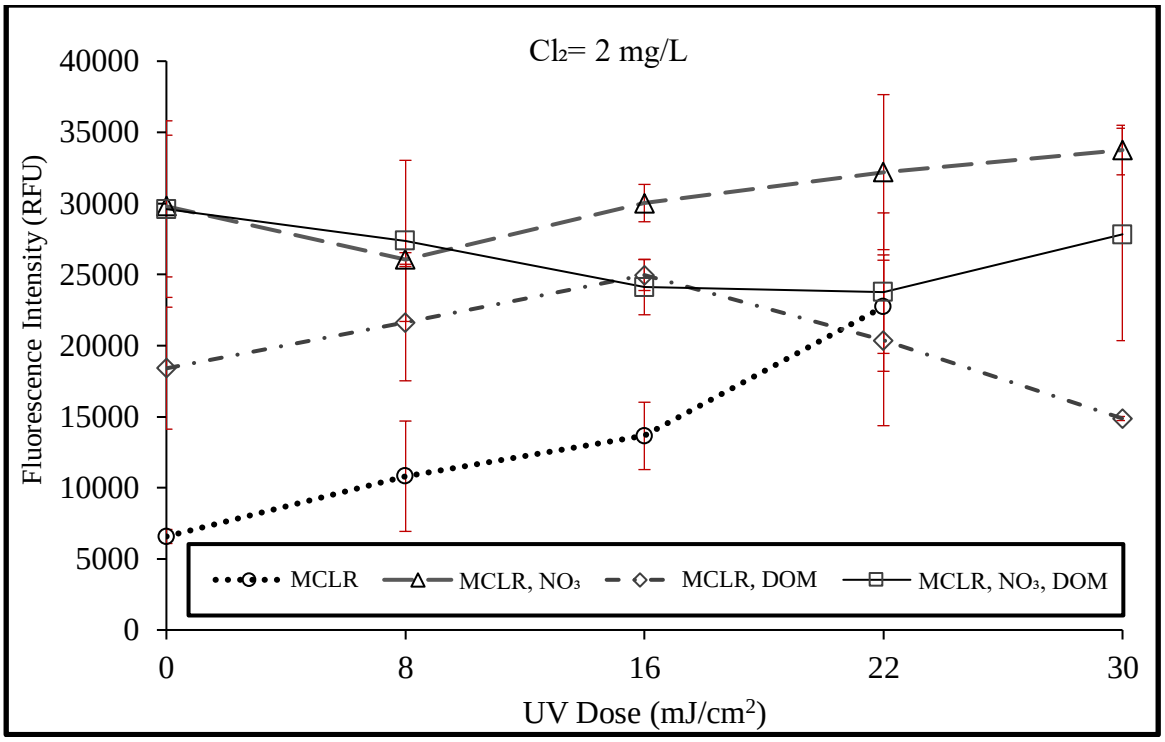

(c)

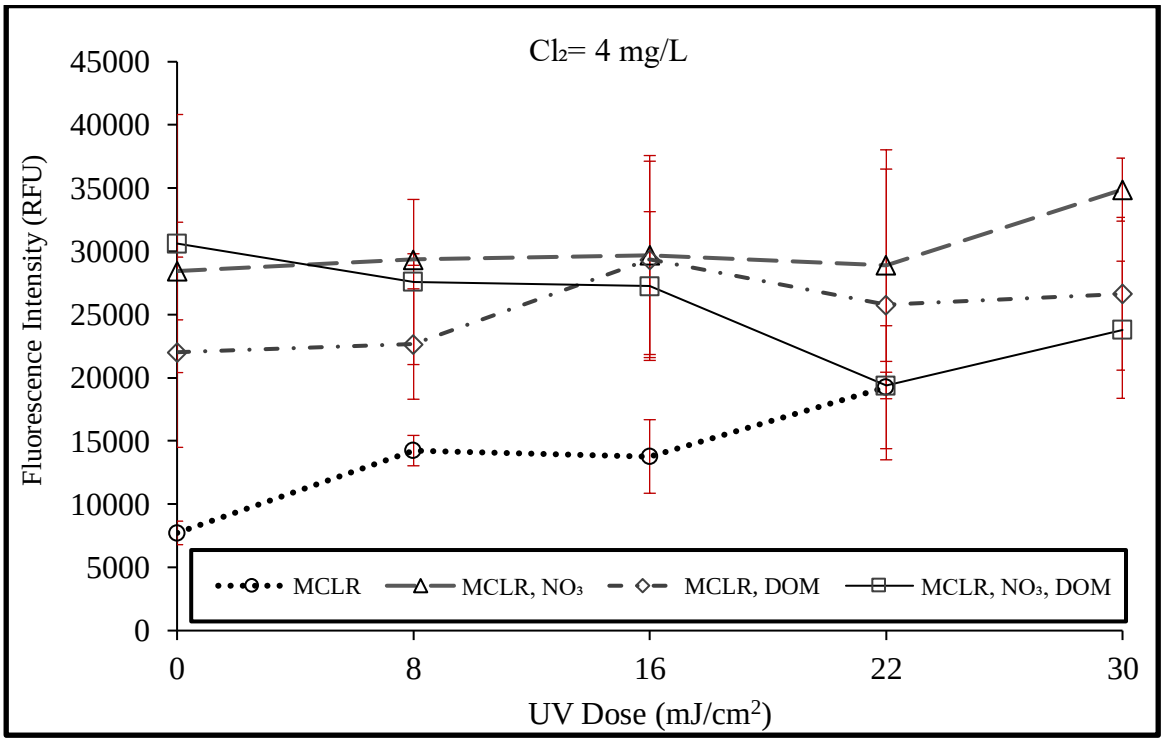

(d)

Figure 20. (Cont'd) Effect of Processes at Given UV Dose and Matrix on Hepatotoxicity of Products after MC-LR Degradation
Data shows the average of three replicates and the error bars are the standard deviations.

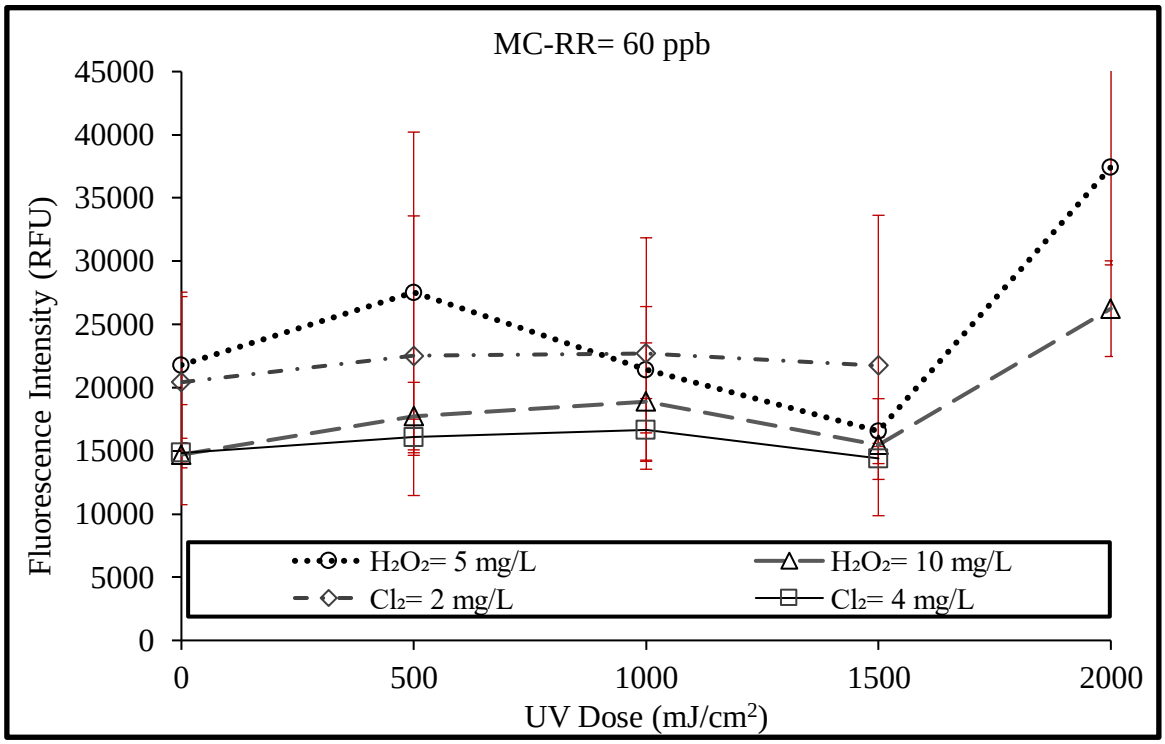

(a)

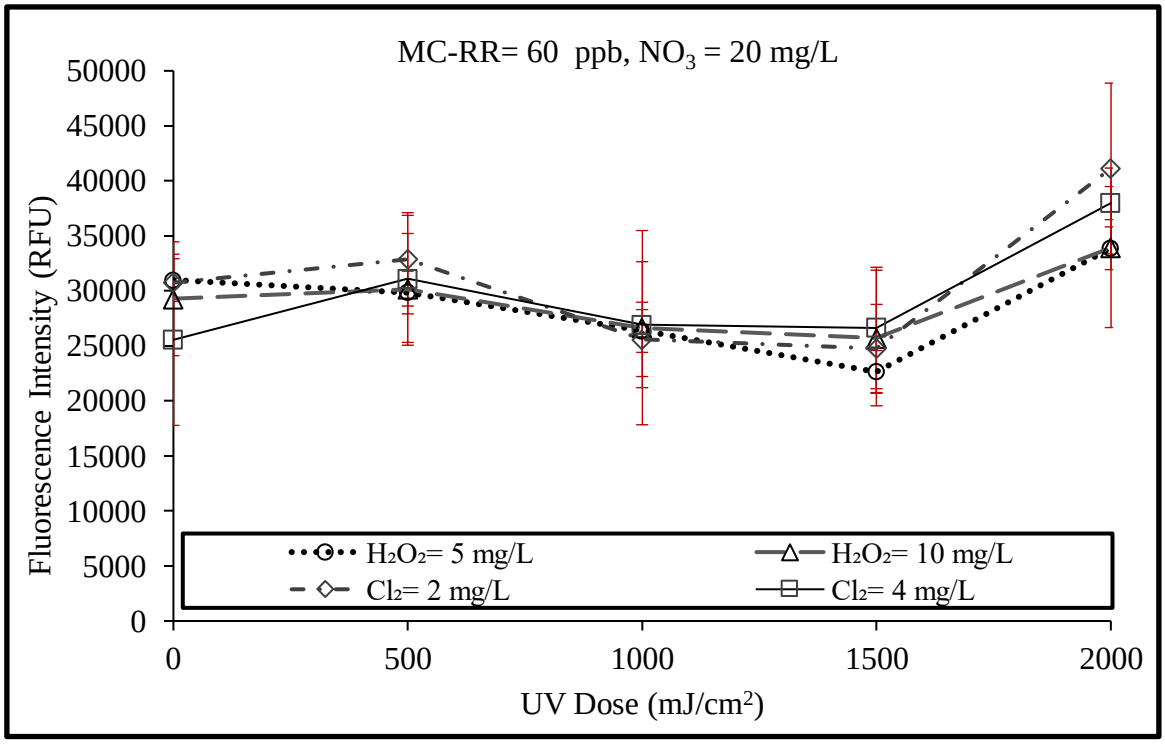

(b)

Figure 21. Effect of Matrix and UV Dose for Different Processes on Hepatotoxicity of Products after MC-RR Degradation

Data shows the average of three replicates and the error bars are the standard deviations.

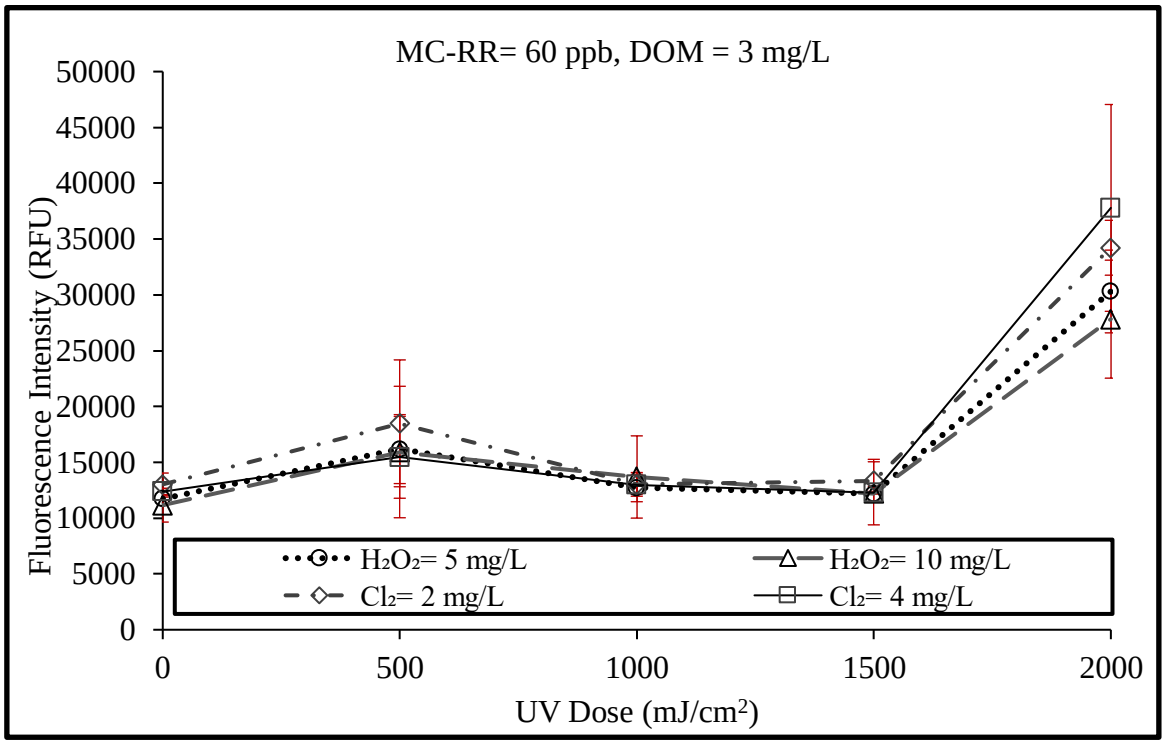

(c)

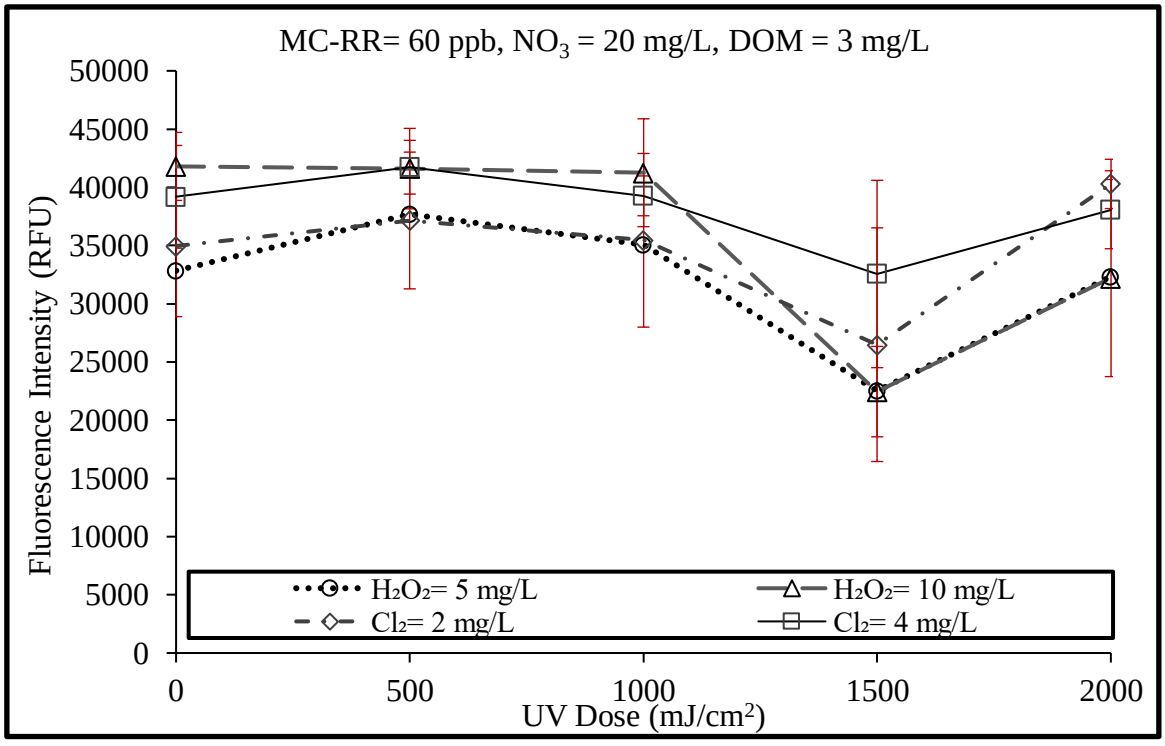

(d)

Figure 21. (Cont'd) Effect of Matrix and UV Dose for Different Processes on Hepatotoxicity of Products after MC-RR Degradation
Data shows the average of three replicates and the error bars are the standard deviations.

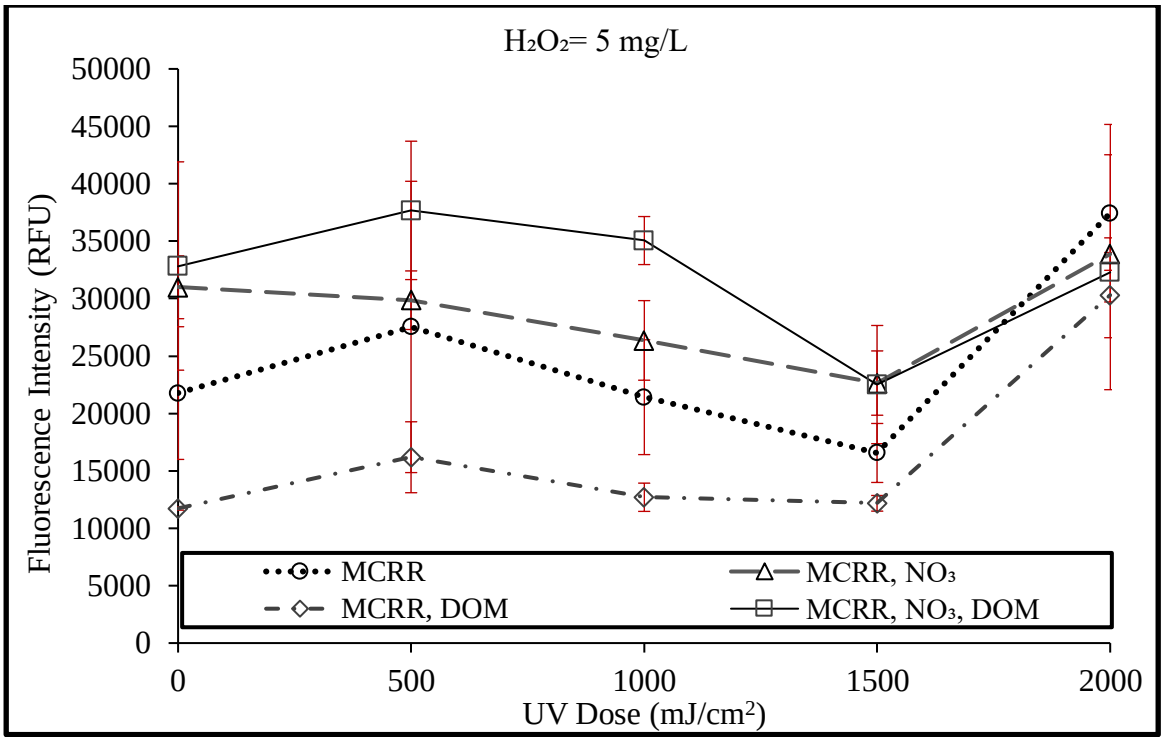

(a)

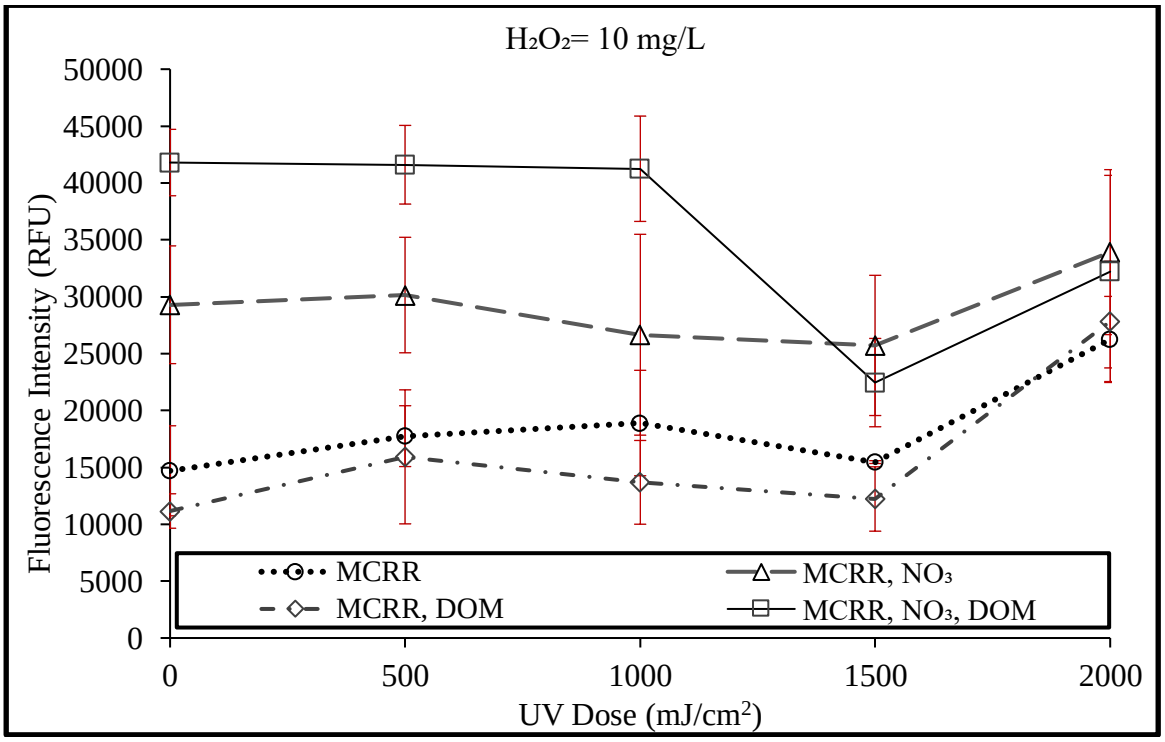

(b)

Figure 22. Effect of Processes at Given UV Dose and Matrix on Hepatotoxicity of Products after MC-RR Degradation
Data shows the average of three replicates and the error bars are the standard deviations.

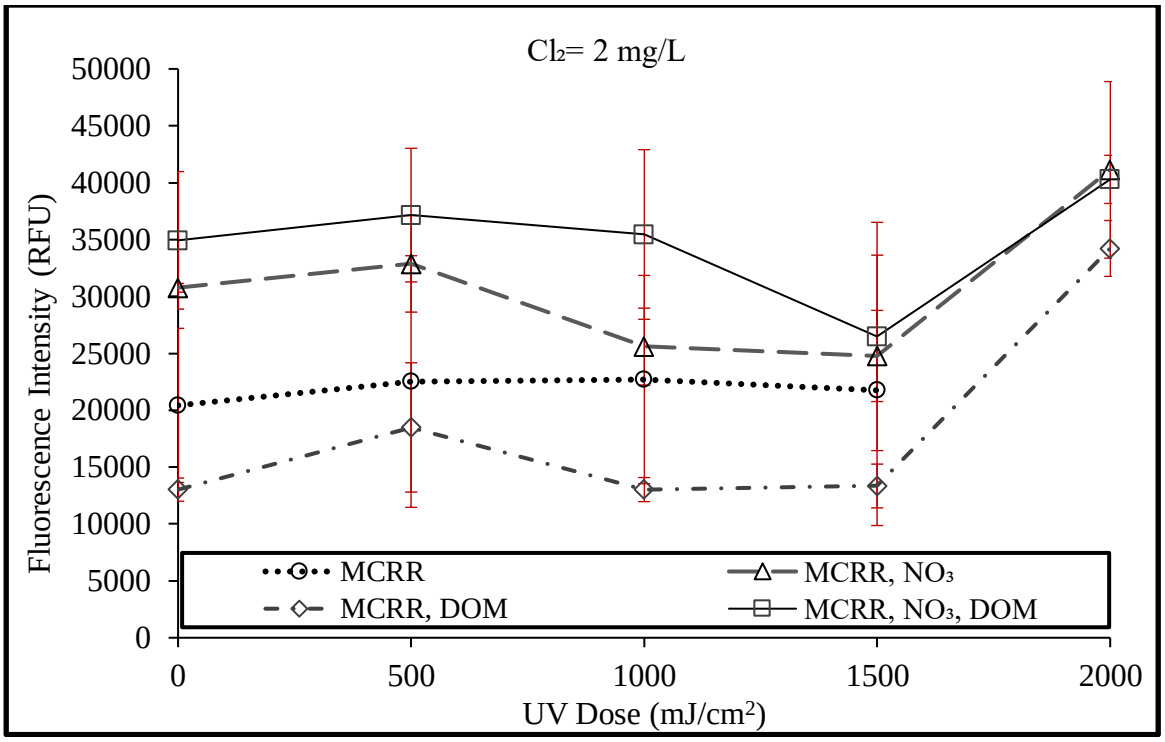

(c)

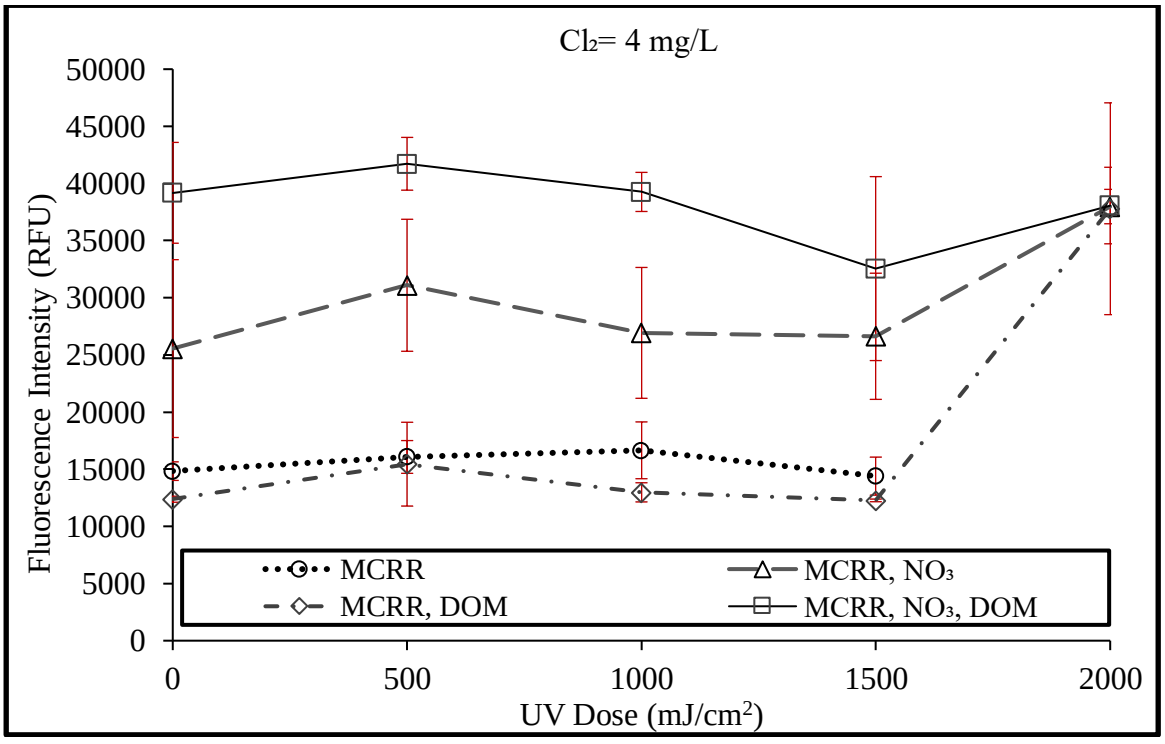

(d)

Figure 22. (Cont'd) Effect of Processes at Given UV Dose and Matrix on Hepatotoxicity of Products after MC-RR Degradation
Data shows the average of three replicates and the error bars are the standard deviations.

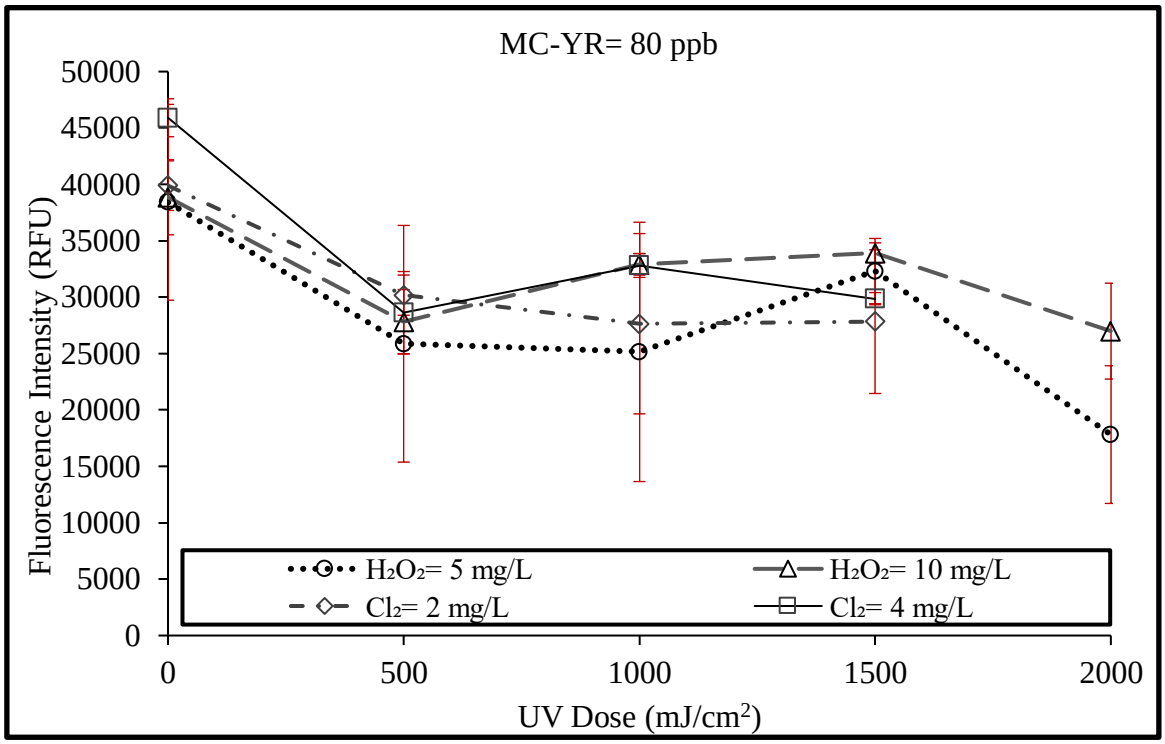

(a)

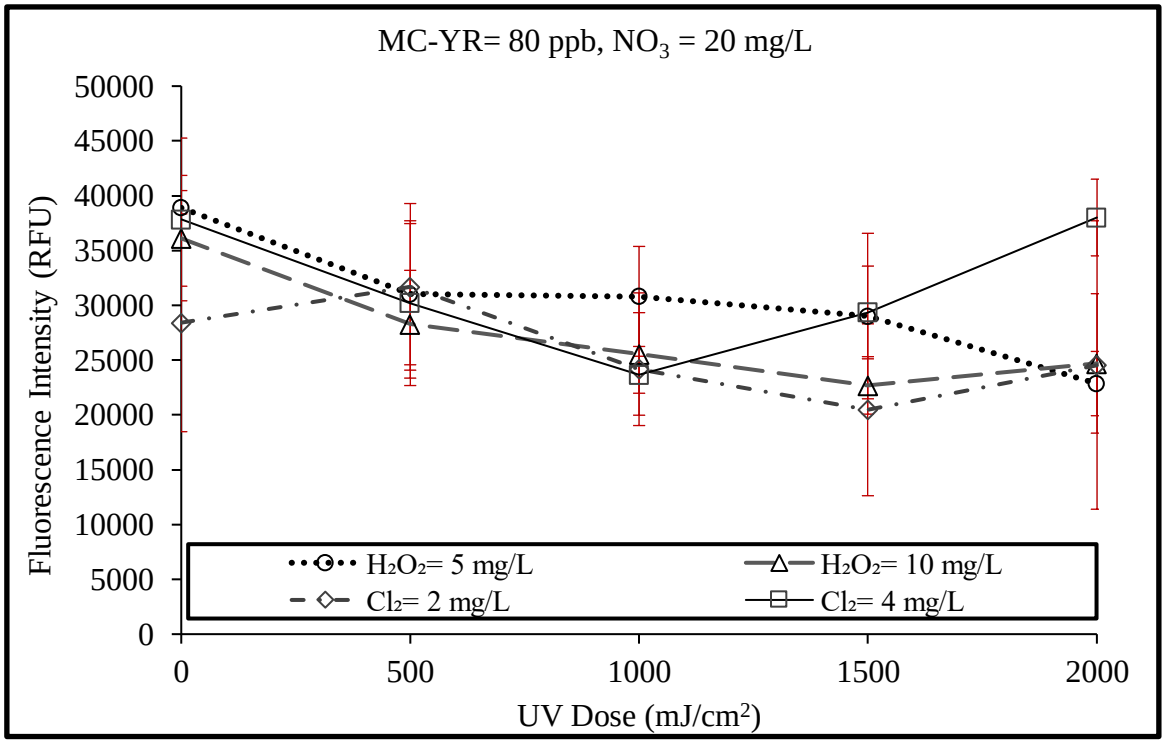

(b)

Figure 23. Effect of Matrix and UV Dose for Different Processes on Hepatotoxicity of Products after MC-YR Degradation

Data shows the average of three replicates and the error bars are the standard deviations.

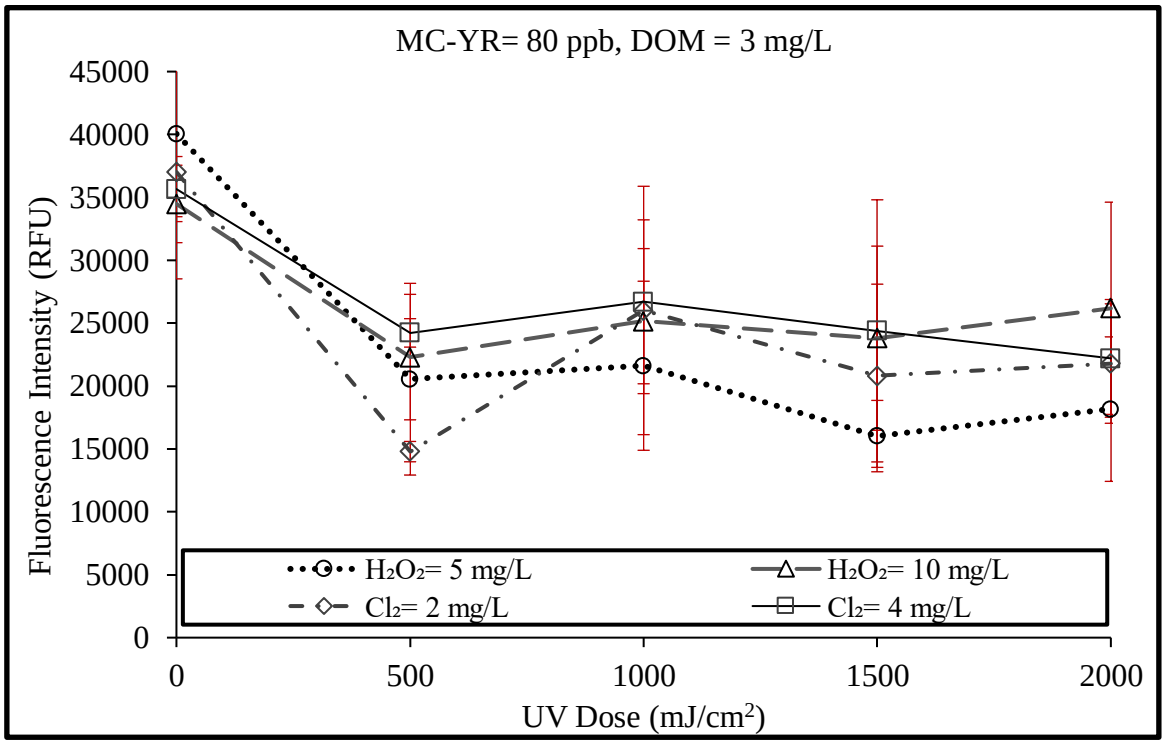

(c)

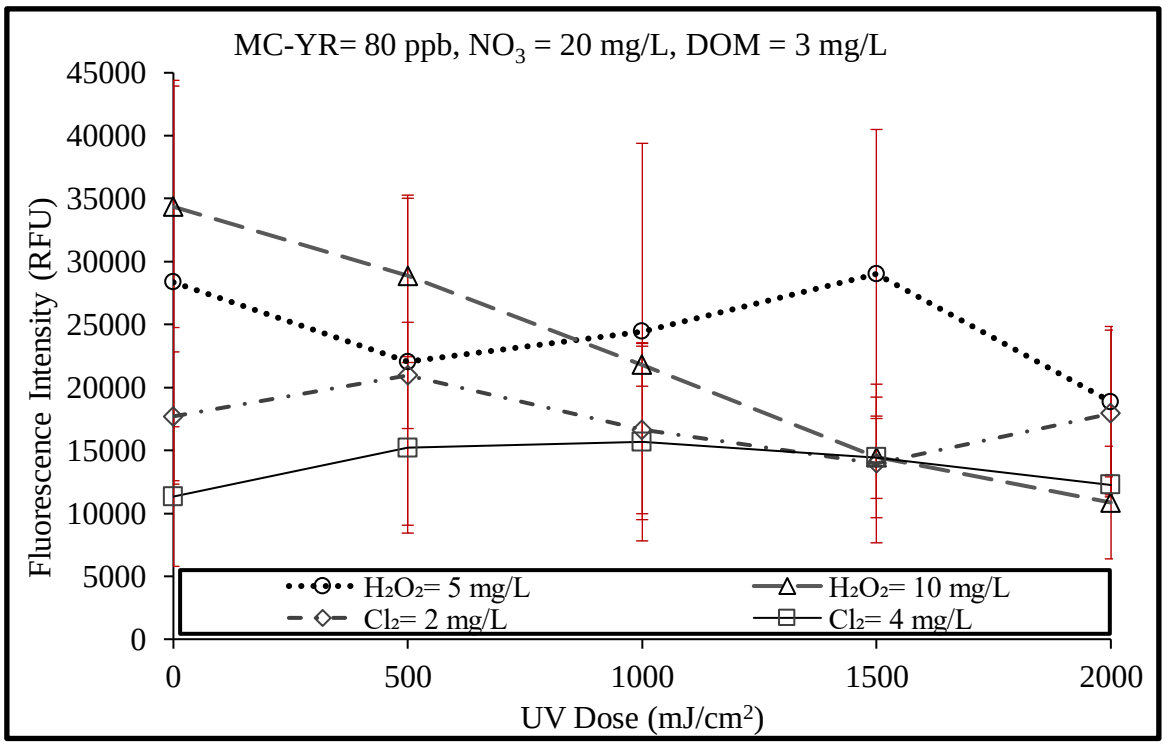

(d)

Figure 23. (Cont'd) Effect of Matrix and UV Dose for Different Processes on Hepatotoxicity of Products after MC-YR Degradation
Data shows the average of three replicates and the error bars are the standard deviations.

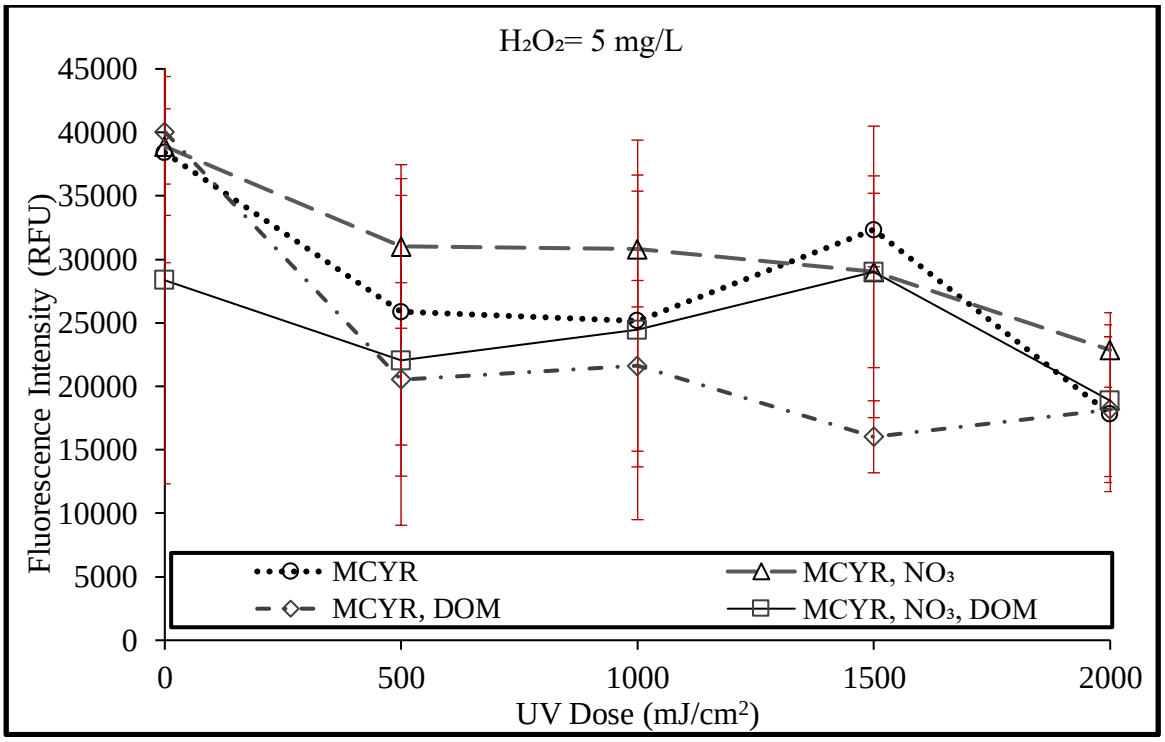

(a)

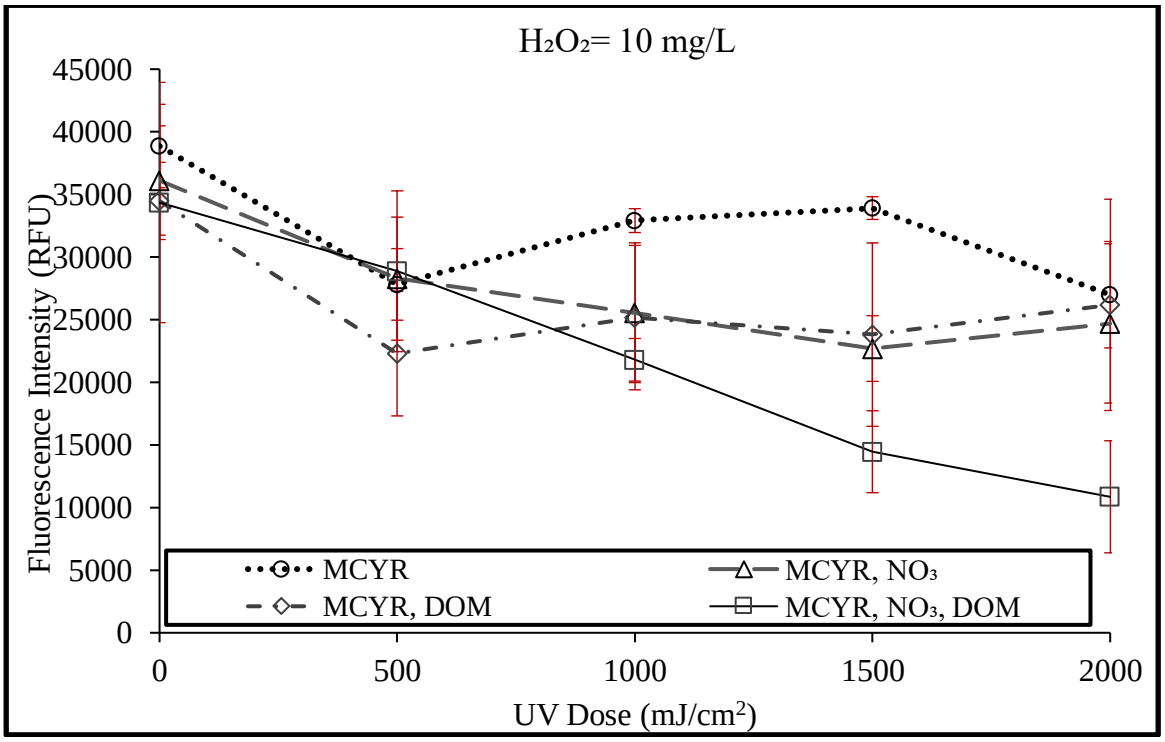

(b)

Figure 24. Effect of Processes at Given UV Dose and Matrix on Hepatotoxicity of Products after MC-YR Degradation
Data shows the average of three replicates and the error bars are the standard deviations.

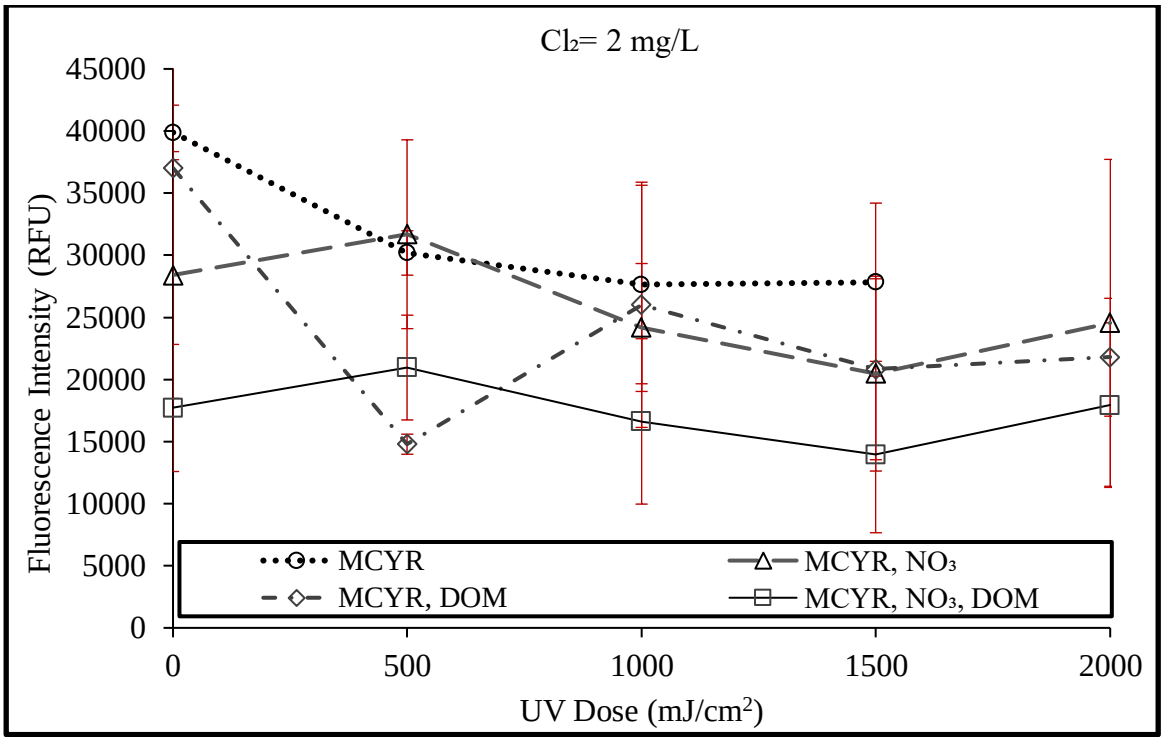

(c)

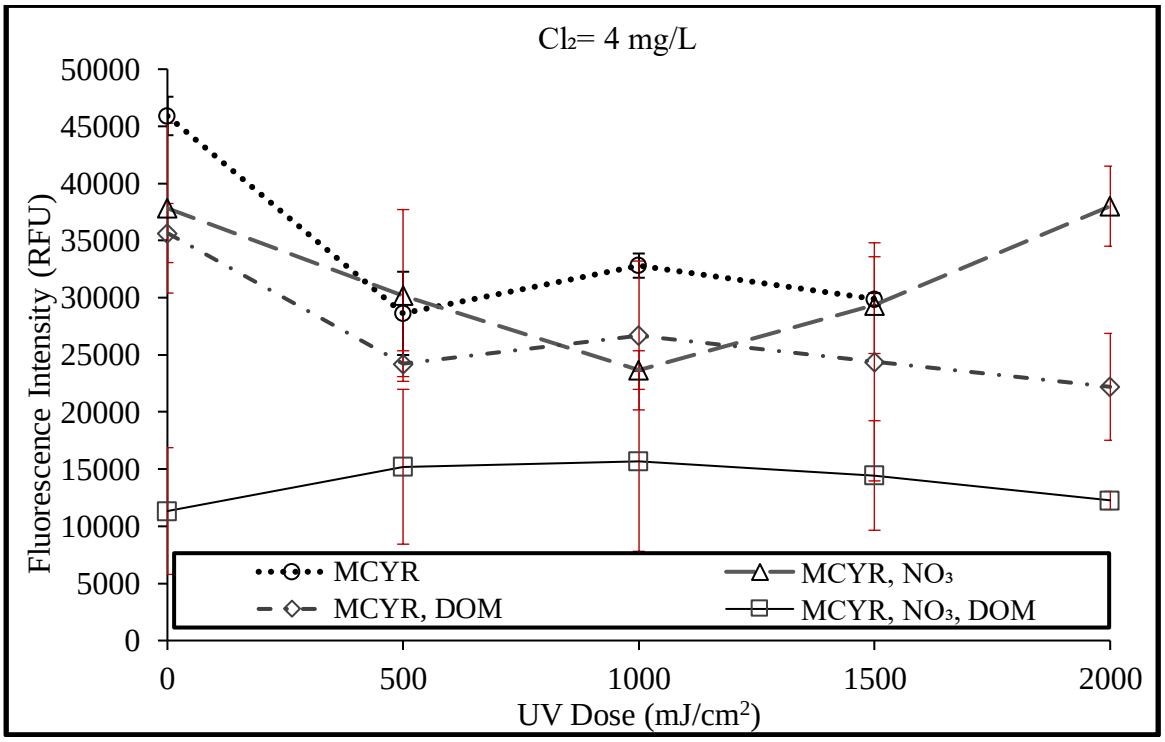

(d)

Figure 24. (Cont'd) Effect of Processes at Given UV Dose and Matrix on Hepatotoxicity of Products after MC-YR Degradation
Data shows the average of three replicates and the error bars are the standard deviations.

4.3.2. Ames II (Genotoxicity)

As mentioned earlier in the method section, the Ames II test was conducted to measure the genotoxicity of parent compounds. Based on the Ames Modified ISO kits form EPBI, the experiment included 23 samples including three background samples, one positive control, one negative control, one blank as mentioned in method section (3.5.3.) and six dilutions of each MCs. Bacterial dilution steps were tested to ensure mutagen exposure occurred during bacterial logarithmic growth phase for optimal results.

Assay endpoints were read based on colorimetric changes. Yellow and partial yellow wells were scored as positive and purple wells were scored as negative. The negative controls had small numbers of reversions, positive controls had many revertants and reagent sterility control did not have any revertants.

The Ames II assay was valid because three criteria were met: 1) Blank wells were sterile (purple) and the assays were not contaminated, 2) Average score for negative or background control were between 0 and 15 revertant wells per 48-well section on day 3, and 3) Average score for positive (standard mutagen) controls was more than 25 revertant wells per 48-well section on day 3.

Depending on number of revertant wells in tested samples and revertant wells in negative controls, different levels of significance were assigned. The quick reference chart and advanced statistical methods provided by EBPI were used to assign the significance to mutagenicity results. The result using *TA100* strain is shown in Table 18. The results were qualitative, and each response was classified in four categories: no response, possible response, positive response, and strong positive response. MC-LR and -YR showed no response and MC-RR showed possible response.

Therefore, MC-LR and -YR were not bacterial mutagens. Same result was demonstrated in previous studies (Žegura, Štraser, and Filipič 2011). However, the *in vitro* studies with mammalian cells and and *in vivo* rodent studies can show that both toxins lead to reactive oxygen species formation, DNA damage and micronuclei formation (Žegura et al. 2011).

MC-RR is a real threat with a high exposure potential in some countries, however, its genotoxicity and chronic effects have not yet been adequately studied (Díez-Quijada et al. 2019).

Table 18. Ames II Test for Parent Toxins

Toxin	Read Revertant Wells	Revertant Ratio (RR)	Response Category
Background	12		
Background	13		
Background	19		
Positive Control	48	2.601258659	
Positive Control	48		
Blank	0	0	
MC-LR – Dilution 1	11	0.596121776	No Response
MC-LR – Dilution 2	14	0.758700442	
MC-LR – Dilution 3	12	0.650314665	
MC-LR – Dilution 4	11	0.596121776	
MC-LR – Dilution 5	9	0.487735999	
MC-LR – Dilution 6	12	0.650314665	
MC-RR – Dilution 1	4	0.216771555	Possible Response
MC-RR – Dilution 2	10	0.541928887	
MC-RR – Dilution 3	9	0.487735999	
MC-RR – Dilution 4	9	0.487735999	
MC-RR – Dilution 5	8	0.43354311	
MC-RR – Dilution 6	5	0.270964444	
MC-YR – Dilution 1	3	0.162578666	No Response
MC-YR – Dilution 2	8	0.43354311	
MC-YR – Dilution 3	16	0.86708622	
MC-YR – Dilution 4	10	0.541928887	
MC-YR – Dilution 5	4	0.216771555	
MC-YR – Dilution 6	9	-	

4.4.The effect of UV/H_2O_2 and UV/Cl_2 AOPs on Formation of DBPs

Natural organic matter is a major DBP precursor (Xinran Zhang et al. 2015), and the presence of organic matter in the system raises concerns for DBPs formation. Besides, high chlorine doses and long contact times can result in carcinogenic DBPs (Zhang et al. 2016). Therefore, the DBPs formation test was essential in this study. The same batches and AOPs experiments were conducted with no MCs to collect samples for DBPs analysis. THMs, HAAs, and NDMA were studied in the current project.

For THMs and HAAs analysis, Liu and the research team optimized the critical factors in the derivatization step including the volume and concentration of acidic methanol, the amount and concentration of Na_2SO_4 solution, the volume of saturated $NaHCO_3$ solution, and derivatization time and temperature (Liu et al. 2013). The following results on THMs and HAAs formation are based on their findings on the optimum extraction method. The data are average values of triplicate samples.

For post-AOP tests such as toxicity assays or mass spectrometry, enzymatic options are recommended quench H_2O_2 (Keen et al. 2013). Therefore, bovine catalase was used to quench H_2O_2 in MCs AOPs experiences that were followed by LC/MS-MS and PP2A analysis. For the samples that include chlorinated DBP analysis chlorine is the recommended option to quench H_2O_2 (Keen et al. 2013). UV/H_2O_2 samples needed higher chlorine dose compared to UV/Cl_2 samples to achieve same residual chlorine.

The reaction between chlorine and H_2O_2 is much faster than the reaction between chlorine and DOM (Keen et al. 2013). Consequently, a slight increase to no increase in DBP formation was expected in UV/H_2O_2 samples because of the increased initial chlorine dose required to quench H_2O_2 (Keen et al. 2013).

4.4.1. Trihalomethanes

Figures 25-32 show the effect of matrices and UV dose for different processes on THMs formation and comparison of methods at given UV dose and matrix for each THM.

In most cases, the water matrix, UV dose, oxidant dose, and different processes (UV/Cl_2 vs. UV/H_2O_2) did not show a significant effect on the four THMs that were studied.

Chloroform was increased with algal DOM presence in hydrogen peroxide processes (Figure 25). According to the t-test, which compared the results of background and metrics with added DOM, the p-value was 0.028 indicating that the results were significantly different. Also, chloroform was suppressed by nitrate and the p-value was 0.066 which was not statically significant (but close to p-value = 0.05).

In UV/H_2O_2 processes, comparing two series of data at different UV dose, the increase in the concentration of hydrogen peroxide decreases the chloroform formation. However, the changes were not statistically significant with the p-values equal to 0.226, 0.134, and 0.135 in background, matrix with nitrate, and matrix with DOM, accordingly. The contribution of DOM in chloroform formation is more explicit in Figure 26.

Algal DOM also increased the formation of bromodichloromethane in UV/H_2O_2 process significantly with the p-value of 0.019 under H_2O_2= 5 mg/L (Figure 27). Dibromochloromethane and bromodichloromethane had higher concentrations compared with dibromochloromethane and bromodichloromethane.

The chlorine dose should be limited to a range that avoids the maximum contaminant level (MCL) of total THMs (TTHMs) of 80 µg/L in the treated water (U.S. EPA 2020). In our study, the maximum TTHM concentration was 46.26 µg/L belonging to the

background matrix that was treated using Cl_2 = 4 mg/L and UV = 2000 mJ/cm_2, which is much less than the MCL (Figures 33 and 34).

In addition, bromide may form bromate due to UV irradiation, and MCL for bromate in drinking water is 10 µg/L (U.S. EPA 2020). The concentration of bromide in background water (0.0021 mg/L) was minimal and bromate formation in treated water was not a concern.

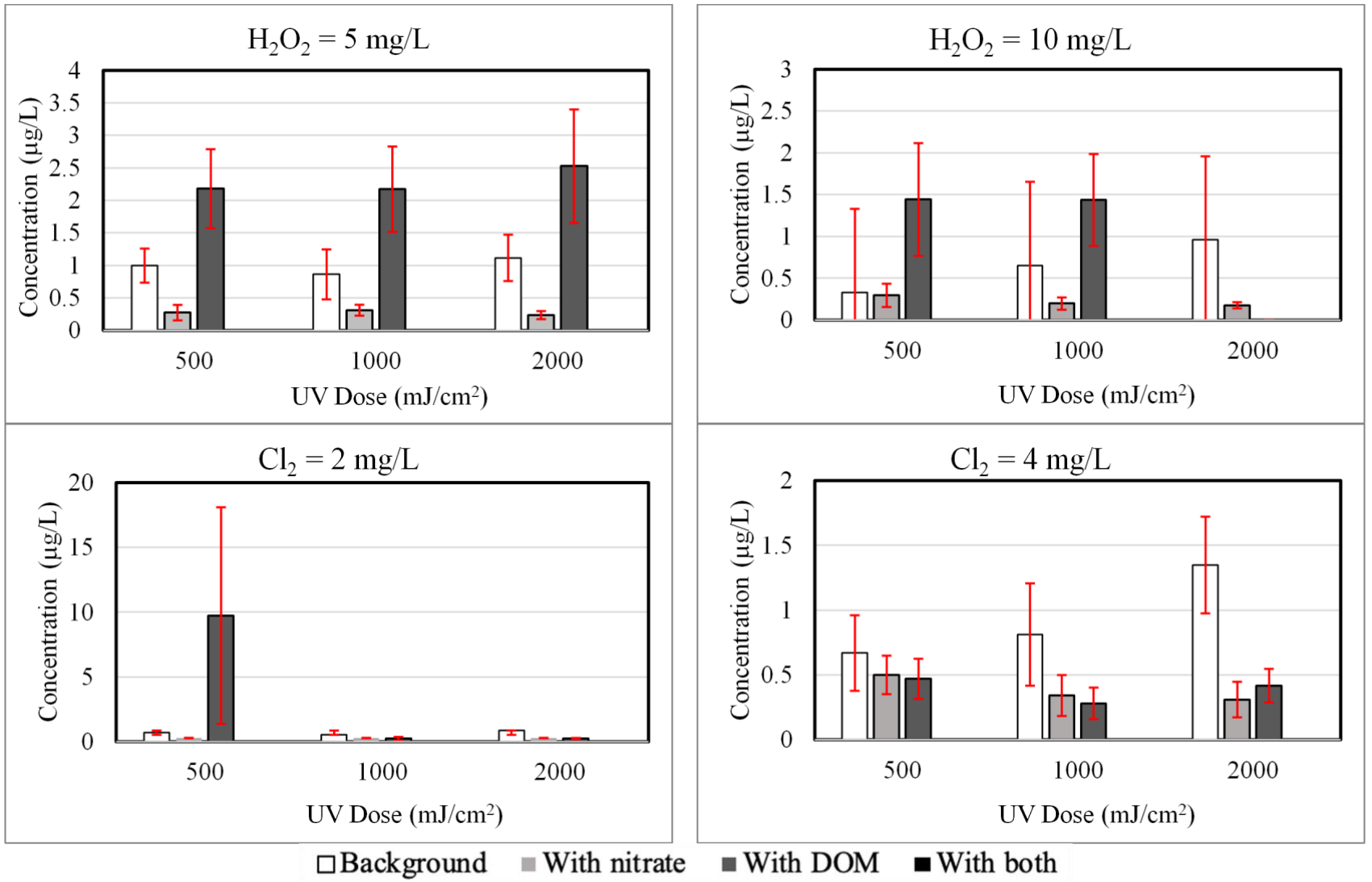

Figure 25. Effect of Matrix and UV Dose for Different Processes on Chloroform
Figure shows the average of three separate experiments with the error bars showing standard deviation.

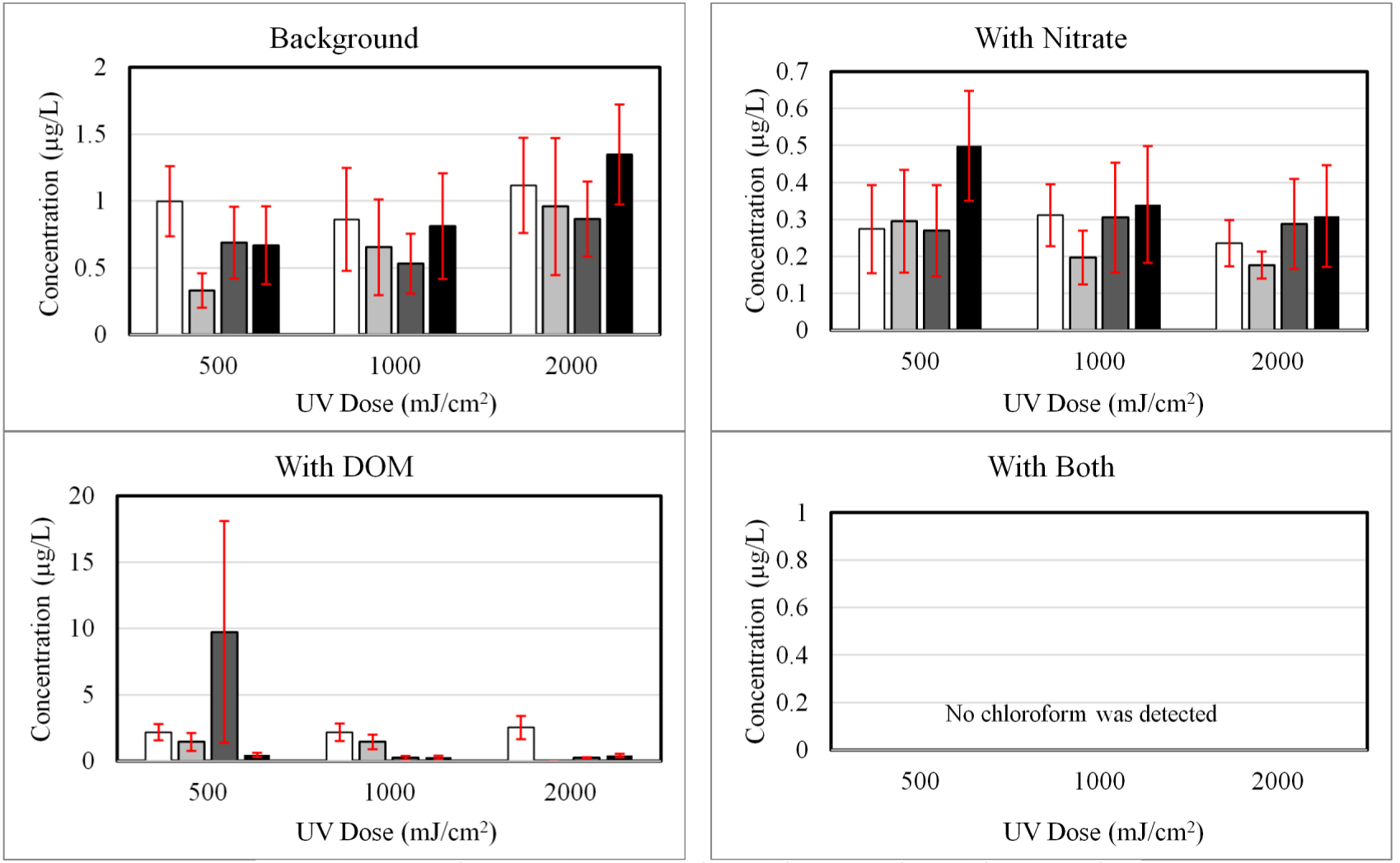

Figure 26: Comparison of Effect of Processes at given UV Dose and Matrix on Chloroform Formation
Figure shows the average of three separate experiments with the error bars showing standard deviation.

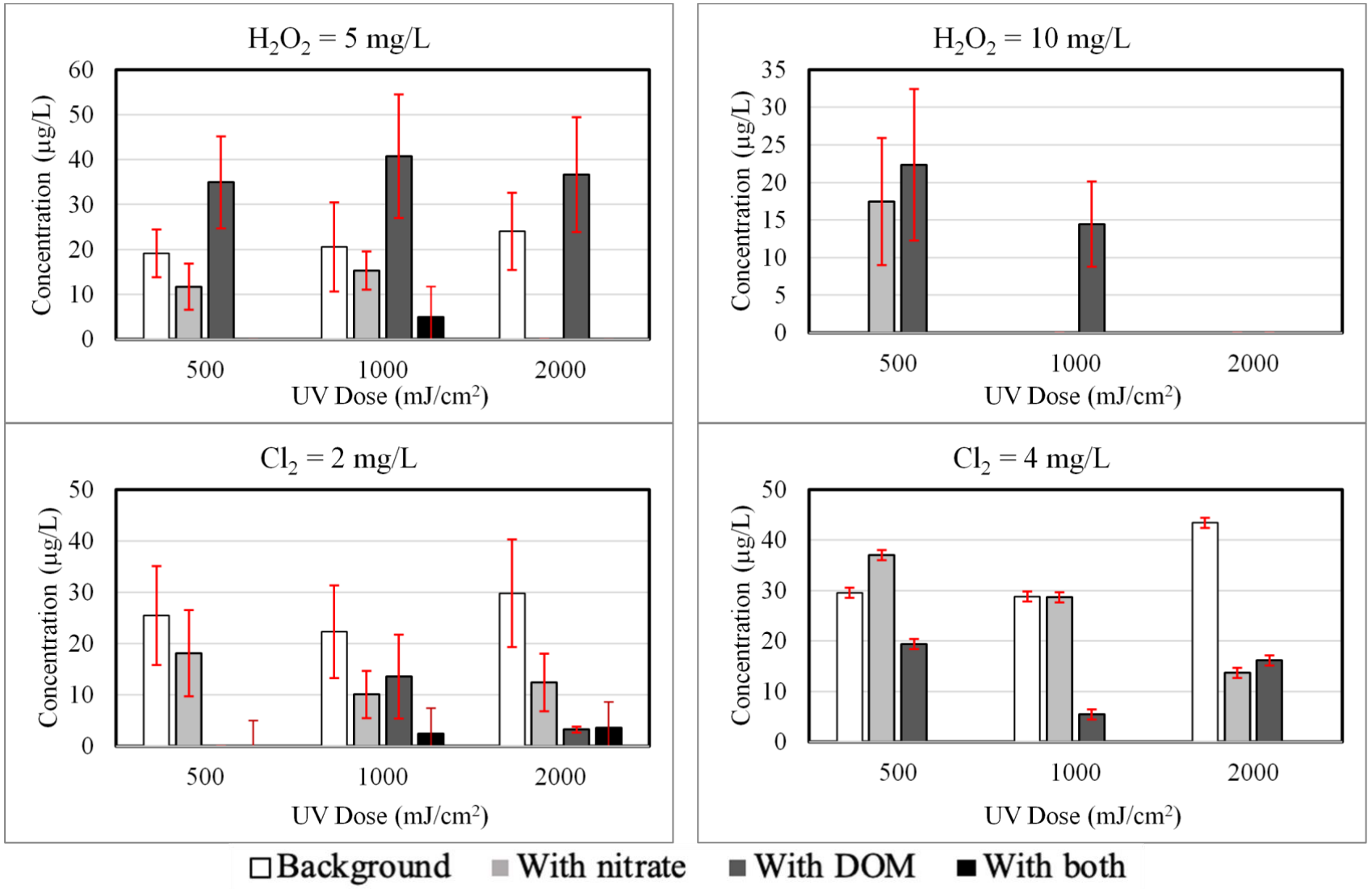

Figure 27. Effect of Matrix and UV Dose for Different Processes on Bromodichloromethane Formation
Figure shows the average of three separate experiments with the error bars showing standard deviation.

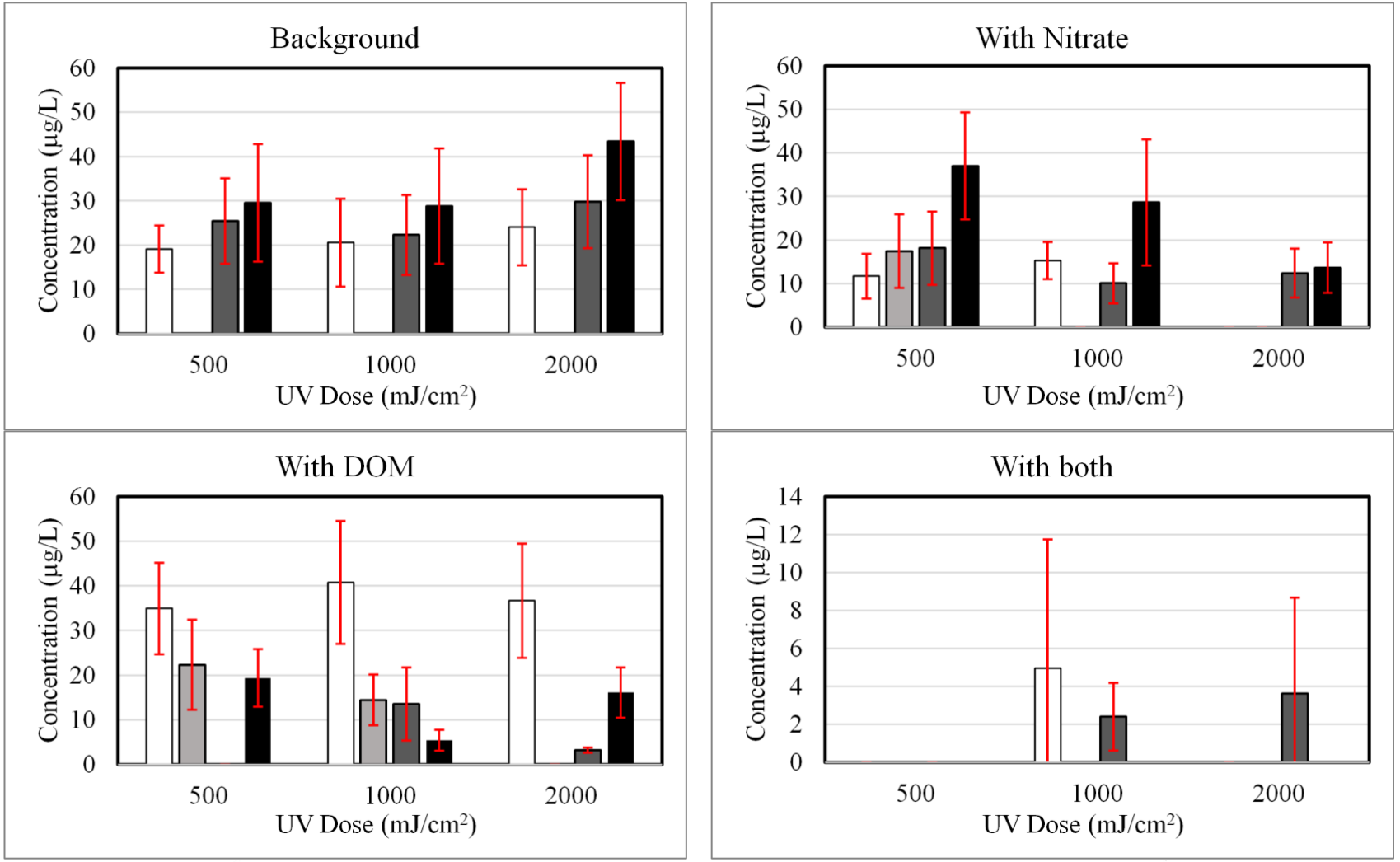

Figure 28. Comparison of Effect of Processes at Given UV Dose and Matrix on Bromodichloromethane Formation
Figure shows the average of three separate experiments with the error bars showing standard deviation.

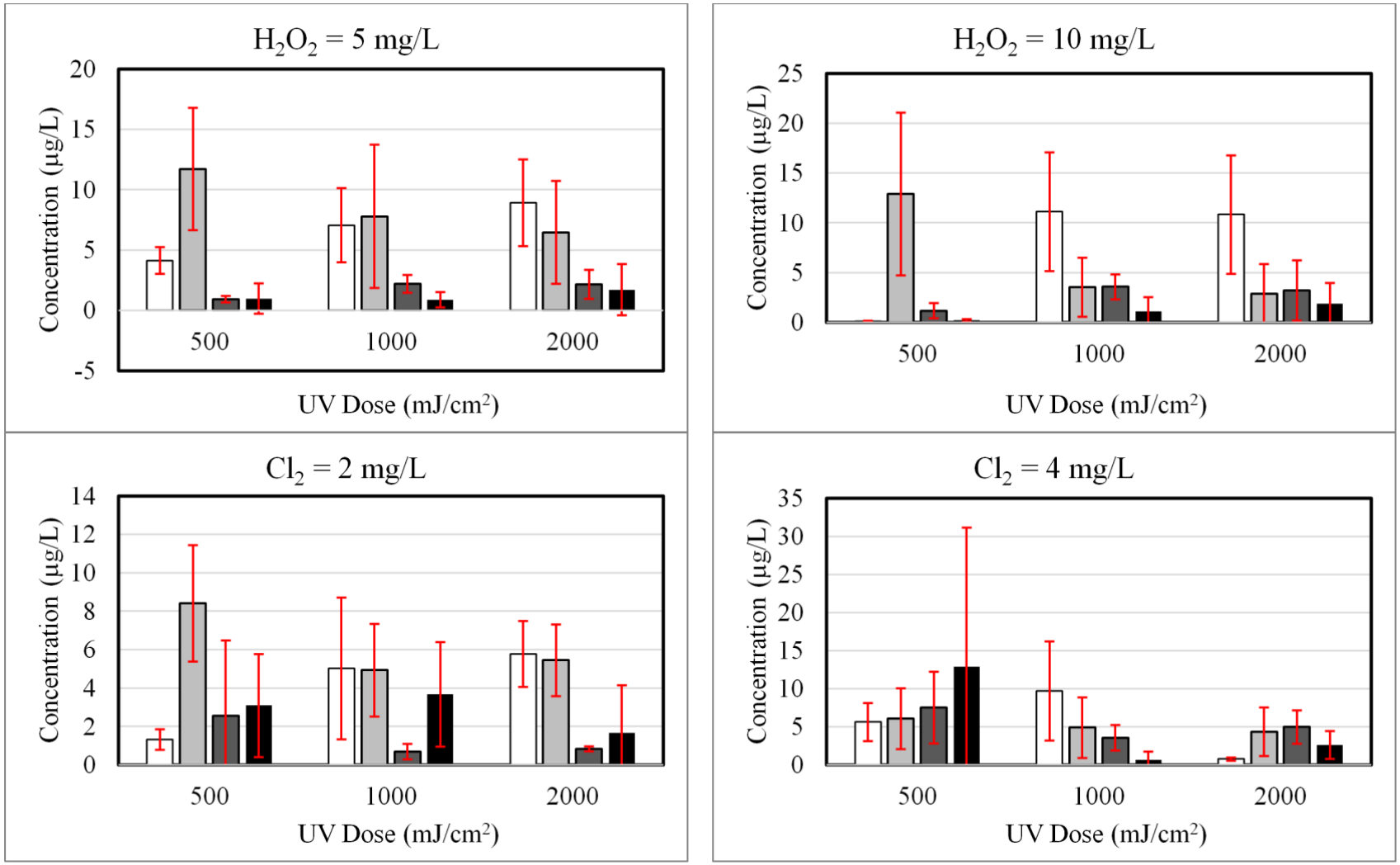

Figure 29. Effect of Matrix and UV Dose for Different Processes on Dibromochloromethane Formation
Figure shows the average of three separate experiments with the error bars showing standard deviation.

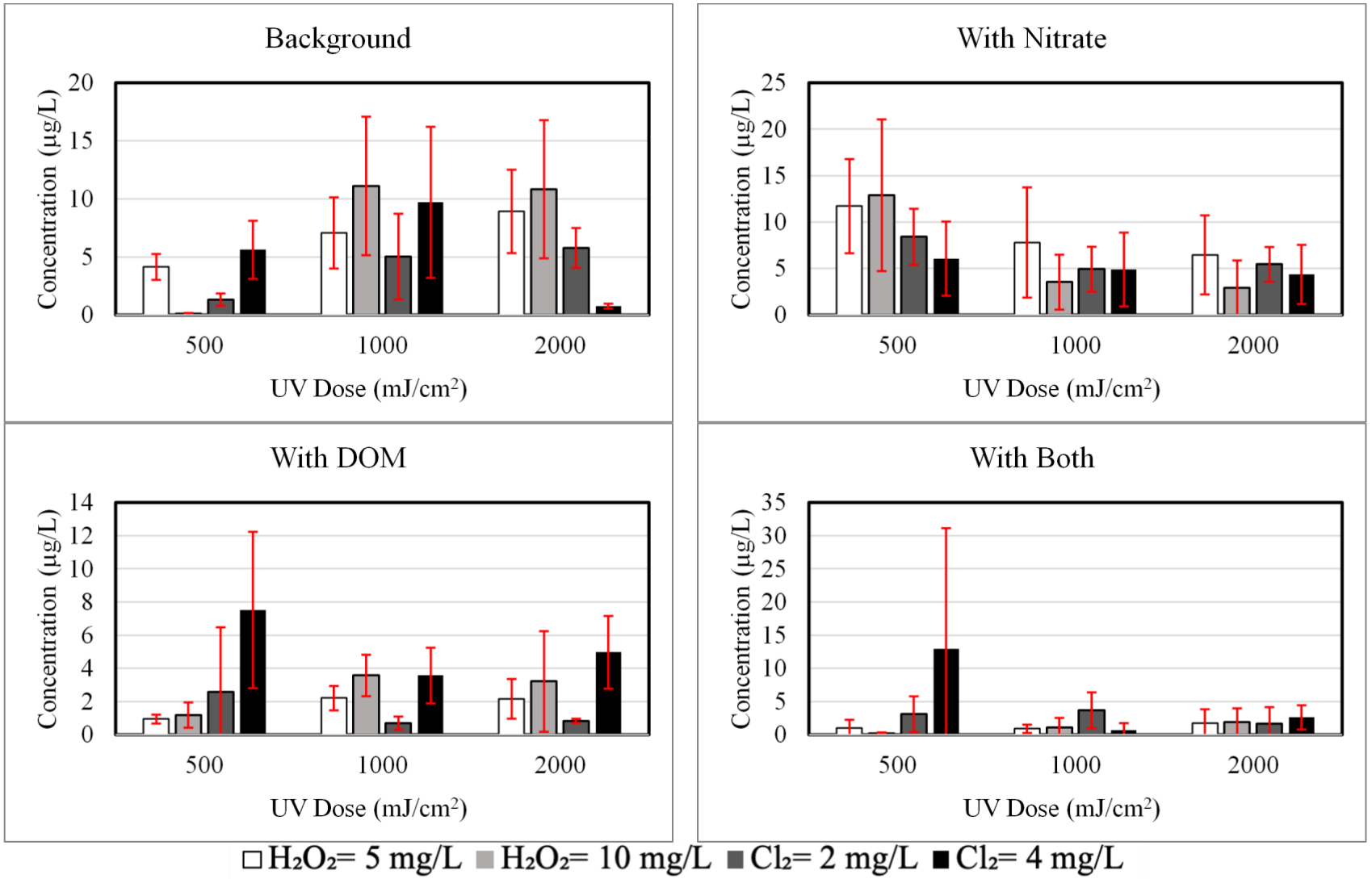

Figure 30: Comparison of Effect of Processes at Given UV Dose and Matrix on Dibromochloromethane Formation
Figure shows the average of three separate experiments with the error bars showing standard deviation.

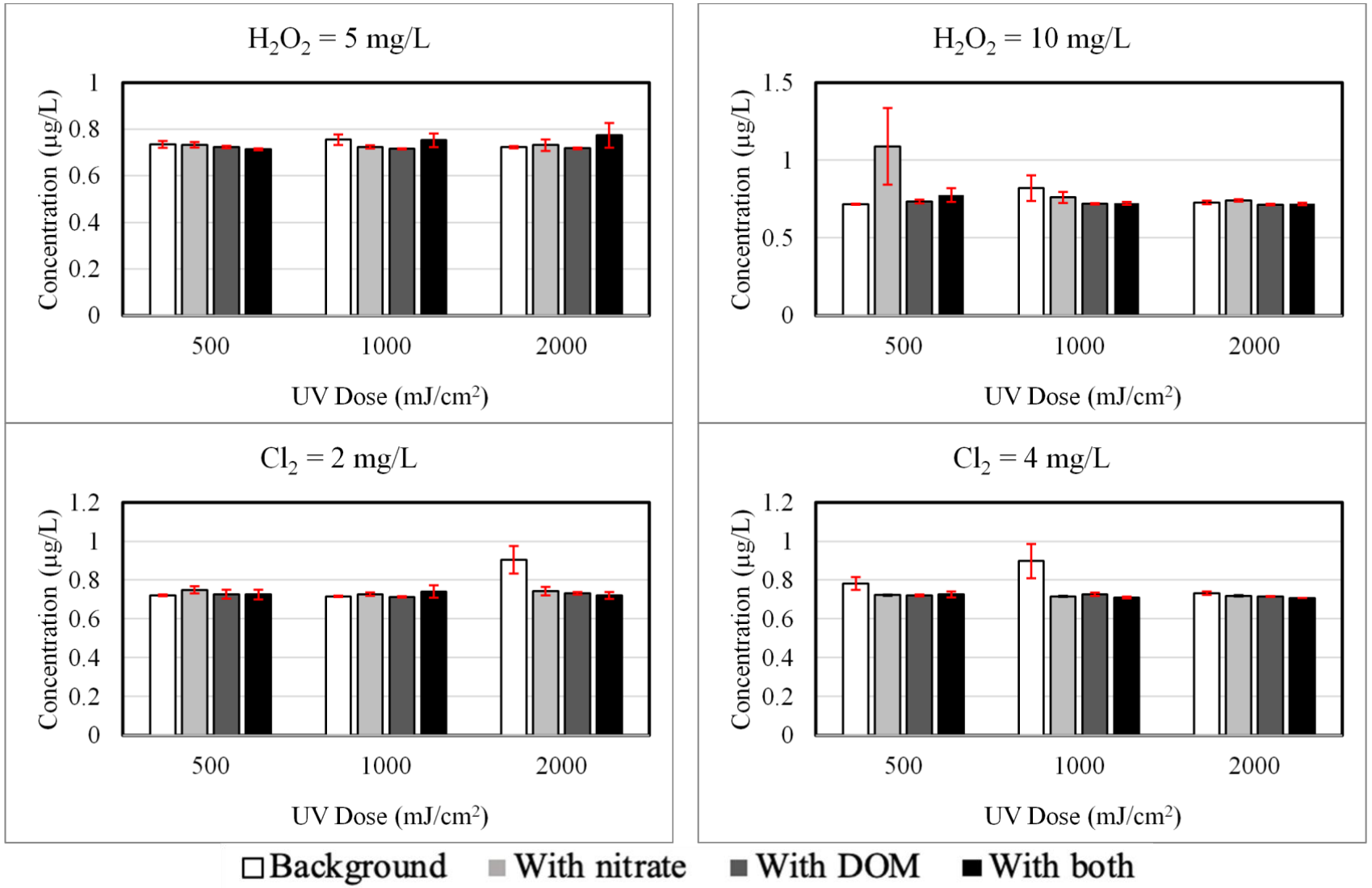

Figure 31. Effect of Matrix and UV Dose for Different Processes on Bromoform Formation
Figure shows the average of three separate experiments with the error bars showing standard deviation.

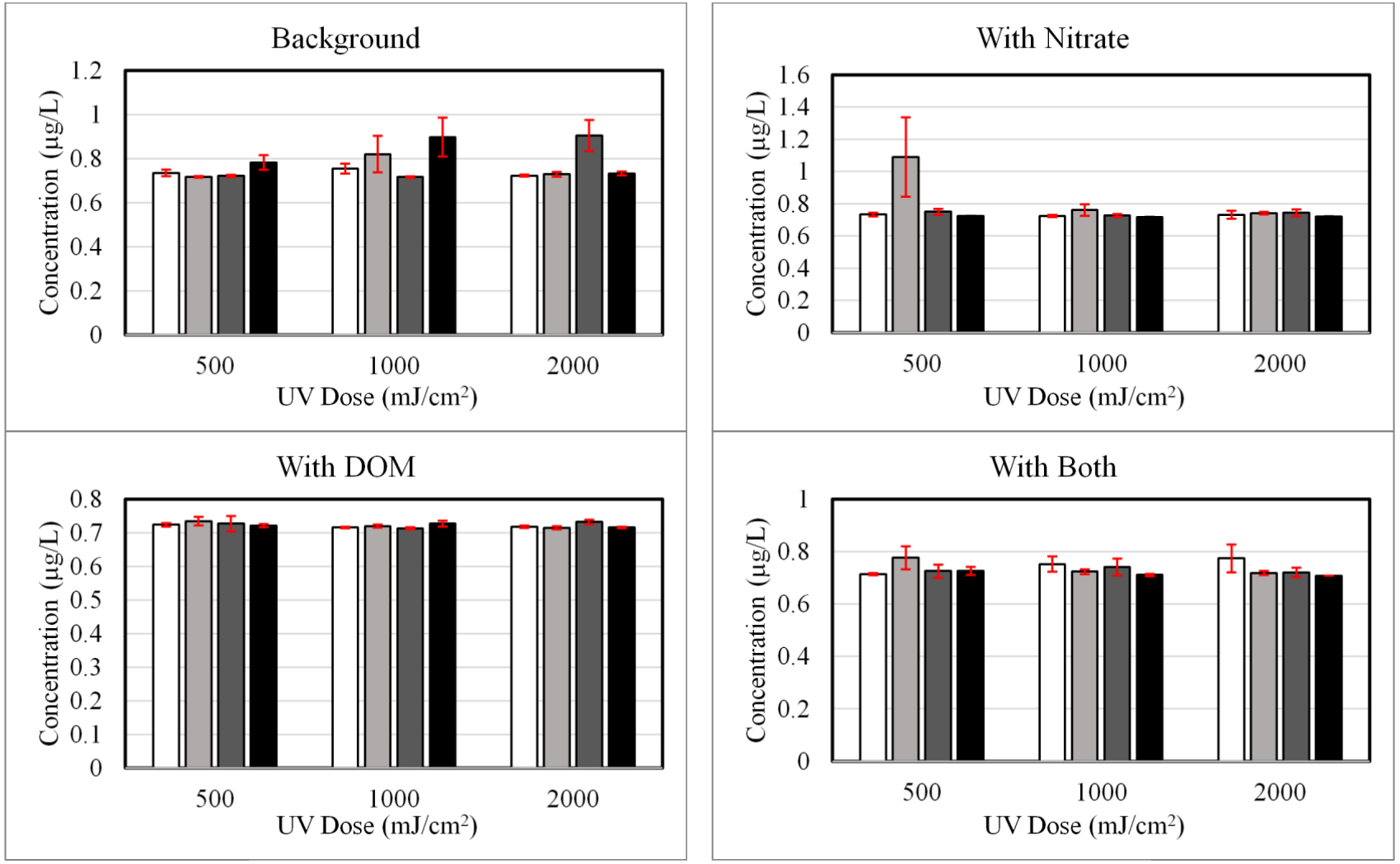

Figure 32: Comparison of Effect of Processes at Given UV Dose and Matrix on Bromoform Formation
Figure shows the average of three separate experiments with the error bars showing standard deviation.

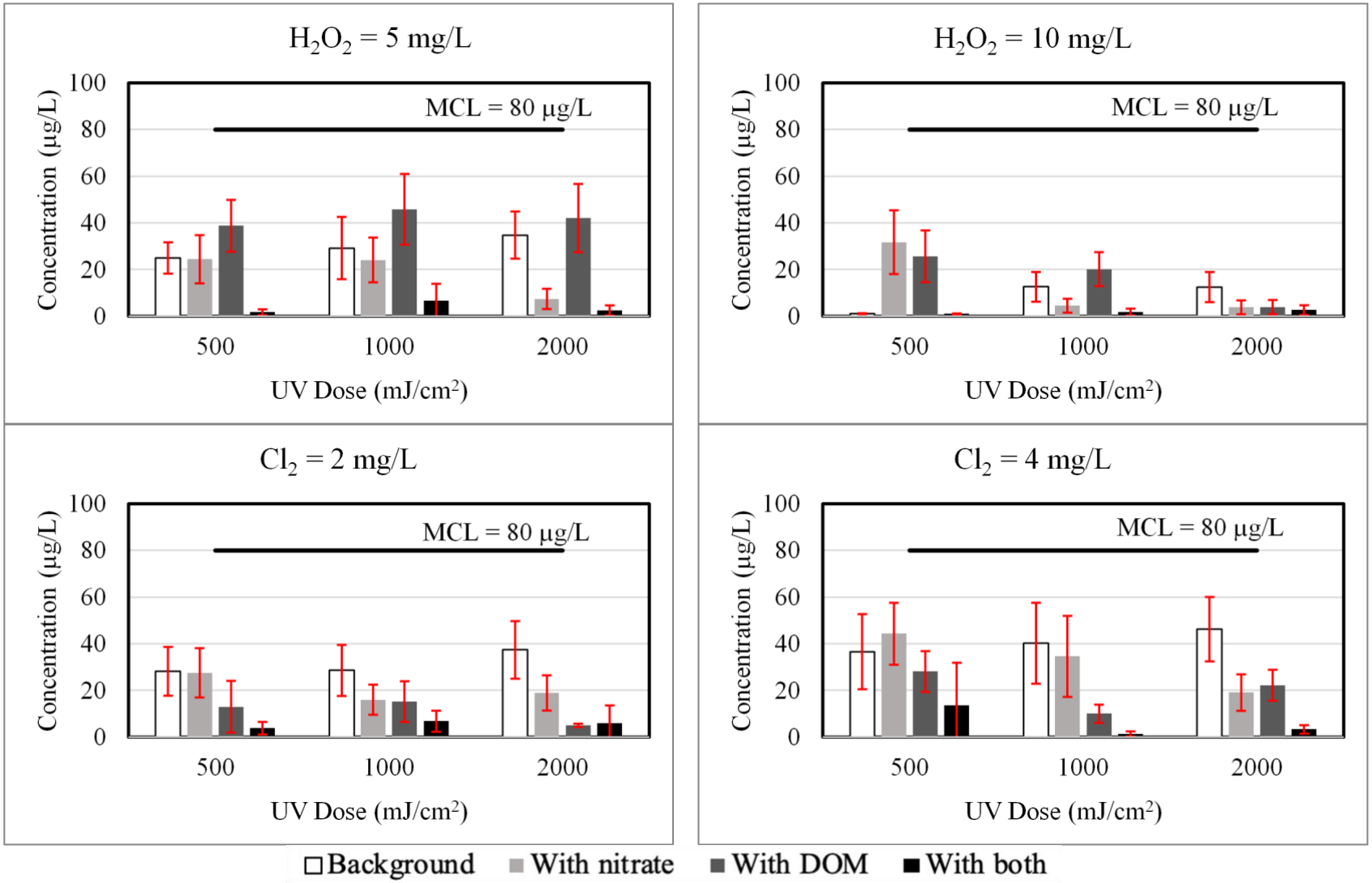

Figure 33. Effect of Matrix and UV Dose for Different Processes on TTHMs formation
Figure shows the average of three separate experiments with the error bars showing standard deviation.

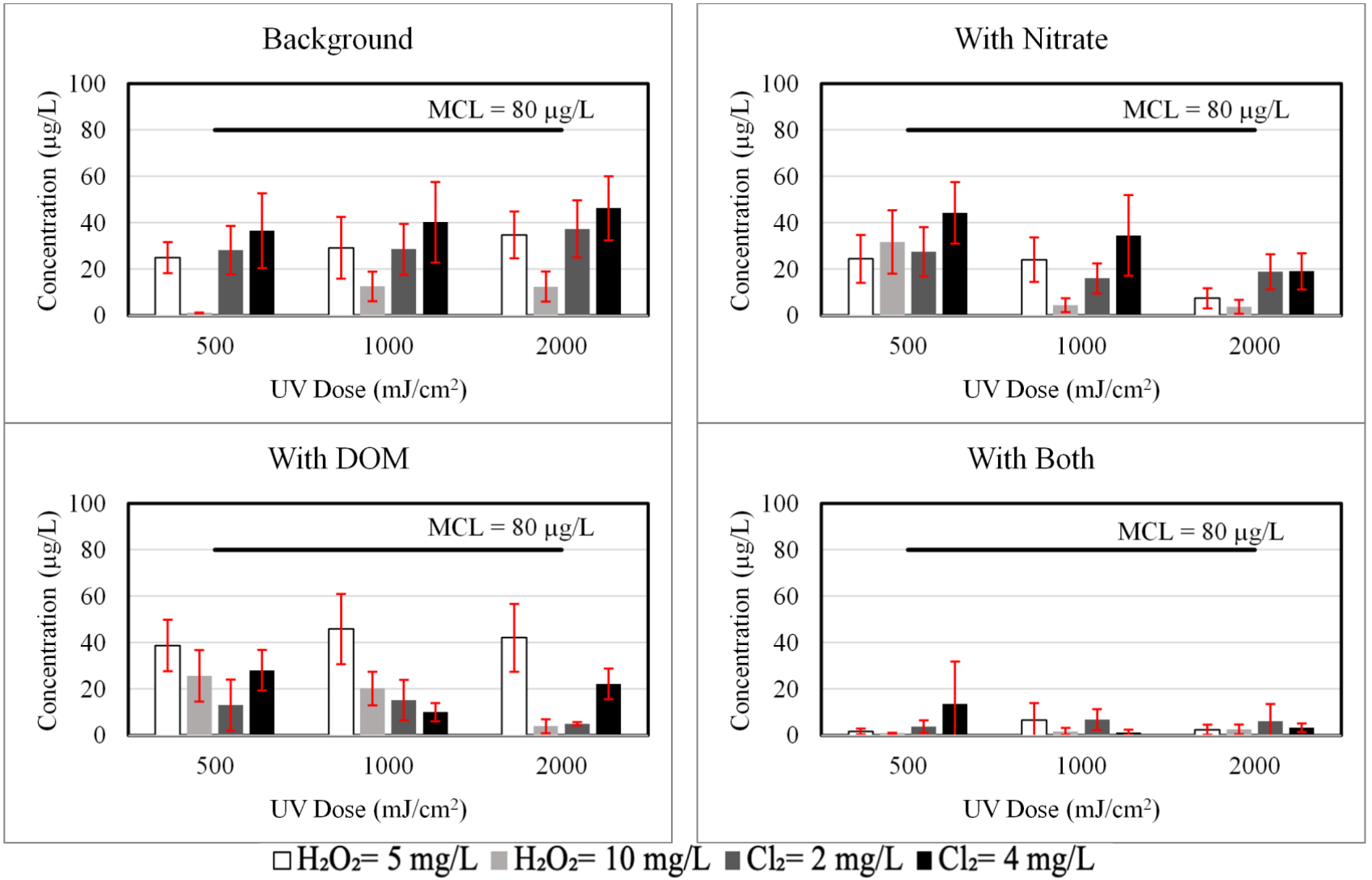

Figure 34: Comparison of Effect of Processes at given UV Dose and Matrix on TTHMs Formation
Figure shows the average of three separate experiments with the error bars showing standard deviation.

4.4.2. Haloacetic acids

Nine HAAs were studied in this project, among which only three HAAs were detected in the treated samples: tribromoacetic acid (Figures 35-36), monochloroacetic acid (Figures 37-38), and chlorodibromoacetic acid (Figures 39-40). The sample matrix impacted HAA formation. For instance, tribromoacetic acid formation was higher at sample containing nitrate (Figure 36). However, the difference was not statistically significant, and the p-value was 0.130 and 0.120 for UV/H_2O_2 and UV/Cl_2, respectively.

No correlation was observed between the type of process or the level of treatment and HAA formation.

Monochloroacetic acid was formed during UV/H_2O_2 processes, which was significantly suppressed by the addition of nitrate and algal DOM to the background matrix (Figure 39). The p-values for comparing the results of different matrices were 0.039 and 0.035 for matrix with nitrate and matrix with DOM, respectively.

The MCL of total HAAs (THAAs) is 60 µg/L in drinking water (U.S. EPA 2020). In our study, the maximum total HAAs was 127.8 µg/L belonging to matrix containing 20 mg/L NO_3 treated by H_2O_2 5 mg/L under UV = 1000 mJ/cm_2. However, in most of the samples total HAAs concentration was less than MCL (Figures 41-42) and only seven samples exceed the MCL.

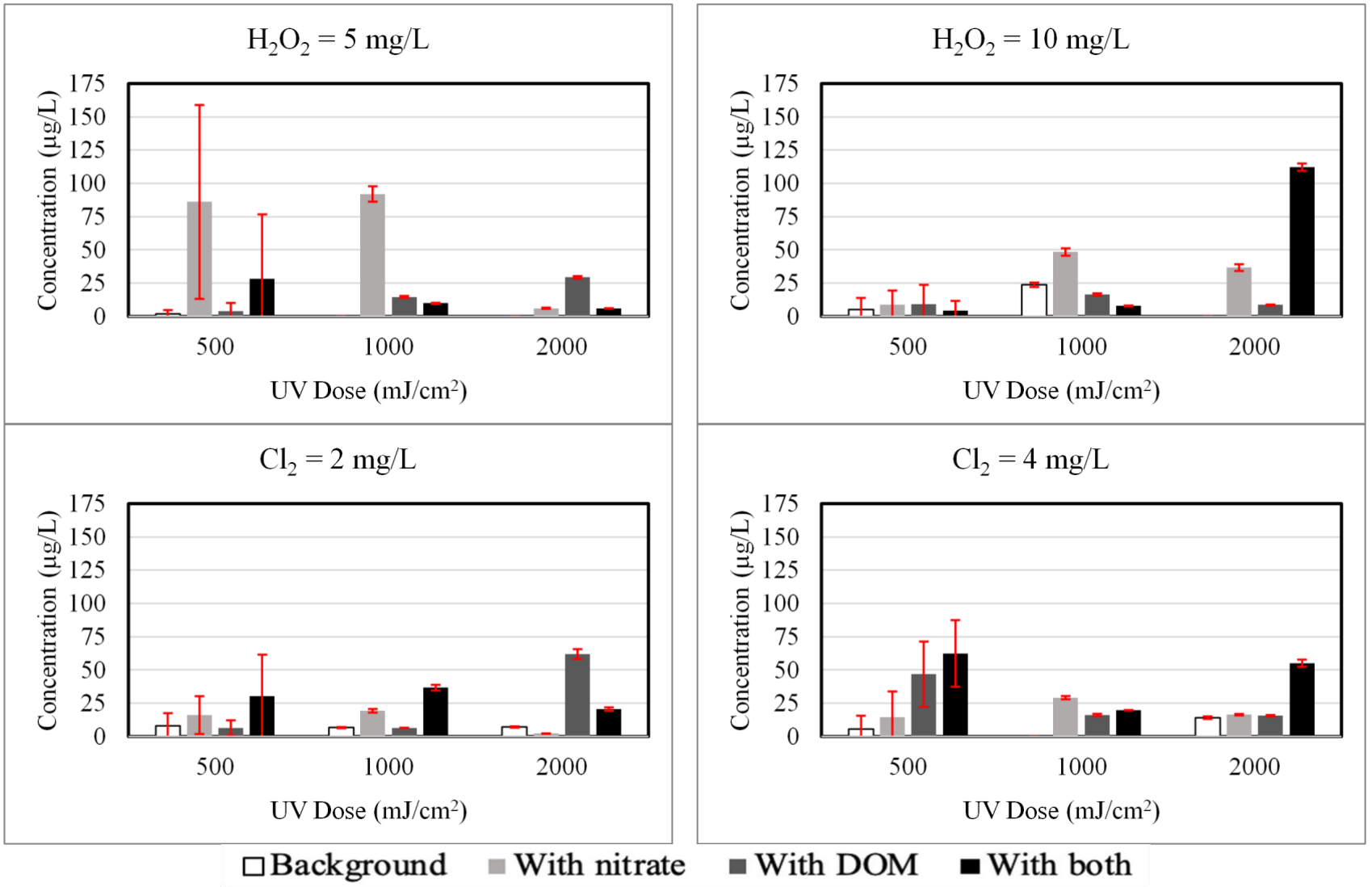

Figure 35. Effect of Matrix and UV Dose for Different Processes on Tribromoacetic Acid Formation
Figure shows the average of three separate experiments with the error bars showing standard deviation.

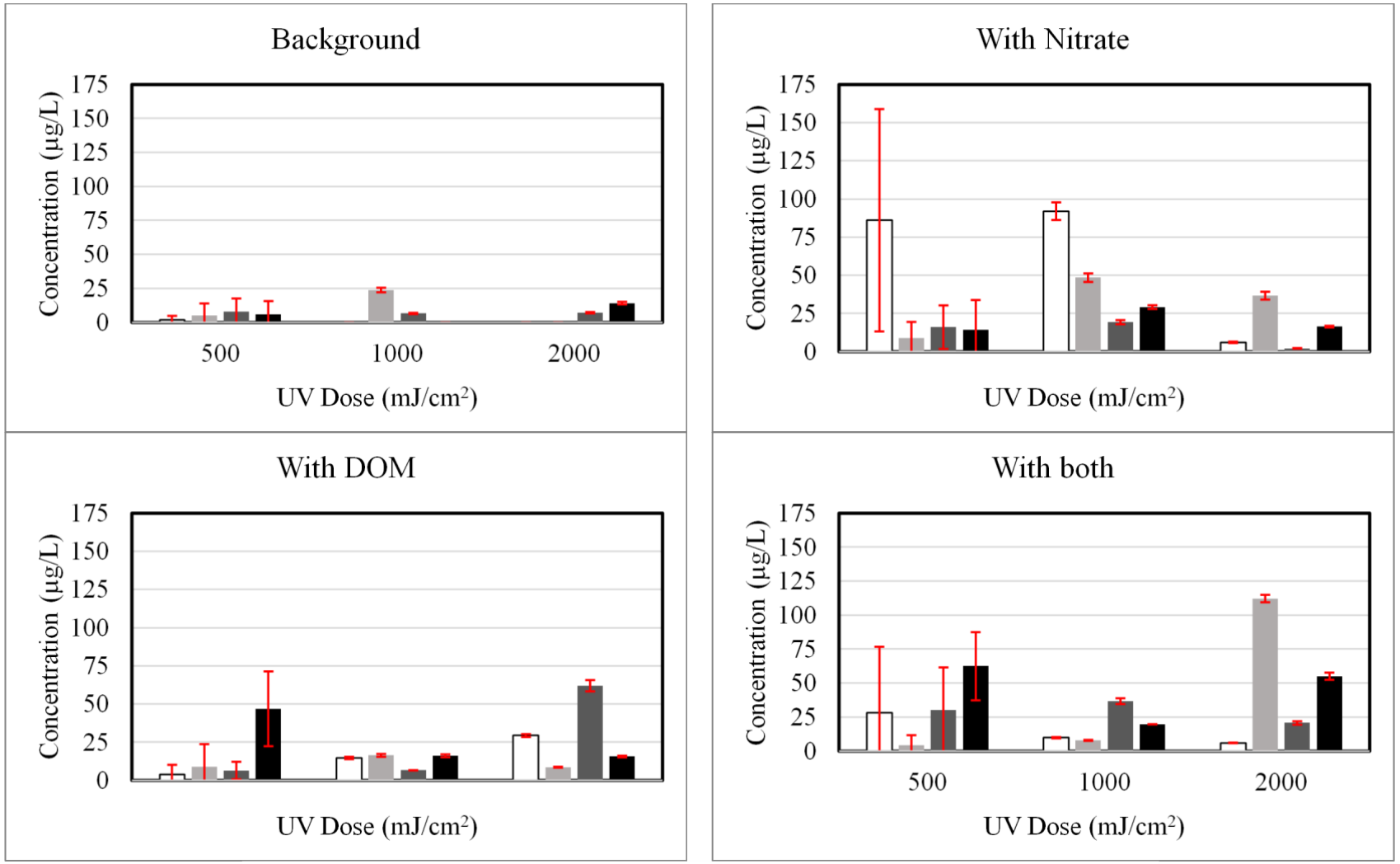

Figure 36. Comparison of Effect of Processes at Given UV Dose and Matrix on Tribromoacetic Acid Formation
Figure shows the average of three separate experiments with the error bars showing standard deviation.

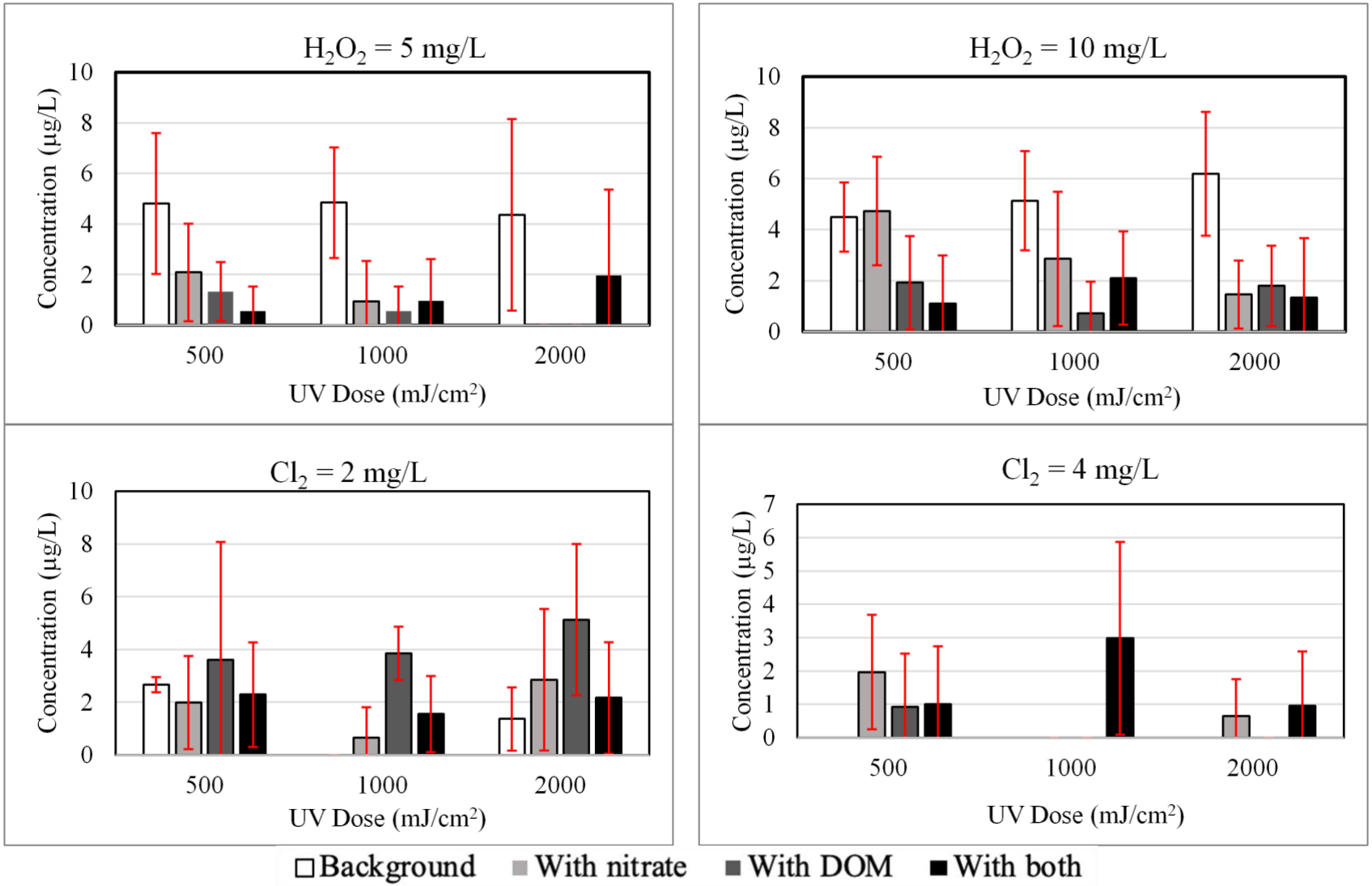

Figure 37. Effect of Matrix and UV Dose for Different Processes on Monochloroacetic Acid Formation
Figure shows the average of three separate experiments with the error bars showing standard deviation.

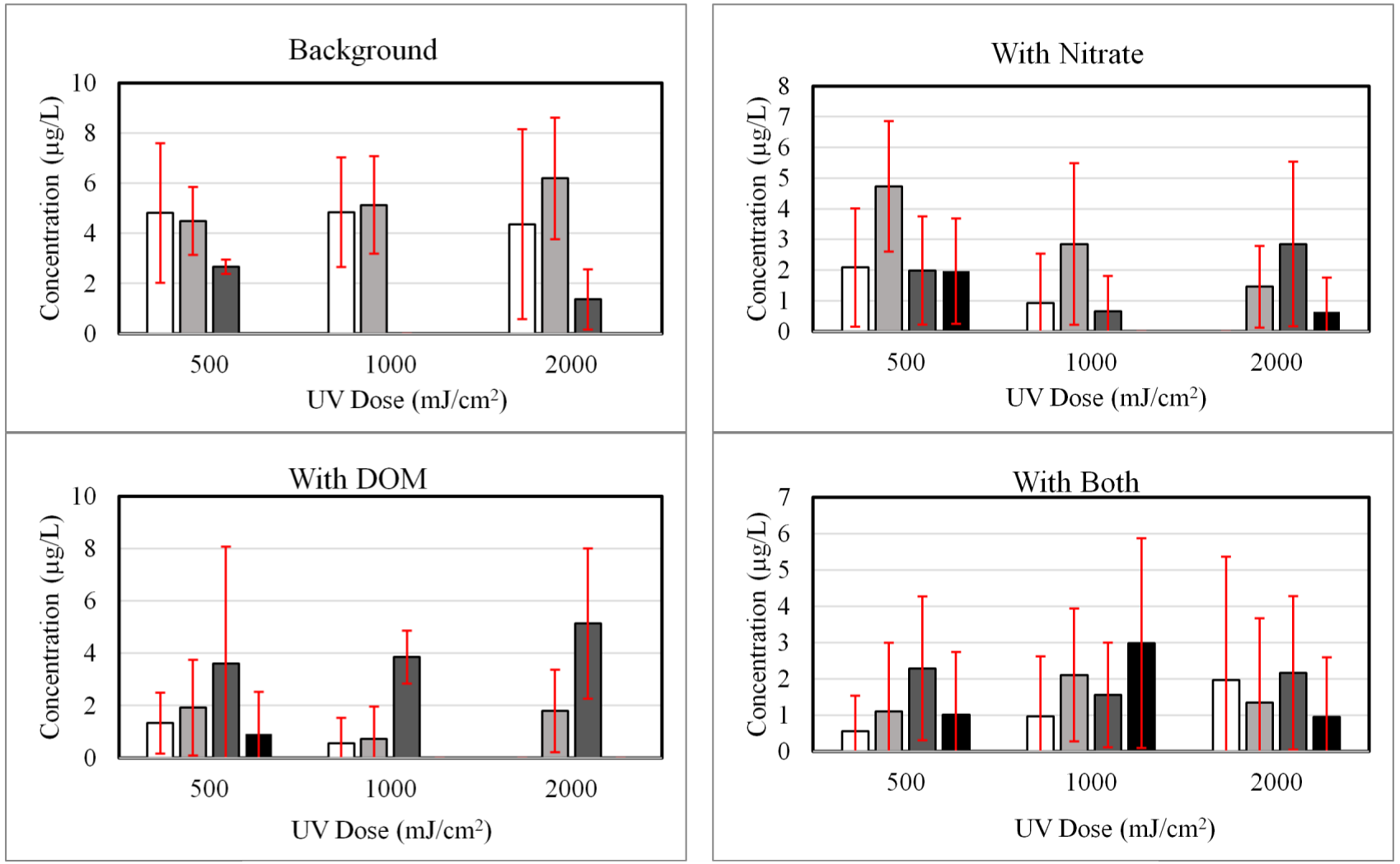

Figure 38. Comparison of Effect of Processes at Given UV Dose and Matrix on Monochloroacetic Acid Formation
Figure shows the average of three separate experiments with the error bars showing standard deviation.

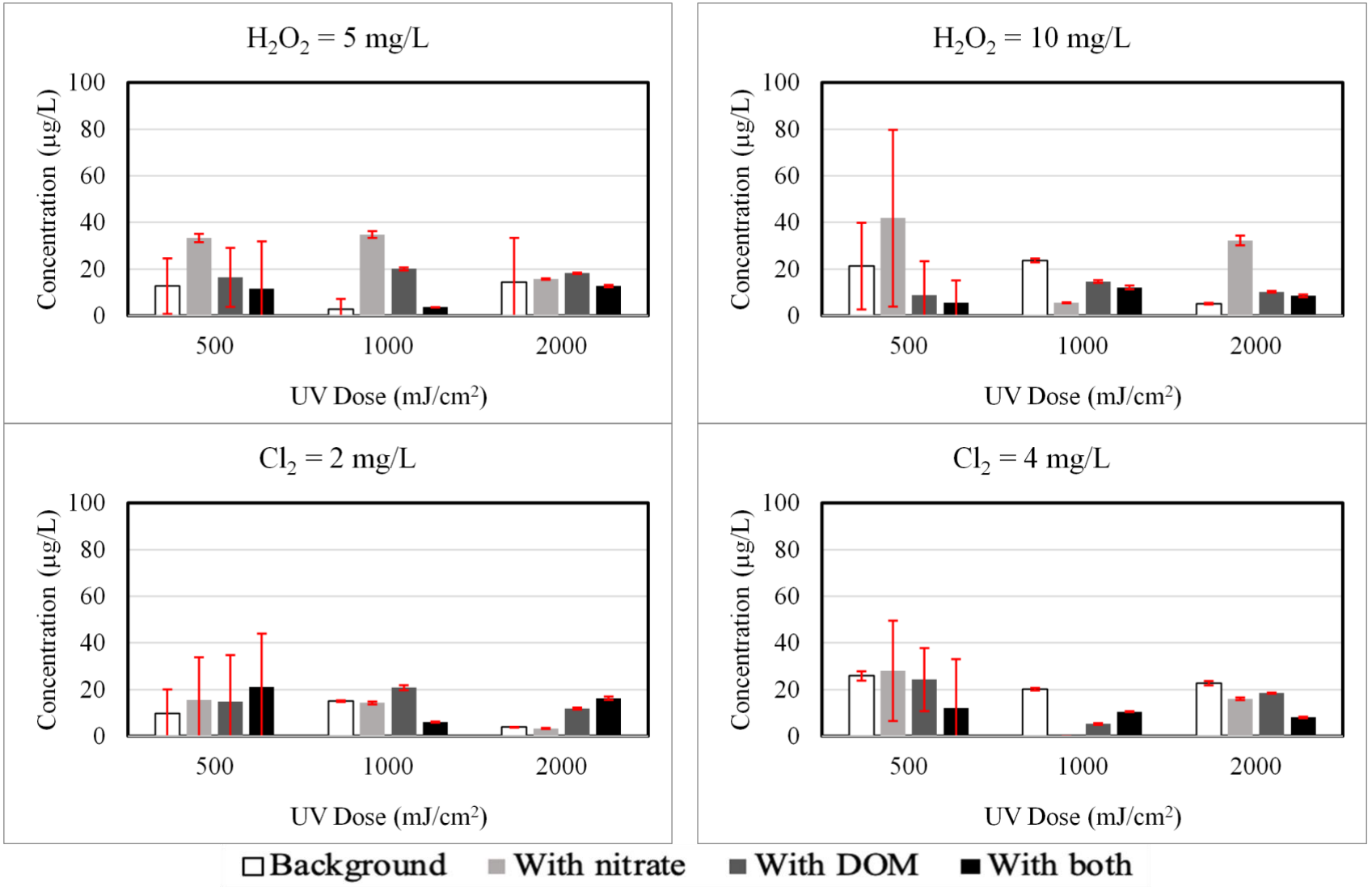

Figure 39. Effect of Matrix and UV Dose for Different Processes on Chlorodibromoacetic Acid Formation
Figure shows the average of three separate experiments with the error bars showing standard deviation.

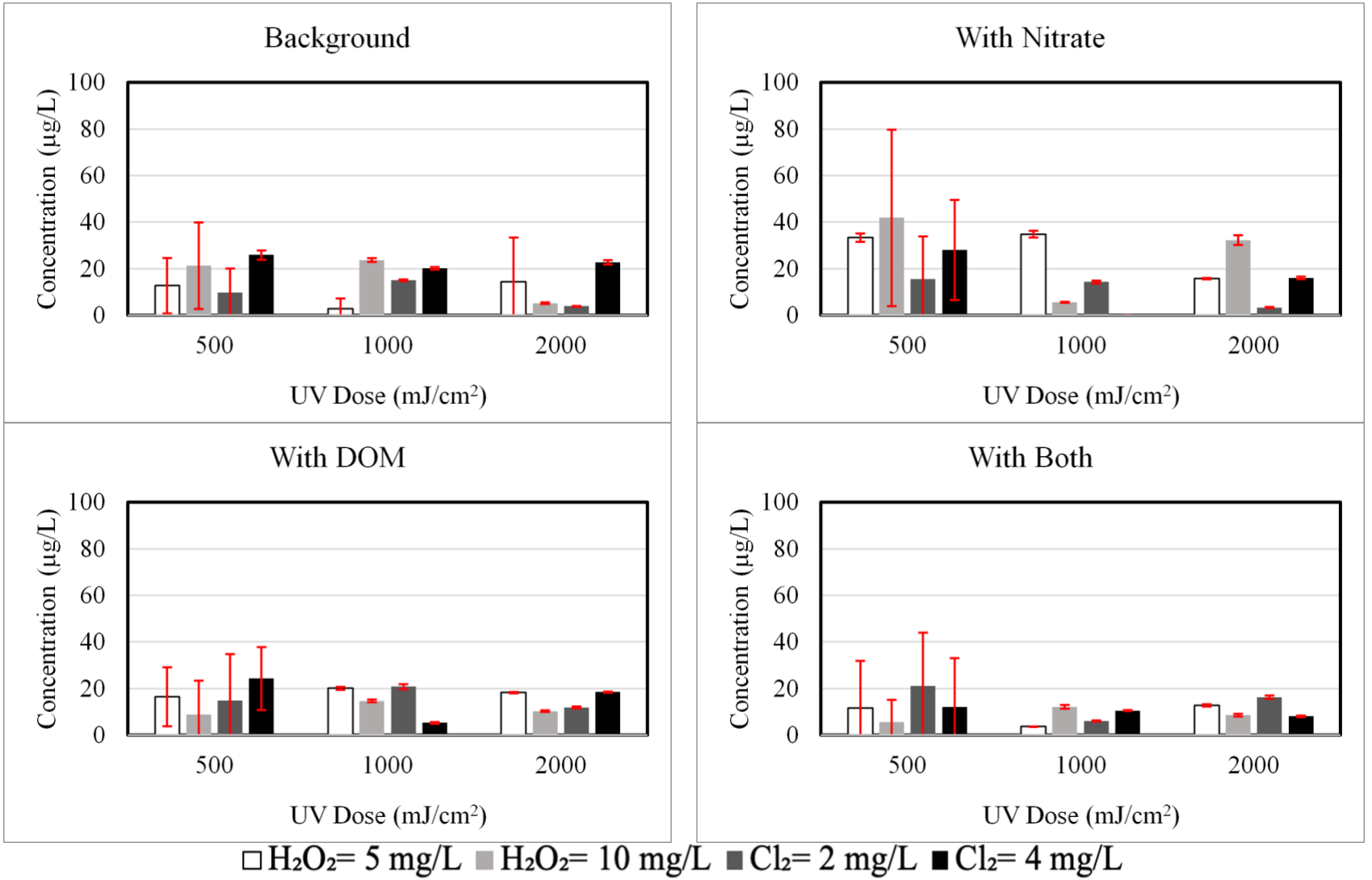

Figure 40. Comparison of Effect of Processes at Given UV Dose and Matrix on Chlorodibromoacetic Acid Formation
Figure shows the average of three separate experiments with the error bars showing standard deviation.

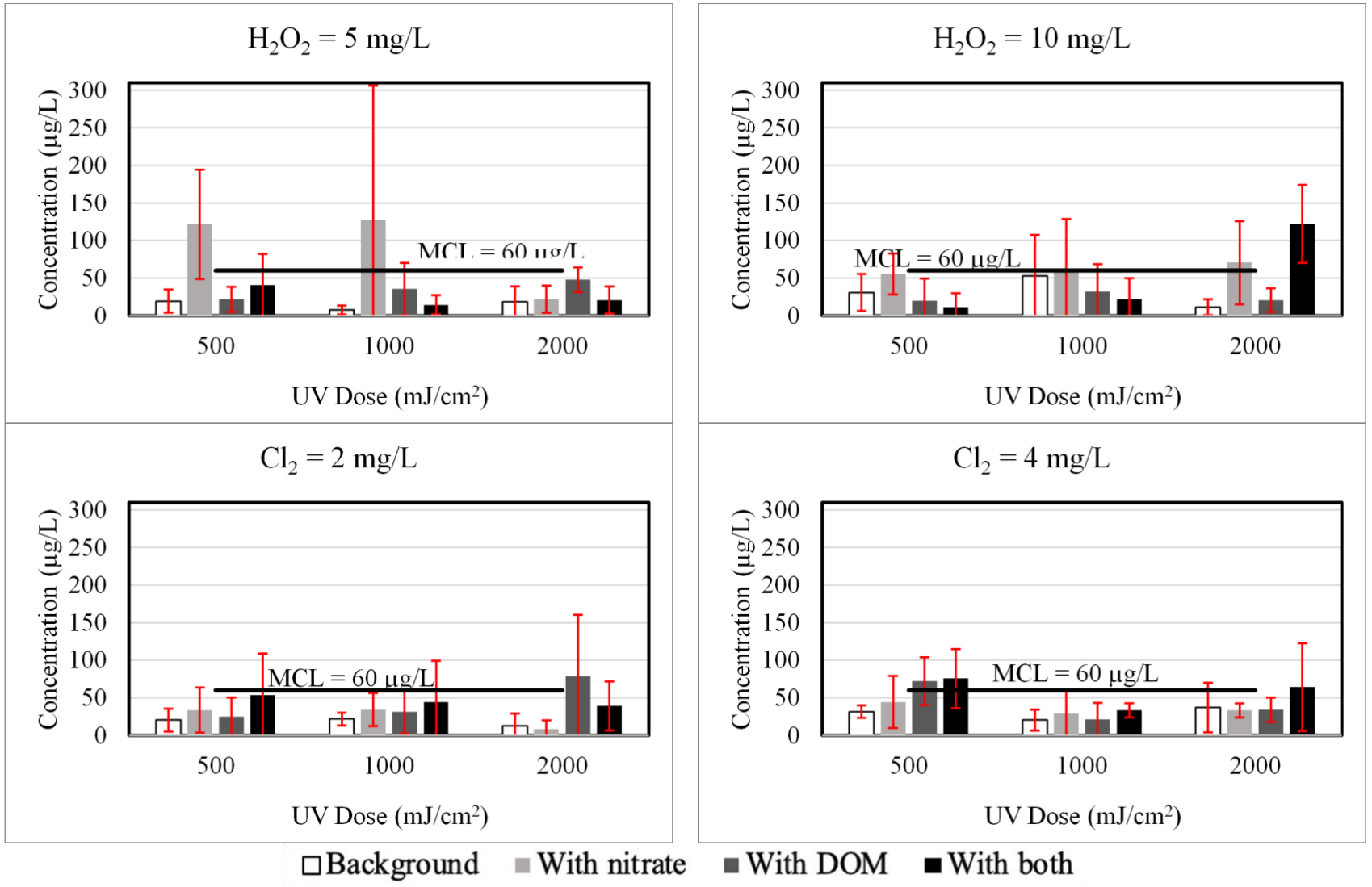

Figure 41. Effect of Matrix and UV Dose for Different Processes on THAAs Formation
Figure shows the average of three separate experiments with the error bars showing standard deviation.

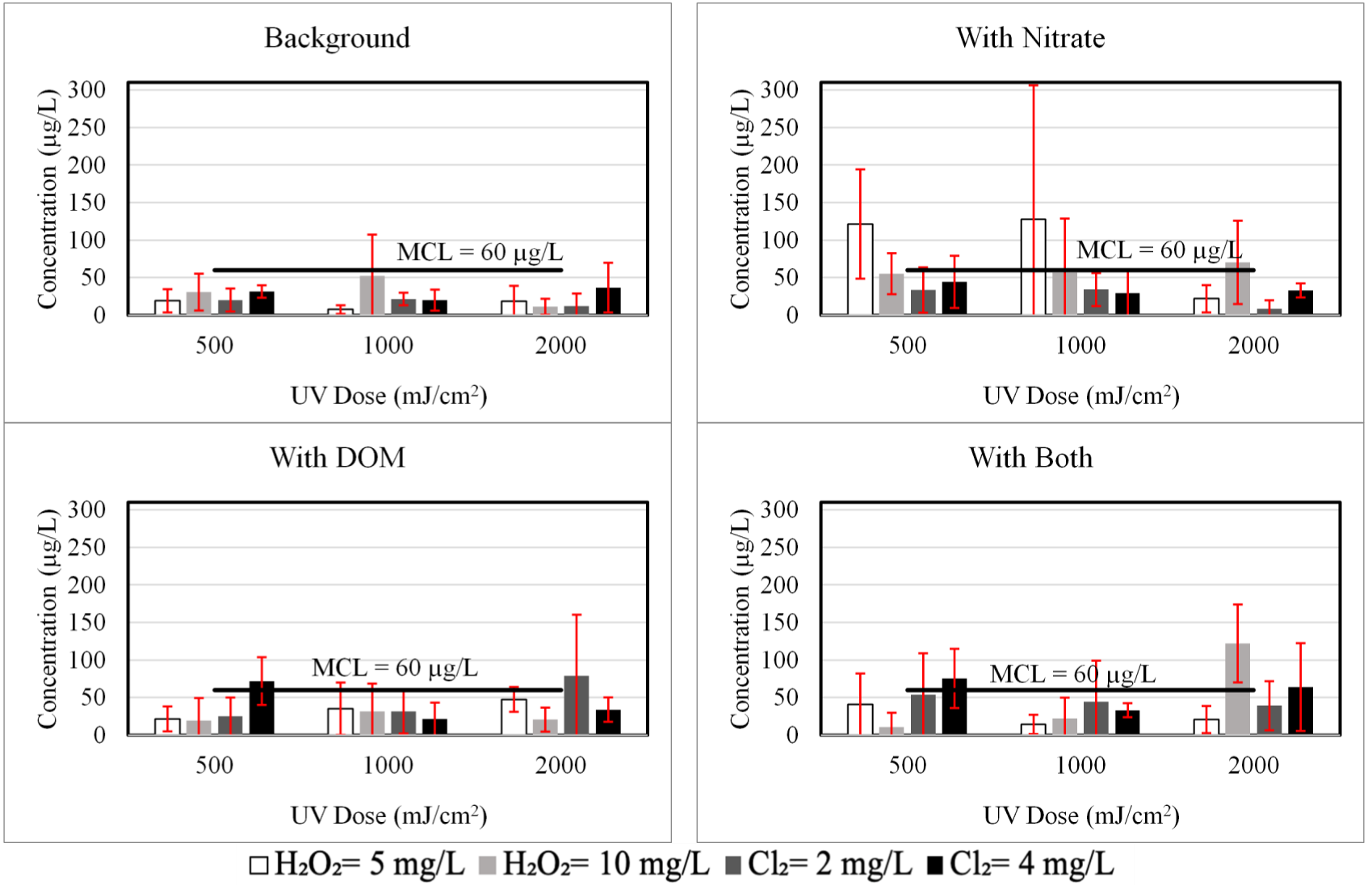

Figure 42. Comparison of Effect of Processes at Given UV Dose and Matrix on THAAs Formation
Figure shows the average of three separate experiments with the error bars showing standard deviation.

4.4.3. Nitrosamines

Both nitrate and algal DOM increased NDMA formation significantly when the samples were treated by UV/H_2O_2 and the p-values were 0.050 and 0.021 for matrix with nitrate and matrix with DOM, respectively, as compared to the background matrix. Same changes were observed using UV/Cl_2 process, however, they were not statistically significant and the p-values were 0.084 and 0.123 for matrix with nitrate and matrix with DOM, respectively.

In all cases, the NDMA in the treated matrix was lower than the health-related advisory level of 10 ng/L (USEPA 2014) under treatment condition.

Nitrate and algal DOM were added at the high end of what is possible, and in full-scale case studies the effects may not be as pronounced. Also, the algal DOM is very nitrogen-rich, which explains the additional formation of NDMA. Figures 43 and 44 demonstrate the effect of matrix and UV dose for different processes on NDMA formation and compare processes at given UV dose and matrix on NDMA formation.

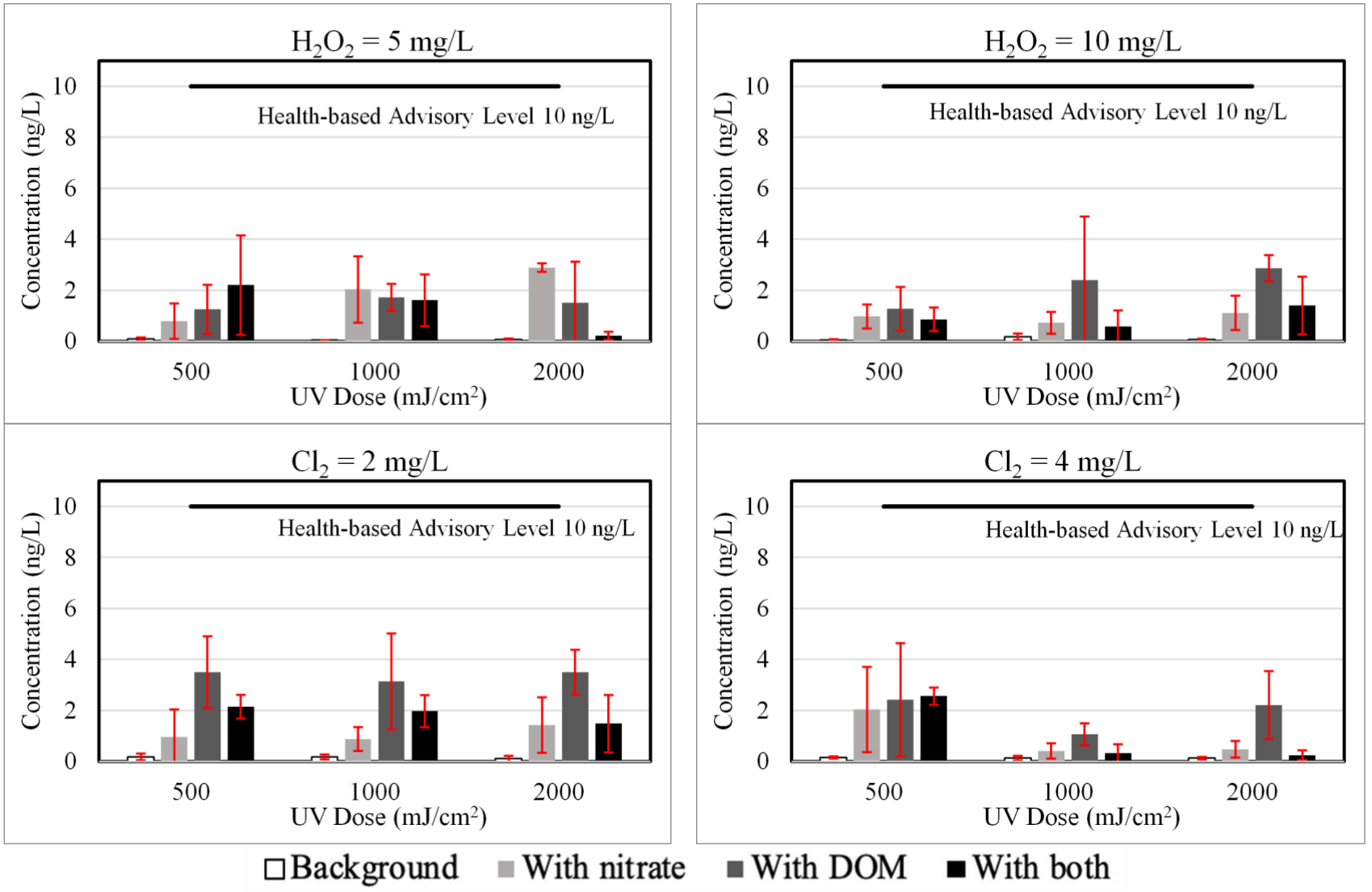

Figure 43. Effect of Matrix and UV Dose for Different Processes on NDMA Formation
Figure shows the average of three separate experiments with the error bars showing standard deviation.

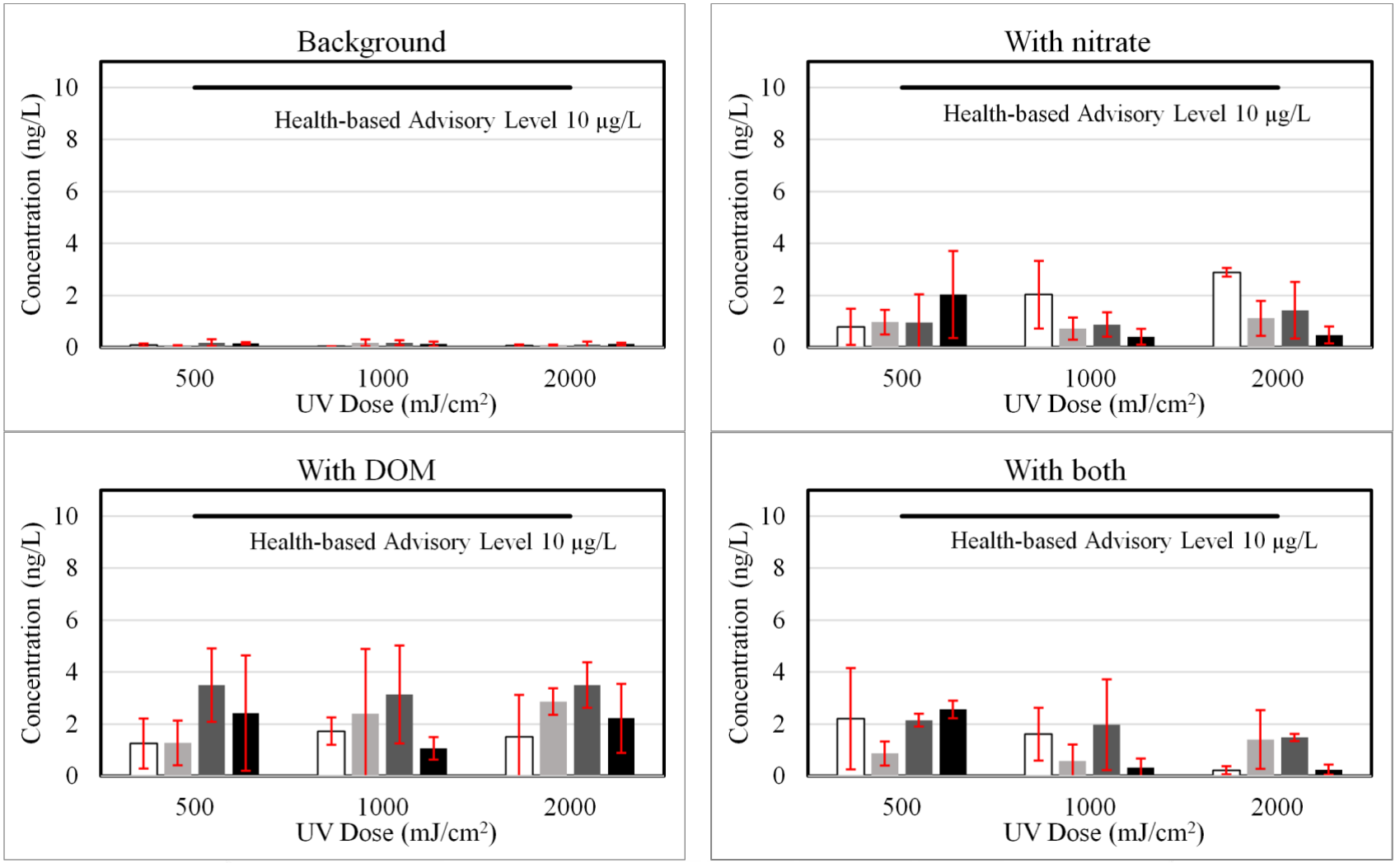

Figure 44. Comparison of Effect of Processes at Given UV Dose and Matrix on NDMA Formation
Figure shows the average of three separate experiments with the error bars showing standard deviation.

4.5. Overall Conclusions

Both UV/H_2O_2 and UV/Cl_2 processes were effective in oxidizing all microcystin variants, including LR, RR, and YR. UV/Cl_2 provided additional oxidation for some microcystins. Based on the observed results the removal efficiency for MC-YR > MC-RR > MC-LR and this result is supported by the previous studies on the reaction of the different amino acids with hydroxyl radical follows.

Even without creating AOP conditions, chlorine and chlorine radicals can degrade microcystins and the addition of chlorine to existing UV disinfection process can remove microcystins up to 90% at Cl_2 = 4 mg/L in background matrix. The removal efficiency of UV/Cl_2 at low UV dose derived from the effect of chlorination.

The background matrix has different inhibitory effects for each toxin because of their relative reactivity with radicals. Higher oxidant dose and higher UV dose help minimizing the impact of the matrix.

The negative effect of DOM as a radical scavenger was observed as expected. The additional radical formation was witnessed in the water matrix with nitrate (NO_3^-). However, having both DOM and nitrate in the water matrix, the effect of DOM as a radical scavenger was higher than the impact of nitrate, creating further radicals. While PP2A assays were inconclusive, the LC/MS results suggest that the Adda group responsible for toxicity is susceptible and likely the products would not exhibit the toxicity of the parent compound.

Based on the results for THMs, chloroform was increased with AOM presence in hydrogen peroxide processes and was suppressed by nitrate. AOM also increased the formation of bromodichloromethane in UV/H_2O_2 process. The maximum TTHM

concentration was 46.26 µg/L belonging to the background matrix that was treated using Cl_2 = 4 mg/L and UV = 2000 mJ/cm_2, which is much less than the MCL.

Three HAAs were detectable in the treated samples, including tribromoacetic acid, chlorodibromoacetic acid, and monochloroacetic acid. HAAs results showed that tribromoacetic acid formation was higher in samples containing nitrate (not statistically significant). No correlation was observed between the type of process or the level of treatment and HAA formation. Monochloroacetic acid was formed during UV/H_2O_2 processes, which was significantly suppressed by the addition of nitrate and algal DOM to the background matrix. The maximum total HAAs was 127.8 µg/L belonging to matrix containing 20 mg/L NO_3 treated by H_2O_2 5 mg/L under UV = 1000 mJ/cm_2. However, in most of the samples total HAAs concentration was less than MCL (60 mg/L).

Findings on NDMA demonstrated that both nitrate and algal DOM increased the formation of NDMA. However, the concentration of nitrate and DOM were on the high end of an environmentally relevant range. Additionally, the level of NDMA was less than 10 ng/L at all treatment conditions and in all background matrices.

4.6. Future Studies

- A detailed study on NDMA formation depending on oxidant concentration and background matrix and an investigation of a threshold of nitrate and algal DOM at which the value begins to rise significantly above the background matrix.
- Investigation of other nitrogenous DBPs (e.g. haloacetonitriles) during UV-based AOPs in presence of algal DOM.
- Testing the background matrix from different DWTPs and comparing the results to determine if the results are generalizable.

- Performing the ADDA-specific ELISA assays to test transformation products and their toxic potential.

REFERENCES

Adams, Jessica L., Edward Tipping, Heidrun Feuchtmayr, Heather T. Carter, and Patrick Keenan. 2018. "The Contribution of Algae to Freshwater Dissolved Organic Matter: Implications for UV Spectroscopic Analysis." *Inland Waters* 8(1):10–21.

Afzal, Atefeh, Thomas Oppenländer, James R. Bolton, and Mohamed Gamal El-Din. 2010. "Anatoxin-a Degradation by Advanced Oxidation Processes: Vacuum-UV at 172 Nm, Photolysis Using Medium Pressure UV and UV/H2O2." *Water Research* 44(1):278–86.

Anderson, Donald M., Siobhan F. E. Boerlage, and Mike B. Dixon. 2017. *Harmful Algal Blooms (HABs) and Desalination: A Guide to Impacts, Monitoring, and Management*.

Atencio, Loyda, Isabel Moreno, Ana I. Prieto, Rosario Moyano, Ana M. Molina, and Ana M. Cameán. 2008. "Acute Effects of Microcystins MC-LR and MC-RR on Acid and Alkaline Phosphatase Activities and Pathological Changes in Intraperitoneally Exposed Tilapia Fish (Oreochromis Sp.)." *Toxicologic Pathology* 36(3):449–58.

Badar, M., Fatima Batool, Safder Shah Khan, Irshad Khokhar, M. K. Qamar, and Ch Yasir. 2017. "Effects of Microcystins Toxins Contaminated Drinking Water on Hepatic Problems in Animals (Cows and Buffalos) and Toxins Removal Chemical Method." *Buffalo Bulletin* 36(1):43–55.

Bajracharya, Asnika, Yen Ling Liu, and John J. Lenhart. 2019. "The Influence of Natural Organic Matter on the Adsorption of Microcystin-LR by Powdered Activated Carbon." *Environmental Science: Water Research and Technology* 5(2):256–67.

Bolton, James R. and Karl G. Linden. 2003. "Standardization of Methods for Fluence (UV Dose) Determination in Bench-Scale UV Experiments." *Journal of Environmental Engineering* 129(3):209–15.

Butler, Ned, James C. Carlisle, Regina Linville, and Barbara Washburn. 2009. *Microcystins: A Brief Overview of Their Toxicity and Effects, with Special Reference to Fish, Wildlife, and Livestock*.

Buxton, George V., Clive L. Greenstock, W. Phillips Helman, and Alberta B. Ross. 1988. "Critical Review of Rate Constants for Reactions of Hydrated Electrons, Hydrogen Atoms and Hydroxyl Radicals (·OH/·O − in Aqueous Solution." *Journal of Physical and Chemical Reference Data* 17(2):513–886.

Carmichael, Wayne W. and Jisi An. 1999. "Using an Enzyme Linked Immunosorbent Assay (ELISA) and a Protein Phosphatase Inhibition Assay (PPIA) for the Detection of Microcystins and Nodularins." *Natural Toxins* 7(6):377–85.

Carmichael, Wayne W. and Gregory L. Boyer. 2016. "Health Impacts from Cyanobacteria Harmful Algae Blooms: Implications for the North American Great Lakes." *Harmful Algae* 54:194–212.

Cerreta, G., Melina A. Roccamante, Isabel Oller, S. Malato, and L. Rizzo. 2019. "Contaminants of Emerging Concern Removal from Real Wastewater by UV/Free Chlorine Process: A Comparison with Solar/Free Chlorine and UV/H2O2 at Pilot Scale." *Chemosphere* 236:124354.

Chae, Soryong, Tahereh Noeiaghaei, Yoontaek Oh, In S. Kim, and Jin-Soo Park. 2019. "Effective Removal of Emerging Dissolved Cyanotoxins from Water Using Hybrid Photocatalytic Composites." *Water Research* 149:421–31.

Chang, Jing, Zhong-lin Chen, Zhe Wang, Ji-min Shen, and Qian Chen. 2014. "ScienceDirect Ozonation Degradation of Microcystin-LR in Aqueous Solution : Intermediates , Byproducts and Pathways." *Water Research* 63:52–61.

Charrois, Jeffrey W. A., Markus W. Arend, Kenneth L. Froese, and Steve E. Hrudey. 2004. "Detecting N -Nitrosamines in Drinking Water at Nanogram per Liter Levels Using Ammonia Positive Chemical Ionization." *Environmental Science & Technology* 38(18):4835–41.

Chen, Jian, Liang Bin Hu, Wei Zhou, Shao Hua Yan, Jing Dong Yang, Yan Feng Xue, and Zhi Qi Shi. 2010. "Degradation of Microcystin-LR and RR by a Stenotrophomonas Sp. Strain EMS Isolated from Lake Taihu, China." *International Journal of Molecular Sciences* 11(3):896–911.

Chen, Shucheng, Zhihua Chen, Samira Siahrostami, Taeho Roy Kim, Dennis Nordlund, Dimosthenis Sokaras, Stanislaw Nowak, John W. F. To, Drew Higgins, Robert Sinclair, Jens K. Nørskov, Thomas F. Jaramillo, and Zhenan Bao. 2018. "Defective Carbon-Based Materials for the Electrochemical Synthesis of Hydrogen Peroxide." *ACS Sustainable Chemistry & Engineering* 6(1):311–17.

Cook, D. and G. Newcombe. 2008. "Comparison and Modeling of the Adsorption of Two Microcystin Analogues onto Powdered Activated Carbon." *Environmental Technology* 29(5):525–34.

Daly, Robert I., Lionel Ho, and Justin D. Brookes. 2007. "Effect of Chlorination on Microcystis Aeruginosa Cell Integrity and Subsequent Microcystin Release and Degradation." *Environmental Science and Technology* 41(12):4447–53.

Danner, Kelsey M., Megan A. Mave, Audrey H. Sawyer, Seungjun Lee, and Jiyoung Lee. 2018. "Removal of the Algal Toxin Microcystin-LR in Permeable Coastal Sediments: Physical and Numerical Models." *Limnology and Oceanography* 63(4):1593–1604.

Deng, Yang, Meiyin Wu, Huiqin Zhang, Lei Zheng, Yaritza Acosta, and Tsung-Ta D. Hsu. 2017. "Addressing Harmful Algal Blooms (HABs) Impacts with Ferrate(VI): Simultaneous Removal of Algal Cells and Toxins for Drinking Water Treatment." *Chemosphere* 186:757–61.

Devi, Salam Sonia and Dinabandhu Sahoo. 2015. "Culturing Algae." Pp. 555–79 in.

Díez-Quijada, Leticia, María Puerto, Daniel Gutiérrez-Praena, María Llana-Ruiz-Cabello, Angeles Jos, and Ana M. Cameán. 2019. "Microcystin-RR: Occurrence, Content in Water and Food and Toxicological Studies. A Review." *Environmental Research* 168(April 2018):467–89.

Domino, M. M., D. J. Munch, P. S. Fair, Y. Xie, J. W. Munch, A. M. Pawlecki-Vonderheide, J. W. Hodgeson, D. Becker, J. Collins, and Barth R.E. 2003. "EPA Method 552.3." (1990):1–66.

Dotson, Aaron D., Olya Keen, Debbie Metz, and Karl G. Linden. 2010. "UV/H2O2 Treatment of Drinking Water Increases Post-Chlorination DBP Formation." *Water Research* 44(12):3703–13.

Draper, William M., Dadong Xu, Paramjit Behniwal, Michael J. McKinney, Prasanna Jayalath, Jagdev S. Dhoot, and Donald Wijekoon. 2013. "Optimizing LC-MS-MS Determination of Microcystin Toxins in Natural Water and Drinking Water Supplies." *Analytical Methods* 5(23):6796–6806.

Drogui, P., S. Elmaleh, M. Rumeau, C. Bernard, and A. Rambaud. 2001. "Hydrogen

Peroxide Production by Water Electrolysis: Application to Disinfection." *Journal of Applied Electrochemistry* 31(8):877–82.

Duan, Xiaodi, Toby Sanan, Armah De La Cruz, Xuexiang He, Minghao Kong, and Dionysios D. Dionysiou. 2018. "Susceptibility of the Algal Toxin Microcystin-LR to UV/Chlorine Process: Comparison with Chlorination." *Environmental Science and Technology* 52(15):8252–62.

Eke, Joyner, Priyesh Wagh, and Isabel C. Escobar. 2018. "Ozonation, Biofiltration and the Role of Membrane Surface Charge and Hydrophobicity in Removal and Destruction of Algal Toxins at Basic PH Values." *Separation and Purification Technology* 194(November 2017):56–63.

Fang, Jingyun, Jun Ma, Xin Yang, and Chii Shang. 2010. "Formation of Carbonaceous and Nitrogenous Disinfection By-Products from the Chlorination of Microcystis Aeruginosa." *Water Research* 44(6):1934–40.

Fang, Jingyun, Xin Yang, Jun Ma, Chii Shang, and Quan Zhao. 2010. "Characterization of Algal Organic Matter and Formation of DBPs from Chlor(Am)Ination." *Water Research* 44(20):5897–5906.

Flechtner, James R. 2017. *Desktop Evaluation of Alternatives - GenX and Other PFAS Treatment Options Study*.

Francis, George. 1878. "Poisonous Australian Lake." *Nature* 18(444):11–12.

Gang, Dianchen, Thomas E. Clevenger, and Shankha K. Banerji. 2003. "Relationship of Chlorine Decay and THMs Formation to NOM Size." *Journal of Hazardous Materials* 96(1):1–12.

Gibco. 2020. "Gibco BG-11 Media." Retrieved (https://www.thermofisher.com/order/catalog/product/A1379901#/A1379901).

Gobler, Christopher J., JoAnn M. Burkholder, Timothy W. Davis, Matthew J. Harke, Tom Johengen, Craig A. Stow, and Dedmer B. Van de Waal. 2016. "The Dual Role of Nitrogen Supply in Controlling the Growth and Toxicity of Cyanobacterial Blooms." *Harmful Algae* 54:87–97.

Goslan, Emma H., Céline Seigle, Diane Purcell, Rita Henderson, Simon A. Parsons, Bruce Jefferson, and Simon J. Judd. 2017. "Carbonaceous and Nitrogenous Disinfection By-Product Formation from Algal Organic Matter." *Chemosphere* 170:1–9.

Graham, JL, KA Loftin, and Neil Kamman. 2009. "Monitoring Recreational Freshwaters." *Lakeline* 18–24.

Hall, T., J. Hart, B. Croll, and R. Gregory. 2000. "Laboratory-Scale Investigations of Algal Toxin Removal by Water Treatment." *Water and Environment Journal* 14(2):143–49.

He, Xuexiang, Armah A. de la Cruz, Anastasia Hiskia, Triantafyllos Kaloudis, Kevin O'Shea, and Dionysios D. Dionysiou. 2015. "Destruction of Microcystins (Cyanotoxins) by UV-254 Nm-Based Direct Photolysis and Advanced Oxidation Processes (AOPs): Influence of Variable Amino Acids on the Degradation Kinetics and Reaction Mechanisms." *Water Research* 74:227–38.

He, Xuexiang, Yen-Ling Liu, Amanda Conklin, Judy Westrick, Linda K. Weavers, Dionysios D. Dionysiou, John J. Lenhart, Paula J. Mouser, David Szlag, and Harold W. Walker. 2016. "Toxic Cyanobacteria and Drinking Water: Impacts, Detection, and Treatment." *Harmful Algae* 54:174–93.

He, Xuexiang, Miguel Pelaez, Judy A. Westrick, Kevin E. O'Shea, Anastasia Hiskia, Theodoros Triantis, Triantafyllos Kaloudis, Mihaela I. Stefan, Armah A. de la Cruz, and Dionysios D. Dionysiou. 2012. "Efficient Removal of Microcystin-LR by UV-C/H2O2in Synthetic and Natural Water Samples." *Water Research* 46(5):1501–10.

Henderson, Rita K., Andy Baker, Simon A. Parsons, and Bruce Jefferson. 2008. "Characterisation of Algogenic Organic Matter Extracted from Cyanobacteria, Green Algae and Diatoms." *Water Research* 42(13):3435–45.

Hitzfeld, Bettina C., Stefan J. Hoger, and Daniel R. Dietrich. 2000. "Cyanobacterial Toxins: Removal during Drinking." 1(July 1999).

Hodgeson, J. W., A. L. Cohen, D. J. Munch, and D. P. Hautman. 1995. "Method 551.1, Determination of Chlorination Disinfection Byproducts, Chlorinated Solvents , and Halogenated Pesticides/Herbicides in Drinking Dater by Liquid-Liquid Extraction and Gas Chromatography with Electron-Capture Detection." 1–61.

Hoeger, Stefan J., Bettina C. Hitzfeld, and Daniel R. Dietrich. 2005. "Occurrence and Elimination of Cyanobacterial Toxins in Drinking Water Treatment Plants." *Toxicology and Applied Pharmacology* 203(3 SPEC. ISS.):231–42.

Ikehara, Tsuyoshi, Shihoko Imamura, Naomasa Oshiro, Satsuki Ikehara, Fukiko Shinjo, and Takeshi Yasumoto. 2008. "A Protein Phosphatase 2A (PP2A) Inhibition Assay Using a Recombinant Enzyme for Rapid Detection of Microcystins." *Toxicon* 51(8):1368–73.

Jiang, Xuewen, Seungjun Lee, Chulkyoon Mok, and Jiyoung Lee. 2017. "Sustainable Methods for Decontamination of Microcystin in Water Using Cold Plasma and UV with Reusable TiO2 Nanoparticle Coating." *International Journal of Environmental Research and Public Health* 14(5):480.

Jurczak, Tomasz, Malgorzata Tarczynska, Katarzyna Izydorczyk, Joanna Mankiewicz, MacIej Zalewski, and Jussi Meriluoto. 2005. "Elimination of Microcystins by Water Treatment Processes—Examples from Sulejow Reservoir, Poland." *Water Research* 39(11):2394–2406.

Kaloudis, Triantafyllos, Sevasti Kiriaki Zervou, Katerina Tsimeli, Theodoros M. Triantis, Theodora Fotiou, and Anastasia Hiskia. 2013. "Determination of Microcystins and Nodularin (Cyanobacterial Toxins) in Water by LC-MS/MS. Monitoring of Lake Marathonas, a Water Reservoir of Athens, Greece." *Journal of Hazardous Materials* 263:105–15.

Kamber, M., S. Fluckiger-Isler, G. Engelhardt, R. Jaeckh, and E. Zeiger. 2009. "Comparison of the Ames II and Traditional Ames Test Responses with Respect to Mutagenicity, Strain Specificities, Need for Metabolism and Correlation with Rodent Carcinogenicity." *Mutagenesis* 24(4):359–66.

Karanfil, Tanju, Ilke Erdogan, and Mark A. Schlautman. 2003. "Selecting Filter Membranes for Measuring DOC and UV254." *American Water Works Association* 95(3):86–100.

Keen, Olya, Aaron D. Dotson, and Karl G. Linden. 2013. "Evaluation of Hydrogen Peroxide Chemical Quenching Agents Following an Advanced Oxidation Process." *Journal of Environmental Engineering* 139(1):137–40.

Keen, Olya and Karl G. Linden. 2013. "Re-Engineering an Artificial Sweetener: Transforming Sucralose Residuals in Water via Advanced Oxidation." *Environmental Science and Technology* 47(13):6799–6805.

Keen, Olya, Nancy G. Love, Diana S. Aga, and Karl G. Linden. 2016. “Biodegradability of Iopromide Products after UV/H2O2 Advanced Oxidation.” *Chemosphere* 144:989–94.

Keen, Olya, Nancy G. Love, and Karl G. Linden. 2012. “The Role of Effluent Nitrate in Trace Organic Chemical Oxidation during UV Disinfection.” *Water Research* 46(16):5224–34.

Keen, Olya, Garrett McKay, Stephen P. Mezyk, Karl G. Linden, and Fernando L. Rosario-Ortiz. 2014. “Identifying the Factors That Influence the Reactivity of Effluent Organic Matter with Hydroxyl Radicals.” *Water Research* 50:408–19.

Kitis, Mehmet. 2004. “Disinfection of Wastewater with Peracetic Acid: A Review.” *Environment International* 30(1):47–55.

Klassen, Normal V., David Marchington, and Heather C. E. McGowan. 1994. “H2O2 Determination by the I3- Method and by KMnO4 Titration.” *Analytical Chemistry* 66(18):2921–25.

Kristiana, Ina, Arron Lethorn, Cynthia Joll, and Anna Heitz. 2014. “To Add or Not to Add: The Use of Quenching Agents for the Analysis of Disinfection by-Products in Water Samples.” *Water Research* 59(0):90–98.

Kumar, Pratik, Krishnamoorthy Hegde, Satinder Kaur Brar, Maximiliano Cledon, and Azadeh Kermanshahi Pour. 2018. “Physico-Chemical Treatment for the Degradation of Cyanotoxins with Emphasis on Drinking Water Treatment - How Far Have We Come?” *Journal of Environmental Chemical Engineering* 6(4):5369–88.

Lee, Doorae, Minhwan Kwon, Yongtae Ahn, Youmi Jung, Seong Nam Nam, Il hwan Choi, and Joon Wun Kang. 2018. “Characteristics of Intracellular Algogenic Organic Matter and Its Reactivity with Hydroxyl Radicals.” *Water Research* 144:13–25.

Li, Lei, Naiyun Gao, Yang Deng, Juanjuan Yao, and Kejia Zhang. 2012. “Characterization of Intracellular & Extracellular Algae Organic Matters (AOM) of Microcystic Aeruginosa and Formation of AOM-Associated Disinfection Byproducts and Odor & Taste Compounds.” *Water Research* 46(4):1233–40.

Liu, Jing and Yu Sun. 2015. “The Role of PP2A-Associated Proteins and Signal Pathways in Microcystin-LR Toxicity.” *Toxicology Letters* 236(1):1–7.

Liu, Wenjun, Susan A. Andrews, Mihaela I. Stefan, and James R. Bolton. 2003. “Optimal Methods for Quenching H2O2 Residuals Prior to UFC Testing.” *Water Research* 37(15):3697–3703.

Liu, Xiaolin, Xiao Wei, Weiwei Zheng, Songhui Jiang, Michael R. Templeton, Gengsheng He, and Weidong Qu. 2013. “An Optimized Analytical Method for the Simultaneous Detection of Iodoform, Iodoacetic Acid, and Other Trihalomethanes and Haloacetic Acids in Drinking Water” edited by Z. Zhou. *PLoS ONE* 8(4):e60858.

Liu, Xiaowei, Zhonglin Chen, Nan Zhou, Jimin Shen, and Miaomiao Ye. 2010. “Degradation and Detoxification of Microcystin-LR in Drinking Water by Sequential Use of UV and Ozone.” *Journal of Environmental Sciences* 22(12):1897–1902.

Liu, Yen Ling, Harold W. Walker, and John J. Lenhart. 2019. “The Effect of Natural Organic Matter on the Adsorption of Microcystin-LR onto Clay Minerals.” *Colloids*

and Surfaces A: Physicochemical and Engineering Aspects 583(July):123964.

Loftin, Keith A., Jimmy M. Clark, Celeste A. Journey, Dana W. Kolpin, Peter C. Van Metre, Daren Carlisle, and Paul M. Bradley. 2016. "Spatial and Temporal Variation in Microcystin Occurrence in Wadeable Streams in the Southeastern United States." *Environmental Toxicology and Chemistry* 35(9):2281–87.

Lopez, Antonio, Anna Bozzi, Giuseppe Mascolo, Ruggiero Ciannarella, and Roberto Passino. 2003. "UV and H2O2/UV Degradation of a Pharmaceutical Intermediate in Aqueous Solution." *Annali Di Chimica* 92(1–2):41–51.

Lu, Jingrang, Ian Struewing, Larry Wymer, Daniel R. Tettenhorst, Jody Shoemaker, and Joel Allen. 2020. "Use of QPCR and RT-QPCR for Monitoring Variations of Microcystin Producers and as an Early Warning System to Predict Toxin Production in an Ohio Inland Lake." *Water Research* 170:115262.

Ma, Min, Ruiping Liu, Huijuan Liu, Jiuhui Qu, and William Jefferson. 2012. "Effects and Mechanisms of Pre-Chlorination on Microcystis Aeruginosa Removal by Alum Coagulation: Significance of the Released Intracellular Organic Matter." *Separation and Purification Technology* 86:19–25.

Mack, John and James R. Bolton. 1999. "Photochemistry of Nitrite and Nitrate in Aqueous Solution: A Review." *Journal of Photochemistry and Photobiology A: Chemistry* 128(1–3):1–13.

Maron, Dorothy M. and Bruce N. Ames. 1983. "Revised Methods for the Salmonella Mutagenicity Test." *Mutation Research/Environmental Mutagenesis and Related Subjects* 113(3–4):173–215.

Martijn, Abraham Jan. 2015. "Impact of the Water Matrix on the Effect and the Side Effect of MP UV/H2O2 Treatment for the Removal of Organic Micropollutants in Drinking Water Production."

Martínez-Huitle, Carlos A. and Enric Brillas. 2008. "Electrochemical Alternatives for Drinking Water Disinfection." *Angewandte Chemie - International Edition* 47(11):1998–2005.

Mash, H. and A. Wittkorn. 2016. "Effect of Chlorination on the Protein Phosphatase Inhibition Activity for Several Microcystins." *Water Research* 95:230–39.

Merel, Sylvain, Michel Clément, and Olivier Thomas. 2010. "State of the Art on Cyanotoxins in Water and Their Behaviour towards Chlorine." *Toxicon* 55(4):677–91.

Moon, Bo-ram, Tae-Kyoung Kim, Moon-kyung Kim, Jaewon Choi, and Kyung-duk Zoh. 2017. "Degradation Mechanisms of Microcystin-LR during UV-B Photolysis and UV/H2O2 Processes: Byproducts and Pathways." *Chemosphere* 185:1039–47.

Mountfort, Douglas O., Patrick Holland, and Jan Sprosen. 2005. "Method for Detecting Classes of Microcystins by Combination of Protein Phosphatase Inhibition Assay and ELISA: Comparison with LC-MS." *Toxicon* 45(2):199–206.

Munch, J. W. and M. V. Bassett. 2004. "Method 521: Determination of Nitrosamines in Drinking Water by Solid-Phase Extraction and Capillary Column Gas Chromatography with Large Volume Injection and Chemical Ionization Tandem Mass Spectrometry (MS/MS)." *EPA Document #: EPA/600/R-05/054* 47.

NCDENR. 2016. *1,4-Dioxane in the Cape Fear River Basin of North Carolina: An Initial Screening and Source Identification Study*.

Nihemaiti, Maolida, Ratish Ramyad Permala, and Jean Philippe Croué. 2020. "Reactivity

of Unactivated Peroxymonosulfate with Nitrogenous Compounds." *Water Research* 169.

Qi, Mei, Yao Dang, Qinglong Xu, Liqin Yu, Chunsheng Liu, Yongchao Yuan, and Jianghua Wang. 2016. "Microcystin-LR Induced Developmental Toxicity and Apoptosis in Zebrafish (Danio Rerio) Larvae by Activation of ER Stress Response." *Chemosphere* 157:166–73.

Radjenovic, Jelena and David L. Sedlak. 2015. "Challenges and Opportunities for Electrochemical Processes as Next-Generation Technologies for the Treatment of Contaminated Water." *Environmental Science and Technology* 49(19):11292–302.

Remucal, C. K. and D. Manley. 2016. "Emerging Investigators Series: The Efficacy of Chlorine Photolysis as an Advanced Oxidation Process for Drinking Water Treatment." *Environmental Science: Water Research & Technology* 2(4):565–79.

Renner, Beatriz, Sabra R. Botch-jones, and Claude R. Mallet. 2019. *Analysis of Microcystins in Urine with 2D-LC-MS / MS – Part III*. Boston.

Rizzo, Luigi, Giusy Lofrano, Carmen Gago, Tatiana Bredneva, Patrizia Iannece, Marta Pazos, Nataliya Krasnogorskaya, and Maurizio Carotenuto. 2018. "Antibiotic Contaminated Water Treated by Photo Driven Advanced Oxidation Processes: Ultraviolet/H2O2 vs Ultraviolet/Peracetic Acid." *Journal of Cleaner Production* 205:67–75.

Rodríguez, Eva, Gretchen D. Onstad, Tomas P. J. Kull, James S. Metcalf, Juan L. Acero, and Urs von Gunten. 2007. "Oxidative Elimination of Cyanotoxins: Comparison of Ozone, Chlorine, Chlorine Dioxide and Permanganate." *Water Research* 41(15):3381–93.

Rositano, J., G. Newcombe, B. Nicholson, and P. Sztajnbok. 2001. "Ozonation of Nom and Algal Toxins in Four Treated Waters." *Water Research* 35(1):23–32.

Sanders, Jon. 2018. "Early Responses to Unregulated Contaminants in the Cape Fear River." *John Locke Foundation* 1–20.

Schmidt, Justine R., Steven W. Wilhelm, and Gregory L. Boyer. 2014. "The Fate of Microcystins in the Environment and Challenges for Monitoring." *Toxins* 6(12):3354–87.

Sedan, Daniela, Martín Laguens, Guido Copparoni, Jorge Oswaldo Aranda, Leda Giannuzzi, Carlos Alberto Marra, and Darío Andrinolo. 2015. "Hepatic and Intestine Alterations in Mice after Prolonged Exposure to Low Oral Doses of Microcystin-LR." *Toxicon* 104:26–33.

Senogles, P. J., J. A. Scott, G. Shaw, and H. Stratton. 2001. "Photocatalytic Degradation of the Cyanotoxin Cylindrospermopsin, Using Titanium Dioxide and UV Irradiation." *Water Research* 35(5):1245–55.

Shang, Lixia, Muhua Feng, Xiangen Xu, Feifei Liu, Fan Ke, and Wenchao Li. 2018. "Co-Occurrence of Microcystins and Taste-and-Odor Compounds in Drinking Water Source and Their Removal in a Full-Scale Drinking Water Treatment Plant." *Toxins* 10(1):26.

Sharma, Virender K., Xin Yu, Thomas J. McDonald, Chetan Jinadatha, Dionysios D. Dionysiou, and Mingbao Feng. 2019. "Elimination of Antibiotic Resistance Genes and Control of Horizontal Transfer Risk by UV-Based Treatment of Drinking Water: A Mini Review." *Frontiers of Environmental Science & Engineering* 13(3):37.

Sichel, C., C. Garcia, and K. Andre. 2011. "Feasibility Studies: UV/Chlorine Advanced

Oxidation Treatment for the Removal of Emerging Contaminants." *Water Research* 45(19):6371–80.
Sillanpää, Mika, Mohamed Chaker Ncibi, and Anu Matilainen. 2018. "Advanced Oxidation Processes for the Removal of Natural Organic Matter from Drinking Water Sources: A Comprehensive Review." *Journal of Environmental Management* 208:56–76.
Song, Weihua, Armah A. De La Cruz, Kathleen Rein, and Kevin E. O'Shea. 2006. "Ultrasonically Induced Degradation of Microcystin-LR and -RR: Identification of Products, Effect of PH, Formation and Destruction of Peroxides." *Environmental Science and Technology* 40(12):3941–46.
Summers, R. Scott, Stuart M. Hooper, Hiba M. Shukairy, Gabriele Solarik, and Douglas Owen. 1996. "Assessing DBP Yield: Uniform Formation Conditions." *Journal - American Water Works Association* 88(6):80–93.
Sun, Julong, Lingjun Bu, Shiyang Chen, Xianlei Lu, Yangtao Wu, Zhou Shi, and Shiqing Zhou. 2019. "Oxidation of Microcystic-LR via the Solar/Chlorine Process: Radical Mechanism, Pathways and Toxicity Assessment." *Ecotoxicology and Environmental Safety* 183(July):109509.
Sun, Julong, Lingjun Bu, Lin Deng, Zhou Shi, and Shiqing Zhou. 2018. "Removal of Microcystis Aeruginosa by UV/Chlorine Process: Inactivation Mechanism and Microcystins Degradation." *Chemical Engineering Journal* 349(April):408–15.
Sun, Mei, Catalina Lopez-Velandia, and Detlef R. U. Knappe. 2016. "Determination of 1,4-Dioxane in the Cape Fear River Watershed by Heated Purge-and-Trap Preconcentration and Gas Chromatography-Mass Spectrometry." *Environmental Science and Technology* 50(5):2246–54.
Sun, Peizhe, Wan-Ning Lee, Ruochun Zhang, and Ching-Hua Huang. 2016. "Degradation of DEET and Caffeine under UV/Chlorine and Simulated Sunlight/Chlorine Conditions." *Environmental Science & Technology* 50(24):13265–73.
Szlag, David, James Sinclair, Benjamin Southwell, and Judy Westrick. 2015. "Cyanobacteria and Cyanotoxins Occurrence and Removal from Five High-Risk Conventional Treatment Drinking Water Plants." *Toxins* 7(6):2198–2220.
Tran, Nam, Patrick Drogui, Jean François Blais, and Guy Mercier. 2012. "Phosphorus Removal from Spiked Municipal Wastewater Using Either Electrochemical Coagulation or Chemical Coagulation as Tertiary Treatment." *Separation and Purification Technology* 95:16–25.
U.S. EPA. 2020. "National Primary Drinking Water Regulations." Retrieved (https://www.epa.gov/ground-water-and-drinking-water/national-primary-drinking-water-regulations).
US EPA. 2016. *Final CCL 4 Chemical Contaminants*.
USEPA. 2014. *EPA - NDMA Technical Fact Sheet*.
USEPA. 2015. "Algal Toxin Risk Assessment and Management Strategic Plan for Drinking Water United States Environmental Protection Agency." (November).
USEPA. 2016. "Six-Year Review 3 Technical Support Document for Disinfectants/Disinfection Byproducts Rules." *U.S. Environmental Protection Agency* 110.
Visentin, Flavia, Siddharth Bhartia, Madjid Mohseni, Sarah Dorner, and Benoit Barbeau.

2019. “Performance of Vacuum UV (VUV) for the Degradation of MC-LR, Geosmin, and MIB from Cyanobacteria-Impacted Waters.” *Environmental Science: Water Research and Technology* 5(11):2048–58.

Wang, Chengkun, Xiaojian Zhang, Jun Wang, and Chao Chen. 2012. “Detecting N-Nitrosamines in Water Treatment Plants and Distribution Systems in China Using Ultra-Performance Liquid Chromatography-Tandem Mass Spectrometry.” *Frontiers of Environmental Science & Engineering* 6(6):770–77.

Watts, Michael J., Erik J. Rosenfeldt, and Karl G. Linden. 2007. “Comparative OH Radical Oxidation Using UV-Cl2 and UV-H 2O2 Processes.” *Journal of Water Supply: Research and Technology - AQUA* 56(8):469–77.

Westerhoff, Paul, George Aiken, Gary Amy, and Jean Debroux. 1999. “Relationships between the Structure of Natural Organic Matter and Its Reactivity towards Molecular Ozone and Hydroxyl Radicals.” *Water Research* 33(10):2265–76.

Woolbright, Benjamin L., C. David Williams, Hongmin Ni, Sean C. Kumer, Timothy Schmitt, Bartholomew Kane, and Hartmut Jaeschke. 2017. “Microcystin-LR Induced Liver Injury in Mice and in Primary Human Hepatocytes Is Caused by Oncotic Necrosis.” *Toxicon* 125:99–109.

Wu, Jing, Dandan Cao, Wei Gao, Kun Lv, Yong Liang, Jianjie Fu, Yan Gao, Yawei Wang, and Guibin Jiang. 2019. “The Atmospheric Transport and Pattern of Medium Chain Chlorinated Paraffins at Shergyla Mountain on the Tibetan Plateau of China.” *Environmental Pollution* 245:46–52.

Yan, Hai, Huasheng Wang, Junfeng Wang, Chunhua Yin, Song Ma, Xiaolu Liu, and Xueyao Yin. 2012. “Cloning and Expression of the First Gene for Biodegrading Microcystin LR by Sphingopyxis Sp. USTB-05.” *Journal of Environmental Sciences* 24(10):1816–22.

Yin, Ran, Li Ling, and Chii Shang. 2018. “Wavelength-Dependent Chlorine Photolysis and Subsequent Radical Production Using UV-LEDs as Light Sources.” *Water Research* 142(June):452–58.

Zeck, A., M. G. Weller, D. Bursill, and R. Niessner. 2001. “Generic Microcystin Immunoassay Based on Monoclonal Antibodies against Adda.” *The Analyst* 126(11):2002–7.

Žegura, Bojana, Alja Štraser, and Metka Filipič. 2011. “Genotoxicity and Potential Carcinogenicity of Cyanobacterial Toxins – a Review.” *Mutation Research/Reviews in Mutation Research* 727(1–2):16–41.

Zhang, Hua, Huijuan Liu, Xu Zhao, Jiuhui Qu, and Maohong Fan. 2011. “Formation of Disinfection By-Products in the Chlorination of Ammonia-Containing Effluents: Significance of Cl2/N Ratios and the DOM Fractions.” *Journal of Hazardous Materials* 190(1–3):645–51.

Zhang, Xinran, Jun He, Shuqi Xiao, and Xin Yang. 2019. “Elimination Kinetics and Detoxification Mechanisms of Microcystin-LR during UV/Chlorine Process.” *Chemosphere* 214:702–9.

Zhang, Xinran, Jing Li, Jer-Yen Yang, Karl V. Wood, Arlene P. Rothwell, Weiguang Li, and Ernest R. Blatchley III. 2016. “Chlorine/UV Process for Decomposition and Detoxification of Microcystin-LR.” *Environmental Science & Technology* 50(14):7671–78.

Zhang, Xinran, Weiguang Li, Ernest R. Blatchley, Xiaoju Wang, and Pengfei Ren. 2015.

"UV/Chlorine Process for Ammonia Removal and Disinfection by-Product Reduction: Comparison with Chlorination." *Water Research* 68(2602):804–11.

Zhang, Zhong, Yi Hsueh Chuang, Aleksandra Szczuka, Kenneth P. Ishida, Shannon Roback, Megan H. Plumlee, and William A. Mitch. 2019. "Pilot-Scale Evaluation of Oxidant Speciation, 1,4-Dioxane Degradation and Disinfection Byproduct Formation during UV/Hydrogen Peroxide, UV/Free Chlorine and UV/Chloramines Advanced Oxidation Process Treatment for Potable Reuse." *Water Research* 164:114939.

Zhao, Quan, Chii Shang, Xiangru Zhang, Guoyu Ding, and Xin Yang. 2011. "Formation of Halogenated Organic Byproducts during Medium-Pressure UV and Chlorine Coexposure of Model Compounds, NOM and Bromide." *Water Research* 45(19):6545–54.

Zhao, Xi, Jin Jiang, Suyan Pang, Chaoting Guan, Juan Li, Zhen Wang, Jun Ma, and Congwei Luo. 2019. "Degradation of Iopamidol by Three UV-Based Oxidation Processes: Kinetics, Pathways, and Formation of Iodinated Disinfection Byproducts." *Chemosphere* 221:270–77.

Zhao, Yuan-Yuan, Jessica Boyd, Steve E. Hrudey, and Xing-Fang Li. 2006. "Characterization of New Nitrosamines in Drinking Water Using Liquid Chromatography Tandem Mass Spectrometry." *Environmental Science & Technology* 40(24):7636–41.

APPENDIX

A1. Preliminary Data for Selecting the Filter

Type of Filter	**TOC (mg/L)**	**TN (mg/L)**
Ultrapure water	0.08244	Not detectable
Mixed cellulose ester 0.45 reagent water	0.04783	Not detectable
Nylon 0.45 reagent water	1.001	0.2352

A2. BG11 Media Formulations

BG-11 media formulations optimized for Cyanobacteria (Gibco, Them Fisher Science, Cat. No. A1379901) are as below (Gibco 2020):

Item, Formula, (%w/v)

- Boric Acid, H_3BO_3, 0.00287%
- Manganese chloride tetrahydrate, $MnCl_2$-$4H_2O$, 0.00181%
- Zinc sulfate heptahydrate, $ZnSO_4$-$7H_2O$, 0.00022%
- Sodium molybdate dihydrate, Na_2MoO_4, 0.00039%
- Copper sulfate pentahydrate, $CuSO_4$-$5H_2O$, 0.00008%
- Sodium Nitrate, $NaNO_3$, 0.15000%
- Calcium chloride dihydrate, $CaCl_2$-$2H_2O$, 0.00270%
- Ferric ammonium citrate (green), C_6H_5 4yFe_xN_yO7, 0.00120%
- EDTA, EDTA, 0.00010%
- Potassium Phosphate Dibasic, K_2HPO_4, 0.00390%
- Magnesium sulfate heptahydrate, $MgSO_4$-$7H_2O$, 0.00750%
- Sodium carbonate monohydrate, Na_2CO_3-$1H_2O$, 0.00200%

A3. Microcystins SDS Links

Product	Product Number	SDS Link
Microcystin LR Standard, 10 µg/mL, 1mL	300632	SDS
Microcystin LR *Certified* Standard, 0.5 mL	300580	SDS
Microcystin RR Standard, 10 µg/mL, 1 mL	300636	SDS
Microcystin RR *Certified* Standard, 0.5mL	300582	SDS
Microcystin YR Standard, 10 µg/mL, 1 mL	300638	SDS